

---

# Characterizing and Manipulating by Local Electrochemical Techniques

---

## **DISSERTATION**

zur Erlangung des akademischen Grades eines Doktors der Naturwissenschaften  
(Dr. rer. nat.) an der Fakultät für Biologie, Chemie und Geowissenschaften  
der Universität Bayreuth



**UNIVERSITÄT  
BAYREUTH**

vorgelegt von

**Andreas Karg**

geboren in Bayreuth, Deutschland

Bayreuth, 2023



---

# Characterizing and Manipulating by Local Electrochemical Techniques

---

## DISSERTATION

zur Erlangung des akademischen Grades eines Doktors der Naturwissenschaften  
(Dr. rer. nat.) an der Fakultät für Biologie, Chemie und Geowissenschaften  
der Universität Bayreuth



UNIVERSITÄT  
BAYREUTH

vorgelegt von

**Andreas Karg**

geboren in Bayreuth, Deutschland

Bayreuth, 2023



Die vorliegende Arbeit wurde in der Zeit von August 2017 bis Juli 2023 in Bayreuth am Lehrstuhl Physikalische Chemie II unter Betreuung von Herrn Professor Dr. Georg Papastavrou angefertigt.

Vollständiger Abdruck der von der Fakultät für Biologie, Chemie und Geowissenschaften der Universität Bayreuth genehmigten Dissertation zur Erlangung des akademischen Grades einer Doktorin/ eines Doktors der Naturwissenschaften (Dr. rer. Nat.).

Form der Dissertation: Kumulative Dissertation

Dissertation eingereicht am: 18.07.2023

Zulassung durch die Promotionskommission: 26.07.2023

Wissenschaftliches Kolloquium: 18.12.2023

Amtierender Dekan: Prof. Dr. Cyrus Samimi

Prüfungsausschuss:

Prof. Dr. Georg Papastavrou (Gutachter)

Prof. Dr. Markus Retsch (Gutachter/in)

Prof. Dr. Jürgen Senker (Vorsitz)

JProf. Dr. Meike Leiske



*„Ride, si sapis“*

*- Marcus Valerius Martialis (40 - 104)*



# Contents

<b>Contents</b> .....	<b><i>i</i></b>
<b>Zusammenfassung</b> .....	<b><i>iii</i></b>
<b>Summary</b> .....	<b><i>vi</i></b>
<b>1. Introduction</b> .....	<b>1</b>
<b>2. Theory</b> .....	<b>7</b>
<b>2.1 Scanning probe microscopy</b> .....	<b>7</b>
2.1.1 Atomic Force Microscopy .....	7
2.1.2 Direct force measurements .....	8
2.1.3 Calibration .....	10
2.1.4 Colloidal probe technique.....	10
<b>2.2 Surface Forces</b> .....	<b>12</b>
2.2.1 Derjaguin Approximation .....	12
2.2.2 DLVO Theory.....	13
2.2.3 Van der Waals Interactions .....	14
2.2.4 Double-layer interactions.....	14
<b>2.3 Contact mechanics</b> .....	<b>16</b>
<b>2.4 Electrochemistry</b> .....	<b>18</b>
2.4.1 Electrochemical instrumentation .....	18
2.4.2 Micro- and macroelectrodes.....	19
2.4.3 Scanning electrochemical microscopy.....	21
<b>3. Synopsis</b> .....	<b>27</b>
<b>3.1 Outline</b> .....	<b>27</b>
<b>3.2 Content of Joint Publications</b> .....	<b>27</b>
3.2.1 Electrochemical Colloidal Probe for Direct Force Measurements.....	29
3.2.2 Electrochemical Grippers for Micro- and Nanorobotics: Manipulation by Tuning Surface Forces.....	31
3.2.3 An integrated, exchangeable three-electrode electrochemical setup for AFM-based scanning electrochemical microscopy.....	34
<b>3.2 Individual Contributions to Joint Publications</b> .....	<b>38</b>
<b>Manuscripts and Publications</b> .....	<b>43</b>
<b>4. A Versatile and Simple Approach to Electrochemical Colloidal Probes for Direct Force Measurements</b> .....	<b>44</b>

<b>5. Electrochemical Grippers for Micro- and Nanorobotics: Manipulation by Tuning Surface Forces .....</b>	<b>81</b>
<b>6. An integrated, exchangeable three-electrode electrochemical setup for AFM-based scanning electrochemical microscopy .....</b>	<b>123</b>
<b>List of Publications .....</b>	<b>148</b>
<b>Danksagung.....</b>	<b>149</b>
<b>(Eidesstattliche) Versicherungen und Erklärungen .....</b>	<b>151</b>

# Zusammenfassung

Neue Herausforderungen für Energiespeicher und Batterien erfordern ein grundlegendes Verständnis der elektrochemischen Eigenschaften der einzelnen Komponenten. Während auf der makroskopischen Skala eine große Anzahl von Analysemethoden etabliert sind, sind auf der Mikro- und Nanoskala Methoden zur Untersuchung lokaler elektrochemischer Eigenschaften wenig verbreitet. Eine instrumentelle Technik, die es erlaubt, mit hoher Auflösung Oberflächen abzubilden und Objekte zu manipulieren, ist das Rasterkraftmikroskop (engl. atomic force microscope, AFM). Techniken, die AFM und Elektrochemie verbinden sind daher von hohem Interesse für die Energiespeicherentwicklung. Obwohl bereits einige Methoden existieren, die AFM und Elektrochemie kombinieren, gibt es erheblichen Raum für Verbesserung und Innovationen, insbesondere in den Bereichen direkter Kraftmessung und Integration bzw. Aufbau von Messzellen.

Das Ziel dieser Arbeit ist die Entwicklung und Kombination neuer elektrochemischer Methoden für die Analytik, die Manipulation zum kontrollierten Erstellen komplexer Strukturen, sowie die Anwendung dieser Methoden um Grenzflächenprozesse zu untersuchen.

Im ersten Teil dieser Arbeit wurde ein neues Verfahren zur Herstellung kolloidaler Sonden entwickelt, die das Messen definierter Potential-abhängiger Oberflächenwechselwirkungen ermöglichen. Dabei wurde zur Produktion dieser Sonden eine neuartige Herstellungsmethode etabliert, die ausschließlich Standard-Laboraüstung verwendet. Zunächst wurden kommerzielle leitfähige Cantilever via Elektrodisposition elektrisch isoliert. Mithilfe einer Maskierungstechnik wurde dabei ein definiertes Loch in die Isolierschicht des Cantilevers aufgebracht. In dieses wurde mittels eines selbsthergestellten leitfähigen Klebers ein Goldkolloid so aufgebracht, das es elektrischen Kontakt zum leitfähigen Cantilever hatte.

Die so entstandenen elektrochemisch-aktiven kolloidalen Sonden wurden mittels Rasterelektronenmikroskopie, energiedispersiver Röntgenspektroskopie und Cyclovoltammetrie charakterisiert. Zusätzlich wurde mit diesen Cantilevern die potentialabhängige Wechselwirkung eines Goldkolloids und einer Glasoberfläche

untersucht, und diese Messungen mit theoretischen Berechnungen nach der Poisson-Boltzmann Theorie verglichen.

Das zentrale Ziel des zweiten Teils dieser Arbeit war die Entwicklung von Cantilevern mit integrierten Elektroden, die eine definierte Manipulation von  $\mu\text{m}$ - und  $\text{nm}$ - großen Objekten erlauben. Diese wurden durch elektrochemische Abscheidung einer isolierenden Schicht auf einen leitfähigen Cantilever und dem anschließenden definierten Abtragen durch fokussierte Ionenstrahlen erstellt. Die eigentliche Manipulation basiert auf dem externen An/Aus-Schalten der Adhäsion, die zwischen Cantilever und Objekt auftritt, welche durch das Anlegen eines externen Potentials gesteuert wird. Die potentialabhängigen Adhäsionskräfte zwischen diesen Cantilevern und immobilisiertem Silikapartikel wurde bestimmt, um Potentiale, die eine Adhäsion verursachen, die groß genug ist um eine Manipulation dieser Partikel zu erlauben, zu identifizieren. Zusätzlich wurden mögliche Substrate, auf denen die Partikel manipuliert werden sollten, auf ihre Eignung zur Manipulation, insbesondere die auftretende Adhäsion zwischen Substrat und Partikel, untersucht. Hierfür wurden Kraft-Abstandskurven mit einer kolloidalen Silikasonde auf den entsprechenden Substraten gemessen. Das Potenzial dieser Technik zur Manipulation  $\mu\text{m}$ - großer Partikel wurde demonstriert, indem Silikapartikel zu komplexen Strukturen angeordnet wurden.

Im letzten Teil dieser Dissertation wurden kommerzielle Cantilever für elektrochemische Scannmikroskopie (SECM), die die Messung von lokalen elektrochemischen Eigenschaften ermöglichen, mit siebgedruckten Elektroden modifiziert, um externe Referenz- und Gegenelektroden direkt zu integrieren und somit eine makroskopische elektrochemische Zelle zu ersetzen. Die Langzeitbeständigkeit dieser Elektroden wurde experimentell untersucht. Zum Vergleich dieser integrierten Elektroden mit einer kommerziellen elektrochemischen Zelle wurden sowohl die elektrochemischen Eigenschaften der jeweiligen Elektroden gemessen, als auch jeweils eine SECM-Messung durchgeführt und miteinander verglichen. Durch die Integration aller Elektroden auf dem Cantilever war keine zusätzliche Verkabelung nötig, was insbesondere unter Glovebox Bedingungen ein einfacheres Messen einer großen Zahl an Substraten erlaubt. Daher erlaubt die hier

## Zusammenfassung

---

entwickelte Methode einen Verzicht auf eine explizite elektrochemische Flüssigzelle, was zusätzlich in einer Reduktion des Drifts resultiert.

# Summary

New challenges in battery research demand a more fundamental understanding of electrochemical processes on a local scale that play a key role in various battery components. While several analytical techniques have been developed for macroscopic characterization, only a few methods allow to locally resolve the electrochemical behavior on a molecular level. One highly promising method for the measurement of local electrochemistry is the atomic force microscopy (AFM), which allows for high resolution imaging of various interfaces and manipulation of objects. While some combinations of the AFM technique with electrochemical methods already exist, there is still plenty of room for improvements of existing techniques and the development of new applications.

The aim of this work is the development of new electrochemical AFM methods for analytics and manipulation. This newly developed methods are used to study interfacial interactions between electrochemical active AFM-probes and different substrates.

In the first part of this thesis, a new approach to fabricate electrochemically active colloidal probes that offer a defined tip geometry in order to measure potential-dependent surface interactions was established. In difference to previously described electrochemically active colloidal probes, these can be prepared without expensive instrumentation. Commercial electrically conductive cantilevers were insulated by electrical deposition of a commercial insulation color. A temporary masking approach was applied to achieve the non-trivial and well-defined microelectrode at the cantilever probe. These cantilevers and their electrochemical properties were extensively studied using scanning electron microscopy, energy dispersive X-ray scattering, and cyclic voltammetry. Afterward, these novel cantilevers were used to study the potential-dependent interaction of a chemically modified colloidal gold probe against glass surfaces and PEDOT:PSS. The results were in good accordance with theoretical calculations derived from the Poisson-Boltzmann theory.

The aim of the second part of this work was the development of a novel AFM-based approach to nanomanipulation and nanorobotics for electrochemically triggered

## Summary

---

manipulation of objects in the colloidal domain. The cantilevers, which then acted as microgrippers, were purposely produced by coating standard cantilevers with insulating paint, followed by partial removal of this insulation layer by focused ion beam milling. By applying an external potential to the cantilever electrode, the adhesion properties between the cantilever and a colloidal object can be tuned in a well-defined and reproducible manner. The adhesion strength between cantilever electrode and immobilized silica particles was studied by measuring potential-dependent force-distance curves to identify the adhesions sufficient to allow manipulation. Additionally, suitable substrates for manipulation were chosen from different silane-modified and bare glass surfaces. Manipulation was demonstrated on substrates with different adhesive properties, moreover also assessing the limitations of this method. Adhesion behavior has been evaluated quantitatively by direct force measurements in the sphere/plane and plane/sphere geometry. For this, force-distance curves of a colloidal probe against a substrate were measured, and the respective adhesion properties were studied. The viability of manipulation with  $\mu\text{m}$ -precision was shown by manipulating silica particles into complex structures.

Moreover, special AFM cantilevers for scanning electrochemical microscopy (SECM) were modified by screen-printing methods to incorporate a full 3-electrode setup on the cantilever chip. The long-term electrochemical properties of the screen-printed electrodes were studied, while no significant degradation was observed over time. Furthermore, we compared the electrochemical properties of these screen-printed electrodes to the properties of a standard electrochemical cell. SECM images recorded with these modified cantilevers showed similar electrochemical behavior in comparison to the commercial electrochemical cell while displaying stable currents during the scanning of a standard test sample. By integrating all electrodes on the cantilever chip, no additional wiring and no specialized electrochemical cell is needed.

# 1. Introduction

Lithium-ion batteries currently dominate consumer electronics, smartphones, and electric automobiles due to their high energy and energy density<sup>1,2</sup>. However, the long-term use for these batteries in vehicles is damped by their aging processes, which severely harm the lifetime of the batteries<sup>3,4</sup>. Therefore, a fundamental understanding of the degradation and aging mechanisms of batteries and their influence on the key characteristics, like lifetime, energy density, and power density, is mandatory in order to construct better and safer batteries<sup>1,5</sup>. One failure mechanism of batteries is the formation and thickening of a solid electrolyte interface film on the anode, which leads to a loss of lithium inventory and, therefore, resulting in a loss of capacity.

One analytical tool to study the degradation of interfaces in batteries, in particular the formation of the solid electrolyte interface (SEI), is the atomic force microscope (AFM)<sup>6,7</sup>. AFM has been developed by Binnig et al.<sup>8</sup> and is based on the scanning tunneling microscope (STM) that was developed beforehand by the same group<sup>9</sup>. The STM relies on the tunneling effect and allows for atomic resolution on conductive substrates. The AFM, however, allows scanning and imaging of non-conducting substrates as well. It is based on a sharp cantilever tip that is scanned over a surface. Interaction forces between this tip and the substrate result in a bending of the cantilever. The resulting deflection is detected by the optical lever method, precisely a laser beam is reflected on the backside of the cantilever, sequentially a photodiode allows to connect the resulting shift of the laser spot to a voltage<sup>10</sup>.

However, the AFM not only allows for imaging of surfaces with sub-nm- resolution but also the direct measurement of interaction forces down to the pN-scale<sup>11</sup> as well as measuring mechanical properties of a sample. Since the AFM also works in fluid environments, the measurement of forces and deformations of biological samples like cells<sup>12</sup> and proteins<sup>13</sup> is possible. Additionally, by using a colloidal particle as a cantilever tip, the measurement of colloidal interactions allows to investigate the stability of colloidal dispersions<sup>14,15</sup>. Vice-versa, by attaching a single molecule to the tip, the interactions between individual molecules can be measured<sup>16</sup>. Besides the different analytical applications, the AFM was also used to manipulate individual particles by pushing them over a surface<sup>17-19</sup>.

## 1. Introduction

---

In the last decade, AFM was combined with other techniques like Raman spectroscopy<sup>20</sup>, quartz crystal microbalance<sup>21</sup>, microfluidics<sup>22</sup>, or fluorescence microscopy<sup>23</sup> to provide additional orthogonal measurement capabilities. Another promising application is the combination of AFM and electrochemistry<sup>24</sup>. Recently, the measurement of electrodes and charged interfaces using the AFM received increasing attention in literature<sup>25–28</sup>. However, this combination can barely be achieved by the use of standard AFM imaging modes, resulting in the necessity to develop new electrochemical AFM techniques. In the following, a short but not comprehensive overview of existing electrochemical AFM modes is given. In conductive-AFM (c-AFM), sometimes also called current-AFM, the sample conductivity as well as electrochemical properties like charge transport, are studied by a special kind of conductive cantilever probes. In this operating mode, the conductive tip is brought into contact with a sample, and a bias voltage is applied between both. The resulting current, while scanning over the sample, is measured. C-AFM is often used for the measurement of semiconductors and solar cells<sup>29–31</sup>. Kelvin probe microscopy (KPFM) allows the measurement of the surface potential of a sample. The tip is scanned across a sample at constant separation while an alternate current voltage is applied, which drives the cantilever to oscillate. The resulting electrostatic force can be measured by applying a direct current (DC) voltage applied to zero the difference in potential between tip and sample and to prevent mechanical oscillation. This DC voltage corresponds to the surface potential of the sample<sup>32,33</sup>. KPFM is used to study photoelectric materials<sup>34</sup>, semiconductors<sup>35</sup>, and corrosion properties<sup>36,37</sup>. In piezoelectric AFM (PFM), ferroelectric domains get polarized locally by a voltage applied to the tip and are subsequently imaged by the same cantilever<sup>38,39</sup>. Another promising electrical working mode of AFM is AFM-scanning electrochemical microscopy (AFM-SECM). Here, an ultramicroelectrode is used as a tip for electrochemistry and imaging. When a voltage is applied to the tip electrode, local electrochemistry can be imaged by recording the resulting steady-state current while at the same time measuring the topography and mechanical properties. While SECM is a technique that dates back to the 80s<sup>40</sup>, the AFM-SECM remained a niche technique until the introduction of batch fabricated<sup>41–43</sup> and commercial<sup>44</sup> cantilevers. The AFM-SECM is used in the fields of biosensors<sup>45</sup>, catalysis<sup>46</sup>, and battery research<sup>47</sup>.

## 1. Introduction

---

As mentioned beforehand, one of the essential building blocks of an AFM is the AFM cantilever. Especially for these new electrochemical working modes, new electrochemically active cantilevers had to be developed, enhancing the capabilities for AFM measurements towards energy storage analysis. However, here there is still a lot of space for improvements, both for improving the present electrochemically active cantilevers, as well as the development of new ones for other advanced electrochemical working modes.

The main objective of this thesis is the development of new types of electrochemically active AFM-cantilevers to implement new and enhanced electrochemical imaging modes. By the use of specifically produced probes for AFM, it became possible to measure surface forces between a gold colloid with a directly applied potential and a substrate. Additionally, dedicated AFM-cantilevers optimized for electrochemical manipulation of  $\mu\text{m}$ -sized colloids allowed the production of complex colloidal structures. By integrating a complete electrochemical cell into a commercial SECM-cantilever, the prerequisite for a high-throughput AFM-SECM under glovebox conditions without rewiring for every substrate was developed.

In summary, several new electrochemical active AFM-probes have been developed in this work, demonstrating the capabilities of the atomic force microscopy as a tool for both - using electrochemical processes for enhanced measuring and manipulation modes as well as measuring electrochemical processes themselves.

### References

1. Han, X. et al. A review on the key issues of the lithium ion battery degradation among the whole life cycle. *eTransportation* **1**, 100005 (2019).
2. Lu, L., Han, X., Li, J., Hua, J. & Ouyang, M. A review on the key issues for lithium-ion battery management in electric vehicles. *Journal of Power Sources* **226**, 272-288 (2013).
3. Barré, A. et al. A review on lithium-ion battery ageing mechanisms and estimations for automotive applications. *Journal of Power Sources* **241**, 680-689 (2013).
4. Whittingham, M. S. Lithium batteries and cathode materials. *Chemical Reviews* **104**, 4271-4301 (2004).
5. Spitthoff, L., Shearing, P. R. & Burheim, O. S. Temperature, Ageing and Thermal Management of Lithium-Ion Batteries. *Energies* **14**, 1248 (2021).
6. Koltypin, M., Cohen, Y. S., Markovsky, B., Cohen, Y. & Aurbach, D. The study of lithium insertion–deinsertion processes into composite graphite electrodes by in situ atomic force microscopy (AFM). *Electrochemistry communications* **4**, 17-23 (2002).
7. Tripathi, A. M., Su, W.-N. & Hwang, B. J. In situ analytical techniques for battery interface analysis. *Chemical Society Reviews* **47**, 736-851 (2018).
8. Binnig, G., Quate, C. F. & Gerber, C. Atomic force microscope. *Physical Review Letters* **56**, 930 (1986).
9. Binnig, G., Rohrer, H., Gerber, C. & Weibel, E. *Scanning tunneling microscopy* (Springer, Dordrecht, 1982).
10. Meyer, G. & Amer, N. M. Novel optical approach to atomic force microscopy. *Applied Physics Letters* **53**, 1045-1047 (1988).
11. Butt, H.-J., Cappella, B. & Kappl, M. Force measurements with the atomic force microscope: Technique, interpretation and applications. *Surf. Sci. Rep.* **59**, 1-152 (2005).
12. Dufrêne, Y. F., Viljoen, A., Mignolet, J. & Mathelié-Guinlet, M. AFM in cellular and molecular microbiology. *Cellular Microbiology* **23**, 13324 (2021).
13. Wilke, P. et al. A direct biocombinatorial strategy toward next generation, mussel-glycine inspired saltwater adhesives. *Journal of the American Chemical Society* **136**, 12667-12674 (2014).
14. Ducker, W. A., Senden, T. J. & Pashley, R. M. Direct measurement of colloidal forces using an atomic force microscope. *Nature* **353**, 239-241 (1991).
15. Butt, H. J. Measuring electrostatic, van der Waals, and hydration forces in electrolyte solutions with an atomic force microscope. *Biophys. J.* **60**, 1438-1444 (1991).
16. Rief, M., Oesterhelt, F., Heymann, B. & Gaub, H. E. Single molecule force spectroscopy on polysaccharides by atomic force microscopy. *Science* **275**, 1295-1297 (1997).
17. Baur, C. et al. Nanoparticle manipulation by mechanical pushing: underlying phenomena and real-time monitoring. *Nanotechnology* **9**, 360 (1998).
18. Decossas, S., Mazen, F., Baron, T., Brémond, G. & Souifi, A. Atomic force microscopy nanomanipulation of silicon nanocrystals for nanodevice fabrication. *Nanotechnology* **14**, 1272-1278 (2003).

## 1. Introduction

19. Kim, S., Shafiei, F., Ratchford, D. & Li, X. Controlled AFM manipulation of small nanoparticles and assembly of hybrid nanostructures. *Nanotechnology* **22**, 115301 (2011).
20. Chan, K. L. A. & Kazarian, S. G. Tip-enhanced Raman mapping with top-illumination AFM. *Nanotechnology* **22**, 175701 (2011).
21. Gurdak, E., Dupont-Gillain, C. C., Booth, J., Roberts, C. J. & Rouxhet, P. G. Resolution of the vertical and horizontal heterogeneity of adsorbed collagen layers by combination of QCM-D and AFM. *Langmuir* **21**, 10684-10692 (2005).
22. Helfricht, N. et al. Writing with fluid: structuring hydrogels with micrometer precision by AFM in combination with nanofluidics. *Small* **13**, 1700962 (2017).
23. Nishida, S., Funabashi, Y. & Ikai, A. Combination of AFM with an objective-type total internal reflection fluorescence microscope (TIRFM) for nanomanipulation of single cells. *Ultramicroscopy* **91**, 269-274 (2002).
24. Papastavrou, G. Combining electrochemistry and direct force measurements: from the control of surface properties towards applications. *Colloid. Polym. Sci.* **288**, 1201-1214 (2010).
25. Fermín, D. J. Nanoscale probing of electrode surfaces by scanning force microscopy. *CHIMIA International Journal for Chemistry* **60**, 789-794 (2006).
26. Butt, H. Analyzing electric double layers with the atomic force microscope. *Encyclopedia of Electrochemistry: Online* (2007).
27. Kuznetsov, V. & Papastavrou, G. Adhesion of Colloidal Particles on Modified Electrodes. *Langmuir* **28**, 16567-16579 (2012).
28. Kuznetsov, V. & Papastavrou, G. Ion Adsorption on Modified Electrodes as Determined by Direct Force Measurements under Potentiostatic Control. *J. Phys. Chem. C* **118**, 2673-2685 (2014).
29. Lee, L.-T., Ito, S., Benten, H., Ohkita, H. & Mori, D. Current mode atomic force microscopy (C-AFM) study for local electrical characterization of conjugated polymer blends. *Ambio* **41**, 135-137 (2012).
30. Alexeev, A. & Loos, J. Conductive atomic force microscopy (C-AFM) analysis of photoactive layers in inert atmosphere. *Organic Electronics* **9**, 149-154 (2008).
31. De Wolf, P., Snauwaert, J., Clarysse, T., Vandervorst, W. & Hellemans, L. Characterization of a point-contact on silicon using force microscopy-supported resistance measurements. *Applied physics letters* **66**, 1530-1532 (1995).
32. Melitz, W., Shen, J., Kummel, A. C. & Lee, S. Kelvin probe force microscopy and its application. *Surface science reports* **66**, 1-27 (2011).
33. Collins, L., Kilpatrick, J. I., Kalinin, S. V. & Rodriguez, B. J. Towards nanoscale electrical measurements in liquid by advanced KPFM techniques: a review. *Reports on Progress in Physics* **81**, 086101-086193 (2018).
34. Collins, L. et al. Time resolved surface photovoltage measurements using a big data capture approach to KPFM. *Nanotechnology* **29**, 445703 (2018).
35. Rosenwaks, Y., Shikler, R., Glatzel, T. & Sadewasser, S. Kelvin probe force microscopy of semiconductor surface defects. *Physical Review B* **70**, 085320 (2004).
36. Chiba, A., Muto, I. & Hara, N. Cut Edge Corrosion Inhibition by Chromate in Primer of Prepainted 55% Al-Zn Alloy Coated Steel. *Journal of the Electrochemical Society* **158**, C42 (2011).
37. Indira, K., Vanithakumari, S. C., Mudali, U. K. & Mallika, C. Probing the Stability of Superhydrophobic (SHP) Silane Coating on Anodized Ti Substrate Using Kelvin Probe Force Microscope (KPFM). *Transactions of the Indian Institute of Metals* **72**, 3045-3055 (2019).

## 1. Introduction

---

38. Günther, P. & Dransfeld, K. Local poling of ferroelectric polymers. *Applied Physics Letters* **61**, 1137-1139 (1992).
39. Soergel, E. Piezoresponse force microscopy (PFM). *Journal of Physics D: Applied Physics* **44**, 464003 (2011).
40. Bard, A. J., Fan, F. R. F., Kwak, J. & Lev, O. Scanning electrochemical microscopy. Introduction and principles. *Analytical Chemistry* **61**, 132-138 (1989).
41. Eifert, A., Mizaikoff, B. & Kranz, C. Advanced fabrication process for combined atomic force-scanning electrochemical microscopy (AFM-SECM) probes. *Micron* **68**, 27-35 (2015).
42. Dobson, P. S., Weaver, J. M. R., Holder, M. N., Unwin, P. R. & Macpherson, J. V. Characterization of Batch-Microfabricated Scanning Electrochemical-Atomic Force Microscopy Probes. *Analytical Chemistry* **77**, 424-434 (2005).
43. Wain, A. J., Pollard, A. J. & Richter, C. High-Resolution Electrochemical and Topographical Imaging Using Batch-Fabricated Cantilever Probes. *Analytical Chemistry* **86**, 5143-5149 (2014).
44. Nellist, M. R. et al. Atomic force microscopy with nanoelectrode tips for high resolution electrochemical, nanoadhesion and nanoelectrical imaging. *Nanotechnology* **28**, 095711 (2017).
45. Caniglia, G. & Kranz, C. Scanning electrochemical microscopy and its potential for studying biofilms and antimicrobial coatings. *Analytical and Bioanalytical Chemistry* **412**, 6133-6148 (2020).
46. Limani, N., Boudet, A., Blanchard, N., Jusselme, B. & Cornut, R. Local probe investigation of electrocatalytic activity. *Chemical Science* **12**, 71-98 (2021).
47. Mahankali, K., Thangavel, N. K. & Reddy Arava, L. M. In Situ Electrochemical Mapping of Lithium–Sulfur Battery Interfaces Using AFM–SECM. *Nano Letters* **19**, 5229-5236 (2019).

# 2. Theory

## 2.1 Scanning probe microscopy

### 2.1.1 Atomic Force Microscopy

The atomic force microscopy (AFM) is a rather old technique, which was introduced in 1986 by Binnig et al.<sup>1</sup>. Based on the scanning tunneling microscope (STM), which Binnig & Rohrer<sup>2</sup> developed, it allows to study interaction forces of the probe tip. The AFM rapidly became a widely used tool for characterizing interfaces also on non-conductive samples. Imaging sample topography with excellent lateral resolution<sup>3-6</sup> was one of the earliest advantages of an AFM. The recent development of more advanced imaging modes, for example, PeakForce, allows to easily study even more properties of materials, such as elasticity and adhesion<sup>7-9</sup>. Additionally, in recent years AFM has been combined with a wide variety of analytic methods<sup>10-15</sup> which opened the use in different disciplines like biology<sup>16-18</sup>, corrosion science<sup>19-21</sup>, and electrochemistry<sup>22-24</sup>. Furthermore, the AFM allows for directly measuring interaction forces between the probe and a sample surface with a resolution down to the pN-scale<sup>3,25</sup>.

The basic setup of an AFM is shown schematically in figure 2.1. The most essential part of the AFM is the cantilever which acts as a force sensor. This cantilever can have either a sharp tip or a colloidal particle at its free end.

If a force is acting between the cantilever and the surface, the cantilever deflects correspondingly. The deflection is detected by employing the optical lever method<sup>26</sup>. This technique is based on a laser, which is focused on the back of the cantilever, and a position-sensitive photodetector that detects its reflection. As a result, the photodetector senses a different photon distribution if the cantilever is bent. This setup allows for an accurate detection of deflections down to the Å scale.

Lateral and vertical movements of the cantilever are controlled normally by a piezoelectric scanner with sub-nm-precision<sup>3,25</sup>.

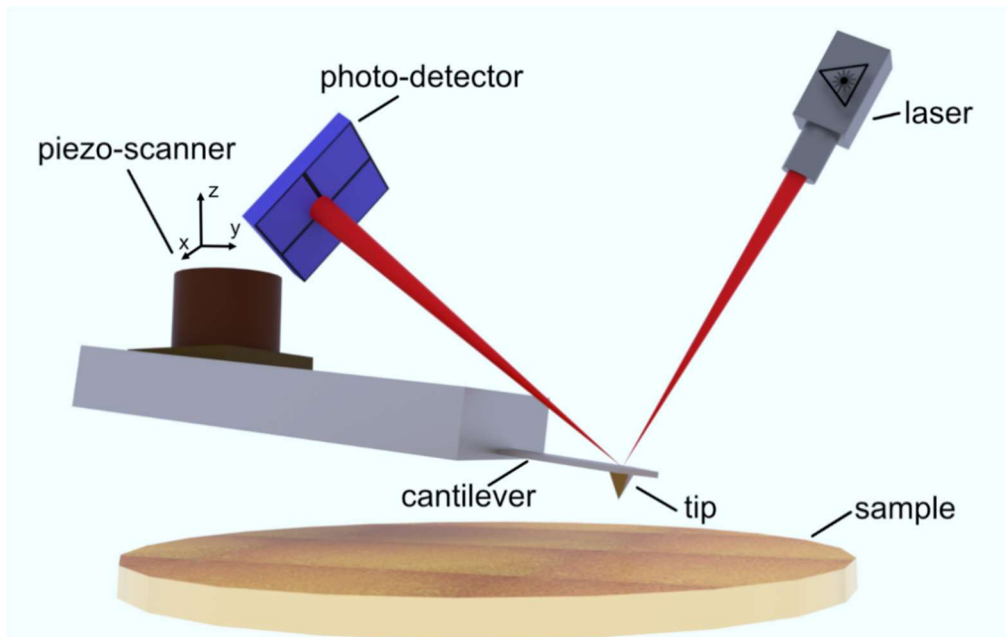


Figure 2.1: Schematic representation of an atomic force microscope (AFM) showing the essential parts of the instrument consisting of a piezo-scanner that moves in  $xyz$  direction, a cantilever that is scanned over the surface, a laser and photo-detector that detects the bending of the cantilever by optical lever method, and the sample that is scanned during the experiment.

### 2.1.2 Direct force measurements

One of the many application fields of force microscopy is the detection of interaction forces by measuring force-distance curves. A schematic example of a force-distance curve is shown in figure 2.2. Here, the force between a colloidal particle and a planar surface is directly measured as a function of the separation distance. A so-called force curve can be divided into an approach and a retraction part. The approach starts far away from the surface, no interaction between the probe and the sample can be observed (cf. fig. 2.2A). Near the surface, the cantilever begins to bend as a result of long-range interactions like electrostatics (cf. fig. 2.2B). In the figure, repulsive long-range interactions are shown. Attractive interactions, like van-der Waals forces, surpass the repulsive long-range forces at smaller separations, leading to a jump-to-contact. If the cantilever is driven further towards the surface, a predefined setpoint, also known as maximum loading force, is reached (cf. fig. 2.2C). Information about the mechanical deformation of the sample can be extracted from this contact. When the piezo movement is reversed, the cantilever gets retracted.

Upon separation, higher forces can be necessary to separate probe and substrate due to adhesion forces. This part of the force vs. distance curve is called jump-from contact

## 2. Theory

(cf. fig. 2.2D). When the cantilever is further retracted, no more interaction forces are observed (cf. fig. 2.2E) and the cantilever deflection is restored to the origin state.

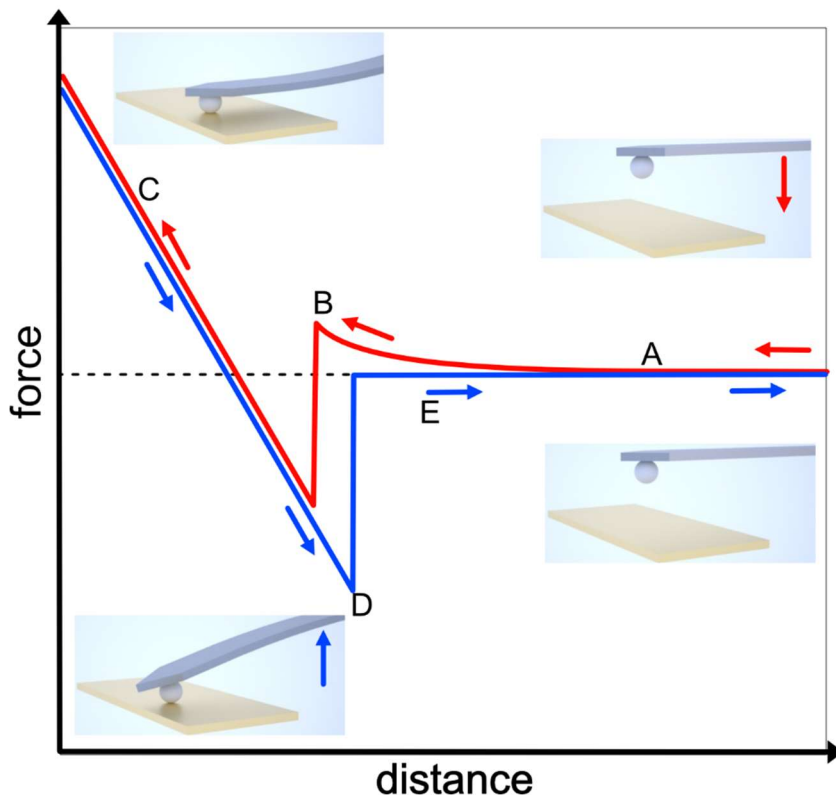


Figure 2.2: Exemplary force-distance curve. The red approach curve and the blue withdraw curve are part of a force vs distance measurement. The insets show the cantilever deflection at different steps schematically.

The raw data measured during a direct force measurement with an AFM, namely the deflection of the cantilever and the displacement of the z-piezo, have to be converted to a force vs. distance curve, as shown in figure 2.2. To convert this data, the optical lever sensitivity (OLS) has to be determined. This is done by measuring force-distance curves against a rigid, flat substrate like freshly cleaved mica. The linear region when the cantilever is in contact with the surface is also called the constant compliance region. This linear regime allows to correlate between the deflection of the cantilever and the photodetector signal.

As long as the deflections are sufficiently small, the cantilever can be regarded as a Hookean spring. Thus, the deflection corresponds directly to the force acting onto it following Hooke's law: ( $F = k Z$ ). As a result, quantitative force measurements are possible with the AFM, provided that the spring constant  $k$  is determined.

## 2. Theory

### 2.1.3 Calibration

Since the cantilevers used in an AFM experiment deviate in their nominal spring constants as a result of the production process, a calibration of each cantilever is necessary to get a real spring constant and, therefore, quantitative force measurements with low errors<sup>27,28</sup>.

In the literature, several different approaches to determine the spring constant of an AFM-cantilever have been reported<sup>29-31</sup>. In this thesis, the so-called 'thermal noise' method was used for all publications. Here, it is briefly introduced: If a cantilever tip is far away from the surface, it will oscillate due to thermal excitation<sup>32</sup>. The cantilever can be considered as harmonic oscillator. The equipartition theorem states a kinetic energy of  $\frac{1}{2}k_B T$  for each degree of freedom in oscillation. For low additional noise and small damping, the resonance peak of the cantilever acquired in the power spectral density data (PSD) can be described by a Lorentzian function<sup>33</sup>. The mean square deflection amplitude  $\langle A^2_0 \rangle$  can be obtained by integrating the Lorentzian curve. This integration allows for the calculation of the spring constant  $k$  from the PSD<sup>3,32</sup>.

$$\frac{1}{2}k \langle A^2_0 \rangle = \frac{1}{2}k_B T \quad (2.1)$$

$$k = \frac{k_B T}{\langle A^2_0 \rangle} \quad (2.2)$$

Where  $k_B$  is the Boltzmann constant,  $T$  is the temperature, and  $k$  is the spring constant of the cantilever. One prerequisite of this calibration method is the need for a previous determination of the optical lever sensitivity (OLS), risking contamination of the probe tip upon sample contact.

Other commonly used cantilever calibration methods are the addition of a known mass to the cantilever and the measurement of the resulting resonance frequency shift<sup>17</sup>, or are based on geometrical considerations<sup>18</sup>.

### 2.1.4 Colloidal probe technique

For quantitative evaluation of AFM measurements, detailed knowledge of the interaction geometry and a defined surface geometry is of uttermost importance. For most topographic AFM applications, sharp cantilever tips are used to achieve a high lateral resolution. Since the exact tip geometry of such tips is hard to access, such

## 2. Theory

cantilevers are commonly not used to determine quantitative interaction forces<sup>34</sup>. The so-called colloidal probe technique, independently developed by Butt et al. and Ducker et al., makes the measurement of interaction forces between colloids in sphere/sphere and sphere/plane geometry possible<sup>34–36</sup>. The colloidal probe technique is based on the attachment of  $\mu\text{m}$ -sized particles with a defined size on the cantilever. These act as a probe. Additionally, a higher force sensitivity results due to the larger interaction area. While classical colloidal probes consist of silica or glass particles, nowadays, a whole range of particles with different orders of magnitudes and different materials and geometries have been used as colloidal probes<sup>37–41</sup>. Figure 2.3 shows SEM images of a standard AFM cantilever with a sharp tip and a colloidal probe cantilever with an attached colloidal particle.

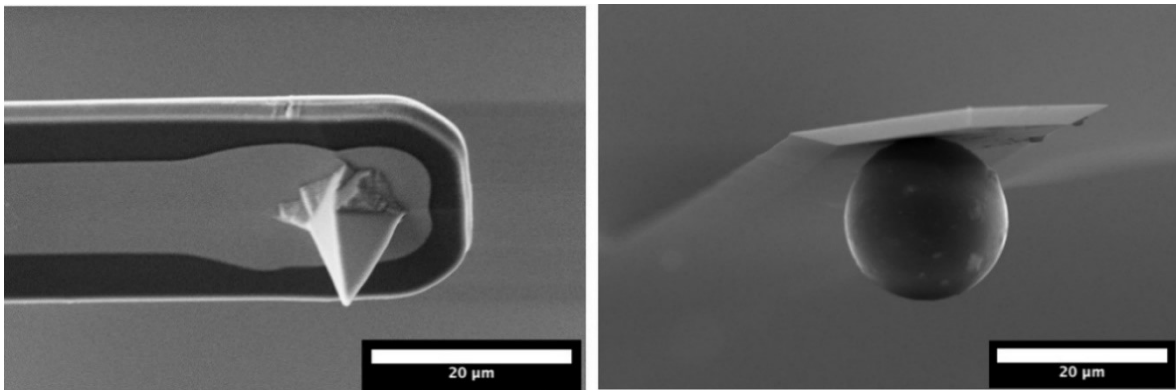


Figure 2.3: SEM images of AFM-cantilevers. Left: Standard AFM cantilever with a sharp tip. Right: colloidal probe cantilever, with a colloidal particle functioning as a tip.

## 2.2 Surface Forces

The colloidal probe technique enabled the quantitative studies of surface forces on a colloidal scale by direct force measurements.

### 2.2.1 Derjaguin Approximation

A detailed knowledge of the interaction geometry is necessary for a quantitative study of colloidal interactions. The Derjaguin approximation relates the force  $F(D)$  acting between two finite spherical objects with a radius of curvature  $R_1$  and  $R_2$  to the free interaction energy per unit area  $W(D)$  between two planar surfaces at this separation  $D$ <sup>42</sup>. Therefore, it is possible to compare measurement results obtained by using different techniques as well as theoretical predictions<sup>43</sup>.

$$F(D) = 2\pi R_{eff} W(D) \quad (2.3)$$

$R_{eff}$  is the effective radius, which is calculated from the radii  $R_1$  and  $R_2$  of the interacting objects for two spheres:

$$R_{eff}^{-1} = R_1^{-1} + R_2^{-1} \quad (2.4)$$

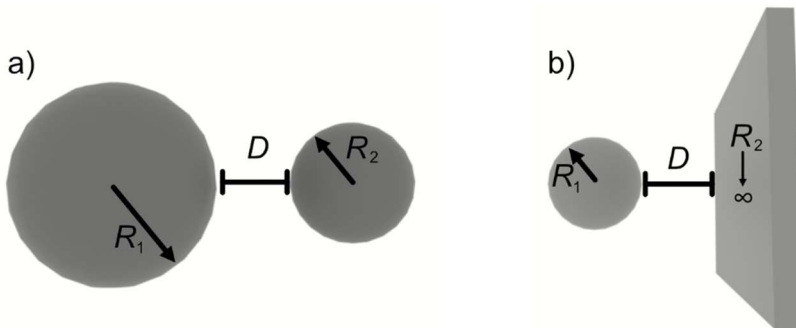


Figure 2.4: Schematic illustration of colloidal interaction forces. a) Interaction of sphere-sphere geometry based on the Derjaguin approximation. b) Schematic of a sphere plane geometry. In both cases,  $D$  is the separation of the objects, while  $R$  is the object's radius.

However, although the Derjaguin approximation has been shown to be valid in many cases also for rough surfaces, the approximation is restricted to distances larger than the characteristic surface roughness of the involved objects<sup>43</sup>. Additionally, it is limited to the case of interaction forces, whose range are significantly smaller than the effective radius  $R_{eff}$  of the interacting bodies ( $D \ll R_{eff}$ ), which is usually fulfilled for

## 2. Theory

colloidal objects<sup>44</sup>. As a result, it is possible to describe the interaction of colloids independently of the geometry of the solid through the Derjaguin approximation<sup>44</sup>.

### 2.2.2 DLVO Theory

The coagulation and stability of colloidal dispersions are of fundamental interest for industrial applications (e.g. dispersion colors). An approach to quantify these properties is described by means of the DLVO theory<sup>45–48</sup>. This theory, named after their developers Derjaguin, Landau, Verwey, and Overbeek, explains the interaction of colloidal particles as the combination of two types of forces: Attractive van der Waals forces, and the repulsive electrostatic double-layer force, which stabilizes these dispersions. A schematic overview of DLVO interaction force profiles depending on the separation distance is shown in figure 2.4. The attractive van der Waals forces dominate near the surface, while for large separations, the contribution of the electrostatic forces governs the DLVO force profile<sup>44</sup>.

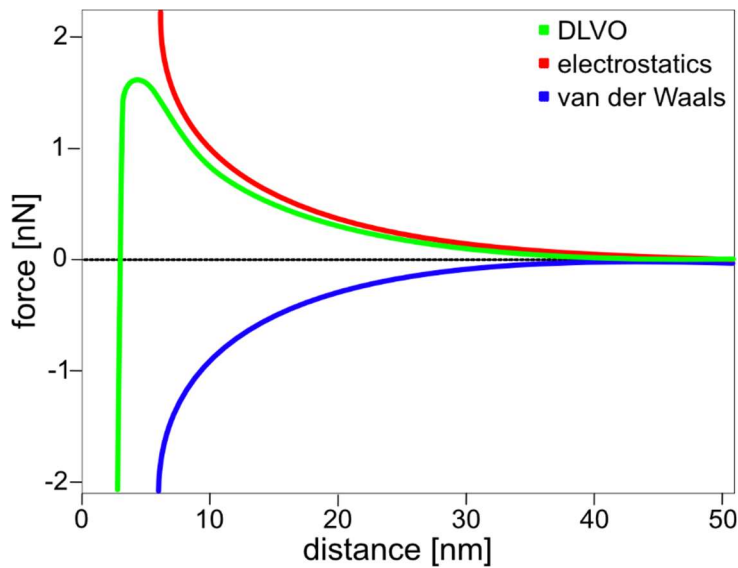


Figure 2.5: Schematic of the interaction forces for diffuse layer interaction (red), van der Waals interactions (blue), and the combination based on the DLVO theory (green)

### 2.2.3 Van der Waals Interactions

Van der Waals forces are caused by dipole interactions. They combine the different dipole-dipole interactions described by Keesom (orientation dipoles), Debye (induced dipoles), and London (dispersion forces). For macroscopic objects, like colloids, the separation-dependent free interaction energy per surface area  $W_{vdw}$  is given by:

$$W_{vdw}(D) = -\frac{A_H}{12\pi D^2} \quad (2.5)$$

Here,  $A_H$  is the so-called Hamaker-constant specific for a material in a medium and represents the strength of van der Waals interactions<sup>44,48</sup>.

### 2.2.4 Double-layer interactions

As a result of ion adsorption or dissociation of surface groups, surfaces are usually charged in aqueous solutions. These surface charges attract oppositely charged counterions. The resulting layer of surface charges, consisting of counterions and coions is the so-called “electric double layer”. In the simplest model of the double layer, the Helmholtz layer, the counterions are directly adsorbed to the surface leading to charge neutralization. The Gouy Chapman model, on the other hand, assumes a diffuse layer caused by thermal motions of the ions<sup>49,50</sup>. Stern combined these models by dividing the double layer into two parts: The Stern-layer, a layer of immobile ions directly adsorbed to the surface, and the Gouy Chapman layer, which consists of mobile ions that follow Poisson-Boltzmann statistics<sup>51,52</sup>. The transition point, where the bound Stern layer ends and the diffuse layer begins, is the so-called shear plane, the potential at this distance the  $\zeta$ -potential<sup>44,53</sup>. In the simplest case of the Stern layer, counterions cannot get infinitely close to the surface due to their size and hydration shell (in water). The distance  $d$  between the centers of the counterions and the surface marks the outer Helmholtz layer<sup>44</sup>. A schematic of the double layer following Stern theory is shown in figure 2.5.

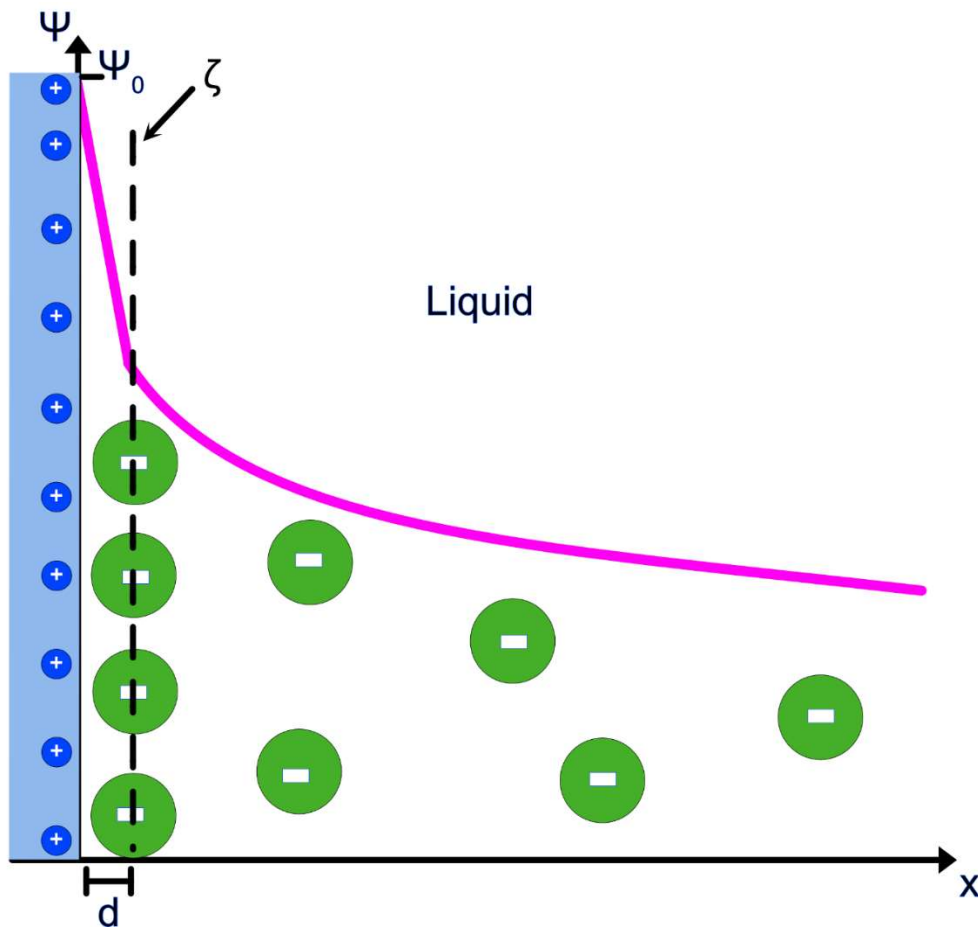


Figure 2.5: Schematic of the simple version of a Stern layer with an electric double layer at the solid/liquid interface with a surface potential  $\psi_0$ <sup>44</sup>. The pink line illustrates the potential as a function of the separation from the charged interface.

The Poisson-Boltzmann theory describes the potential  $\psi$  within a double layer. It combines the Poisson equation (cf. eq. 2.6), which allows the calculation of the potential distribution  $\nabla^2\psi$  near a charged surface with the spatial distribution of ions in solution. Due to their thermal motion, these ions can be described by Boltzmann statistics.

$$\nabla^2\psi = -\frac{\rho_e}{\varepsilon_0\varepsilon_r} \quad (2.6)$$

Here,  $\rho$  is the local electric charge density near the interface,  $\varepsilon_0$  is the vacuum permittivity and  $\varepsilon_r$  the relative permittivity, respectively.

## 2. Theory

When assuming a 1:1 electrolyte and a concentration of background salt higher than the concentration of ions that are dissociated from the surface, the local volume charge density  $\rho$  can be expressed as:

$$\rho_e = ec_0 \left( e^{-\frac{e\psi(x,y,z)}{k_B T}} - e^{\frac{e\psi(x,y,z)}{k_B T}} \right) \quad (2.7)$$

The Poisson-Boltzmann equation is a partial differential equation of second order and therefore has to be solved numerically in most cases. However, for planar homogeneously charged surfaces and low potentials ( $|\psi| \ll 25$  mV at room temperature), it can be linearized to:

$$\frac{\partial^2 \psi}{\partial x^2} \approx \frac{2e^2 c_0}{\epsilon_0 \epsilon_r k_B T} \psi. \quad (2.8)$$

For the boundary conditions  $\psi(x)|_{x \rightarrow 0} = \psi_0$  (surface potential of the charged surface, cf. fig. 2.5) and  $\psi(x)|_{x \rightarrow \infty} = 0$  (bulk potential), the solution to the linearized Poisson-Boltzmann equation is given by:

$$\psi = \psi_0 e^{-\kappa x} \quad (2.9)$$

The decay constant  $\kappa$  is the inverse Debye length, which is a measure for the extension of the electronic diffuse layer. The Debye length for a 1:1 electrolyte at 25°C is given by<sup>44,48</sup>:

$$\kappa^{-1} = \sqrt{\frac{\epsilon_0 \epsilon_r k_B T}{2c_0 e^2}} \approx \frac{0.304 \text{ nm}}{\sqrt{c_0 \text{ L mol}^{-1}}} \quad (2.10)$$

For low potentials, and the case of two identical parallel surfaces of two infinitely extended solids in a distance  $D$  from each other, their Gibbs interaction energy per surface area, can be described as<sup>48</sup>:

$$W_{DL}(D) = 2\epsilon_0 \epsilon_r \kappa \psi_0^2 e^{-\kappa D} \quad (2.11)$$

### 2.3 Contact mechanics

The elastic contact of a sphere with a planar surface is non-trivial since the contact area and the corresponding contact radius are not known a priori. Real particles are never entirely rigid and deform elastically under an applied load. This problem was first addressed by Hertz<sup>54</sup>. Assuming a small contact radius compared to the sphere

## 2. Theory

radius, a frictionless contact, no tensile stress, and no interactions such as adhesion, Hertz derived the force to achieve a given penetration depth  $\delta$ :

$$F_{Hertz} = \frac{4}{3}E^* \sqrt{R_{eff}} \delta^3 \quad (2.12)$$

$E^*$  denotes the combined Young's modulus, which incorporates the Young-moduli of both materials in contact (i.e.  $E_1$  and  $E_2$ , respectively) as well as their Poisson's ratios  $\nu_1$  and  $\nu_2$ :

$$E^* = \left( \frac{1 - \nu_1^2}{E_1} + \frac{1 - \nu_2^2}{E_2} \right)^{-1} \quad (2.13)$$

However, the Hertz model only allows for the calculation of forces between spheres and planar objects while applying an external force. It does not account for the presence of surface forces, which do have an impact on the effective contact area for a real system.

The JKR model, named after Johnson, Kendall, and Roberts, takes such interactions into account, albeit only in the contact area<sup>55</sup>. These forces result in a gain of surface energy for two objects in contact. The adhesion force for the JKR theory is<sup>44,48,53</sup>:

$$F_{JKR} = \frac{3}{2}\pi W_{Adh} R_{eff} \quad (2.14)$$

Figure 2.6 shows schematically adhesive interactions for different contact geometries and for the different contact theories.

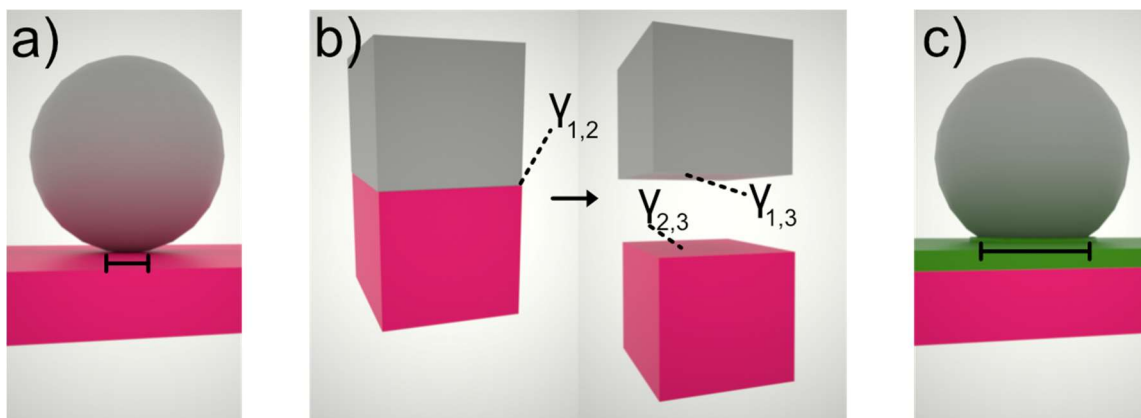


Figure 2.6 Schematic of adhesive interactions. a) Sphere-plane interaction (Hertz model). b) Adhesive contact through interfacial tensions. c) Sphere-plane adhesion based on JKR theory.

### 2.4 Electrochemistry

Electrochemistry is a branch of physical chemistry that studies the relation between electrical potentials with chemical reactions<sup>56</sup>. In the following, first, the essential parts of an electrochemical setup will be described. Then the combination of electrochemistry with scanning probe microscopy, an experimental electrochemical technique that was refined during this work, is explained.

#### 2.4.1 Electrochemical instrumentation

An electrochemical cell is a device that allows the use of defined potentials and currents at electrodes, which interface electronic and ionic conductors, to trigger chemical reactions<sup>57</sup>.

A cell for electrochemical measurements generally consists of at least two electrodes separated by an electrolyte phase<sup>56</sup>, which allows charge transport between the electrodes through its ions. Figure 2.7 shows a schematic of a typical electrochemical cell as used in this work. Of the aforementioned electrodes, the working electrode is typically the focus of an electrochemical experiment. Only here, electrode reactions are supposed to take place at the electrode-electrolyte interface when an external potential is applied towards it<sup>57</sup>. Meanwhile, the counter electrode is the basic part of an electrochemical cell. It is usually chosen to be made of an inert material, like platinum, to prevent chemical reactions like oxidation at this electrode interface. While only two electrodes are needed for an electrochemical experiment to guarantee a stable potential, a three-electrode setup is often used. In a three-electrode setup, the potential of the working electrode is measured against a reference electrode using a voltmeter with a high input impedance. As a result, no significant current flows through the reference electrode. Therefore, the reference electrode has a constant half-cell potential, which acts as a stable reference. Here, often standardized electrodes, like Ag/AgCl or calomel electrodes, are used. Typically, a potentiostat applies a defined potential at the working electrode, while the resulting current flow between the working electrode and counter electrode is measured<sup>56</sup>.

One typical example of an electrochemical method is cyclic voltammetry, which allows for the characterization of electrochemical processes, such as redox reactions. Here, a potential changing linearly with time is applied to the working electrode, and the resulting current is detected<sup>56,58</sup>.

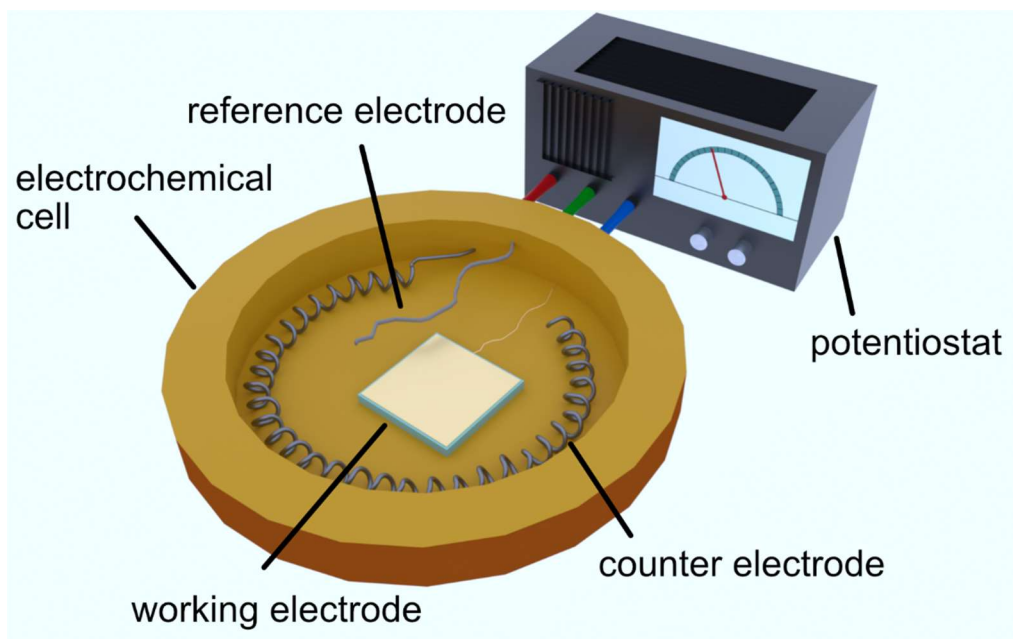


Figure 2.7: Schematic of a setup used for a typical electrochemical experiment, consisting of an electrochemical cell with electrodes (3-electrode-setup) connected to a potentiostat allowing control of the applied potential.

#### 2.4.2 Micro- and macroelectrodes

As mentioned before, the working electrode is typically the center of an experiment in electrochemistry. Their geometric dimensions strongly influence their electronic transport properties. For macroscopic electrodes with a size in the cm-range, the current significantly depends on the processes which lead to an asymptotic current drop while polarizing the electrode. However, for ultramicroelectrodes (UME) or nanoelectrodes, which have a sub- $\mu\text{m}$  dimensions, a time-independent steady-state current  $i$  is established rapidly. As a result, the current  $i$  depends mainly on the critical dimension of the electrode  $r_T$ , the diffusion coefficient  $D_0$ , the stoichiometric number of electrons involved in the redox reaction  $n$ , and the bulk concentration  $c_0$ , as shown in table 2.1. Macro- and ultramicroelectrodes are discerned by their electrical behavior. Typically, one talks of UME if the critical dimension  $r_T$  (such as the radius or the width) is smaller than  $r_T < 25 \mu\text{m}$  or if the electrode dimension  $r$  is significantly smaller than the diffusion layer thickness<sup>56</sup>. Typically, UME appear as disk, sphere, cylinder, or band, and the current depends greatly on their shape<sup>59</sup> (cf table 2.1).

## 2. Theory

Table 2.1: Steady-state current of ultramicroelectrodes depending on their shape<sup>56</sup>

$i_{T,ss}$ (disc electrode)	$i_{T,ss}$ (sphere)	$i_{T,ss}$ (hemisphere)	$i_{T,qss}$ (cylindrical)*
$4nFD_0c_0r_T$	$4\pi nFD_0c_0r_T$	$2\pi nFD_0c_0r_T$	$\frac{2nFAD_0c_0}{r_T \ln \tau}$

\* quasi-steady-state, since  $\tau$  depends on time as an inverse logarithmic function.

In a cyclic voltammogram, the electrode size leads to very different shapes. As shown in figure 2.8 a, no discernable redox peaks are visible for an UME, while for a macroelectrode for the same redox pair, clear peaks can be discerned. For the latter, the current drops visible at higher potentials stem from depletion of redox active molecules near the electrode. The resulting current is controlled by diffusion from the bulk solution. UME's, on the other hand, show a decay to the steady-state current<sup>58</sup>. The diffusion modes for macroelectrodes and UME are shown schematically for an inlaid disc electrode in figure 2.8 b. Because of their fast response times and low Ohmic drop, enhanced mass transport rates, and diminished double layer charging, UME are necessary to study rapid electron transfer kinetics<sup>58,59</sup>. Another application of UME is scanning electrochemical microscopy (SECM), which is introduced in the following chapter.

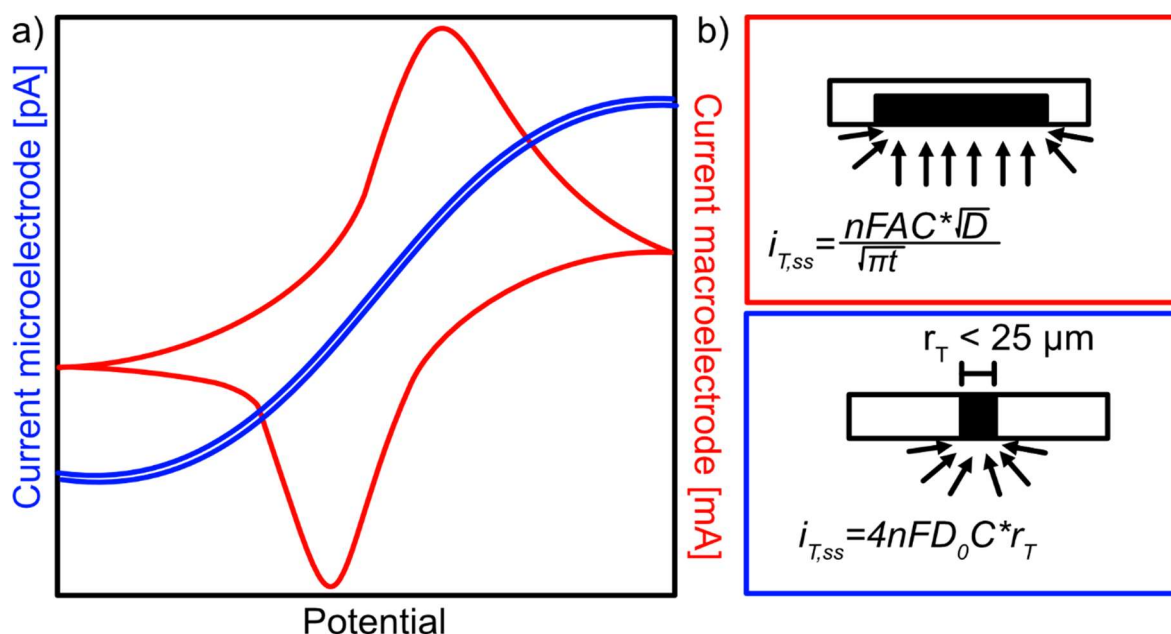


Figure 2.8: Schematic comparison of macroelectrodes (red) and microelectrodes (blue). a) Cyclic voltammograms of macroelectrode and microelectrode. b) Schematic illustration of diffusion modes for macro- and microelectrodes.

### 2.4.3 Scanning electrochemical microscopy

Scanning electrochemical microscopy (SECM), is a rather old technique developed in the 1980s by Bard and coworkers<sup>60</sup>. It was recently applied to a wide range of research areas, like biochemistry<sup>61</sup>, catalysis<sup>62,63</sup> and battery research<sup>64,65</sup>.

The SECM is based on a UME and allows the detection of faradaic currents and, therefore, electrochemical reactions, in a locally resolved manner by scanning the UME at a defined height over the sample while detecting the current caused by local electrochemical reactions. In a classical SECM setup, an UME made from a metal wire embedded in a glass capillary is scanned over the sample using an XY stepper motor for positioning<sup>66</sup>. The principle of one of the most widely used SECM modes, the feedback mode, is shown schematically in figure 2.9. Here, only the tip current  $i_{T,ss}$  is monitored at large separation from the sample surface, while a defined potential is applied to the tip. This current is driven by the flux of the oxidized species **O** from the bulk towards the tip, which are reduced at the UME to the reduced species **R**. The current in a SECM experiment is typically normalized to this so-called bulk current. When the UME is brought closer to an insulator sample, this substrate partially blocks the diffusion of **O** to the tip, leading to a decrease in current  $i_T$  compared to the bulk current  $i_{T,ss}$ . This current drop scales with decreasing tip-substrate distance. The resulting signal when measuring an insulator sample is called negative feedback. Contrarily, when the tip is brought near a conductive substrate with a supplied oxidative potential, **O** gets reduced to **R** at the tip, and **O** gets replenished at the substrate through oxidation. While in this case also, a blockage of diffusion occurs, the speed of the replenishing of the species leads to a higher current  $i_T$ . This so-called positive feedback leads to an increase in current with decreasing tip-substrate distance when measuring conductive substrates<sup>59</sup>.

## 2. Theory

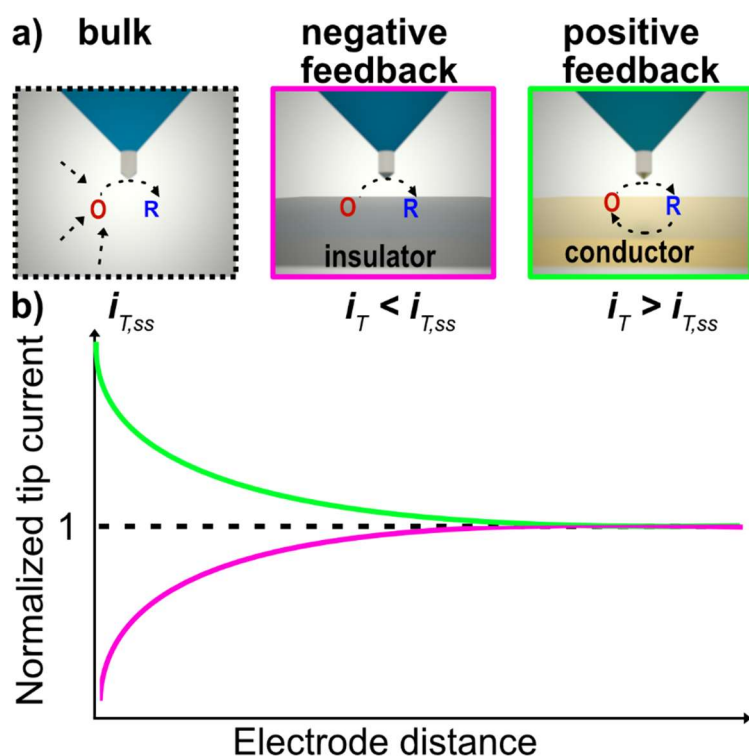


Figure 2.9: Working principle of SECM-feedback mode. a) General principle of feedback mode for a UME at the cantilever tip inserted into a solution containing oxidized species **O**. b) Normalized tip-current for negative (pink) and positive (green) feedback as a function of the electrode distance. The dashed line indicates the bulk current used for normalization.

As shown in figure 2.9, the current of a SECM experiment depends on the tip-substrate separation. Due to the influence of sample electrode reactivity, z-distance control in the nm-range is hard to achieve by classical SECM, where the UME is scanned over the sample at a defined distance. This limitation poses a problem for samples with high roughness and high topographic structures. Additionally, classical SECM has limited lateral resolution<sup>66</sup>. Both of these challenges were overcome by the combination of AFM and SECM, the so-called AFM-SECM. Thus, the local electrochemical sensing capabilities of the SECM were combined with the accurate force control and lateral resolution of the AFM. This combination allows monitoring electrochemical reactions on the sub-micrometer scale independent of sample topography<sup>67–69</sup>. However, because the AFM-SECM cantilever production is complicated, AFM-SECM remained a niche technique. With the introduction of commercial batch-fabricated AFM-SECM cantilevers<sup>70</sup>, the application of AFM-SECM in various research areas has been significantly facilitated<sup>23,71,72</sup>.

### References

1. Binnig, G., Quate, C. F. & Gerber, C. Atomic force microscope. *Phys. Rev. Lett.* **56**, 930 (1986).
2. Binnig, G., Rohrer, H., Gerber, C. & Weibel, E. *Scanning tunneling microscopy* (Springer, Dordrecht, 1982).
3. Butt, H.-J., Cappella, B. & Kappl, M. Force measurements with the atomic force microscope: Technique, interpretation and applications. *Surf. Sci. Rep.* **59**, 1-152 (2005).
4. Gan, Y. Atomic and subnanometer resolution in ambient conditions by atomic force microscopy. *Surface Science Reports* **64**, 99-121 (2009).
5. Giessibl, F. J. AFM's path to atomic resolution. *Materials Today* **8**, 32-41 (2005).
6. Fukuma, T. Subnanometer-scale imaging of nanobio-interfaces by frequency modulation atomic force microscopy. *Biochem. Soc. Trans.* **48**, 1675-1682 (2020).
7. Xu, K. et al. Recent development of PeakForce Tapping mode atomic force microscopy and its applications on nanoscience. *Nanotech. Rev.* **7**, 605-621 (2018).
8. Young, T. J. et al. The use of the PeakForce™ quantitative nanomechanical mapping AFM-based method for high-resolution Young's modulus measurement of polymers. *Meas. Sci. Technol.* **22**, 125703 (2011).
9. Sobhbidari, F. & Hu, Q. Recent advances in the mechanical characterization of shales at nano-to micro-scales: A review. *Mechanics of Materials* **162**, 104043 (2021).
10. Amarouch, M. Y., El Hilaly, J. & Mazouzi, D. AFM and FluidFM Technologies: Recent Applications in Molecular and Cellular Biology. *Scanning* **2018**, 7801274 (2018).
11. Bhat, S. V., Price, J. D. W. & Dahms, T. E. S. AFM-Based Correlative Microscopy Illuminates Human Pathogens. *Front. Cell. Infec. Microbiol.* **11**, 655501 (2021).
12. Dazzi, A. & Prater, C. B. AFM-IR: Technology and applications in nanoscale infrared spectroscopy and chemical imaging. *Chemical reviews* **117**, 5146-5173 (2017).
13. Prats-Mateu, B. & Gierlinger, N. Tip in-light on: Advantages, challenges, and applications of combining AFM and Raman microscopy on biological samples. *Microsc. Res. Tech.* **80**, 30-40 (2017).
14. Handschuh-Wang, S., Wang, T. & Zhou, X. Recent advances in hybrid measurement methods based on atomic force microscopy and surface sensitive measurement techniques. *RSC advances* **7**, 47464-47499 (2017).
15. Fu, W. & Zhang, W. Hybrid AFM for nanoscale physicochemical characterization: recent development and emerging applications. *Small* **13**, 1603525 (2017).
16. Lyubchenko, Y. L. Direct AFM Visualization of the Nanoscale Dynamics of Biomolecular Complexes. *Journal of Physics D: Applied Physics* **51**, (2018).
17. Woolley, A. T., Cheung, C. L., Hafner, J. H. & Lieber, C. M. Structural biology with carbon nanotube AFM probes. *Chemistry & Biology* **7**, R193-R204 (2000).

## 2. Theory

18. Cheong, L.-Z., Zhao, W., Song, S. & Shen, C. Lab on a tip: Applications of functional atomic force microscopy for the study of electrical properties in biology. *Acta Biomaterialia* **99**, 33-52 (2019).
19. Chen, H., Qin, Z., He, M., Liu, Y. & Wu, Z. Application of Electrochemical Atomic Force Microscopy (EC-AFM) in the Corrosion Study of Metallic Materials. *Materials* **13**, 668 (2020).
20. Shinato, K. W., Huang, F. & Jin, Y. Principle and application of atomic force microscopy (AFM) for nanoscale investigation of metal corrosion. *Corrosion Reviews* **38**, 423-432 (2020).
21. Smith, J. R., Larson, C. & Campbell, S. A. Recent applications of SEM and AFM for assessing topography of metal and related coatings—a review. *Transactions of the IMF* **89**, 18-27 (2011).
22. Chotkowski, M., Połomski, D. & Czerwinski, K. Potential Application of Ionic Liquids for Electrodeposition of the Material Targets for Production of Diagnostic Radioisotopes. *Materials* **13**, 5069 (2020).
23. Kempaiah, R., Vasudevamurthy, G. & Subramanian, A. Scanning probe microscopy based characterization of battery materials, interfaces, and processes. *Nano Energy* **65**, 103925 (2019).
24. Liu, X., Wang, D. & Wan, L. Progress of electrode/electrolyte interfacial investigation of Li-ion batteries via in situ scanning probe microscopy. *Science Bulletin* **60**, 839-849 (2015).
25. Hodges, C. S. Measuring forces with the AFM: polymeric surfaces in liquids. *Adv. colloid interface Sci.* **99**, 13-75 (2002).
26. Meyer, G. & Amer, N. M. Novel optical approach to atomic force microscopy. *Appl. Phys. Lett.* **53**, 1045-1047 (1988).
27. Cumpson, P. J., Clifford, C. A. & Hedley, J. Quantitative analytical atomic force microscopy: a cantilever reference device for easy and accurate AFM spring-constant calibration. *Meas. Sci. Tech.* **15**, 1337 (2004).
28. Colton, R. J. *Procedures in scanning probe microscopies* (John Wiley & Sons, New York, 1998).
29. Cleveland, J. P., Manne, S., Bocek, D. & Hansma, P. K. A nondestructive method for determining the spring constant of cantilevers for scanning force microscopy. *Rev. Sci. Instrum.* **64**, 403-405 (1993).
30. Sader, J. E., Chon, J. W. M. & Mulvaney, P. Calibration of rectangular atomic force microscope cantilevers. *Rev. Sci. Instrum.* **70**, 3967-3969 (1999).
31. Burnham, N. A. et al. Comparison of calibration methods for atomic-force microscopy cantilevers. *Nanotechnology* **14**, 1 (2002).
32. Hutter, J. L. & Bechhoefer, J. Calibration of atomic-force microscope tips. *Rev. Sci. Instrum.* **64**, 1868-1873 (1993).
33. Heer, C. V. *Statistical Mechanics, Kinetic theory, and Stochastic Processes* (Academic Press, New York, 2012).
34. Kappl, M. & Butt, H. J. The colloidal probe technique and its application to adhesion force measurements. *Part. Part. Syst. Charact.* **19**, 129-143 (2002).
35. Ducker, W. A., Senden, T. J. & Pashley, R. M. Direct measurement of colloidal forces using an atomic force microscope. *Nature* **353**, 239-241 (1991).
36. Butt, H. J. Measuring electrostatic, van der Waals, and hydration forces in electrolyte solutions with an atomic force microscope. *Biophys. J.* **60**, 1438-1444 (1991).

## 2. Theory

37. Mark, A., Helfricht, N., Rauh, A., Karg, M. & Papastavrou, G. The Next Generation of Colloidal Probes: A Universal Approach for Soft and Ultra-Small Particles. *Small* **15**, 1902976 (2019).
38. Helfricht, N., Mark, A., Dorwling-Carter, L., Zambelli, T. & Papastavrou, G. Extending the limits of direct force measurements: colloidal probes from sub-micron particles. *Nanoscale* **9**, 9491-9501 (2017).
39. Knittel, P., Zhang, H., Kranz, C., Wallace, G. G. & Higgins, M. J. Probing the PEDOT:PSS/cell interface with conductive colloidal probe AFM-SECM. *Nanoscale* **8**, 4475-4481 (2016).
40. Helfricht, N. et al. Probing the adhesion properties of alginate hydrogels: a new approach towards the preparation of soft colloidal probes for direct force measurements. *Soft Matter* **13**, 578-589 (2017).
41. Neugirg, B. R. et al. Long-range interaction forces between 1, 3, 5-cyclohexanetrissamide fibers in crossed-cylinder geometry. *Polymer* **102**, 363-371 (2016).
42. Derjaguin, B. Untersuchungen über die Reibung und Adhäsion, IV. *Kolloid-Zeitschrift* **69**, 155-164 (1934).
43. Rentsch, S., Pericet-Camara, R., Papastavrou, G. & Borkovec, M. Probing the validity of the Derjaguin approximation for heterogeneous colloidal particles. *Phys. Chem. Chem. Phys.* **8**, 2531-2538 (2006).
44. Butt, H.-J., Graf, K. & Kappl, M. *Physics and Chemistry of Interfaces* (John Wiley & Sons, Weinheim, 2013).
45. Derjaguin, B. & Kussakov, M. Anomalous properties of thin polymolecular films. *Acta Physicochimica URSS* **10**, 25-44 (1939).
46. Derjaguin, B. V. Theory of the Stability of Strongly Charged Lyophobic Sols and of the Adhesion of Strongly Charged Particles in Solutions of Electrolytes. *USSR* **14**, 633 (1941).
47. Verwey, E. J. W., Overbeek, J. T. G. & Van Nes, K. Theory of the stability of lyophobic colloids. *J. Phys. Chem.* **51**, 631-636 (1947).
48. Butt, H.-J. & Kappl, M. *Surface and interfacial forces* (John Wiley & Sons, Weinheim. 2018).
49. Gouy, G. Sur la fonction électrocapillaire. *Annales de physique* (1917).
50. Chapman, D. L. LI. A contribution to the theory of electrocapillarity. *The London* (1913).
51. Stern, O. Zur theorie der elektrolytischen doppelschicht. *Zeitschrift für Elektrochemie und angewandte physikalische Chemie* **30**, 508-516 (1924).
52. Carnie, S. L., Chan, D. Y. C., Mitchell, D. J. & Ninham, B. W. The structure of electrolytes at charged surfaces: The primitive model. *J. Chem. Phys.* **74**, 1472-1478 (1981).
53. Israelachvili, J. N. *Intermolecular and surface forces* (American Press, New York, 1992).
54. Hertz, H. Ueber die Berührung fester elastischer Körper. *J. für die reine und angewand. Math.* **92**, 22 (1882).
55. Johnson, K. L., Kendall, K. & Roberts, A. A. D. Surface energy and the contact of elastic solids. *Pro. R. Soc. Lond. A* **324**, 301-313 (1971).
56. Bard, A. J. & Faulkner, L. R. *Fundamentals and applications* (Wiley, New York, 2001).
57. Atkins, P., De Paula, J. & Keeler, J. *Phys. Chem.* (2018).
58. Compton, R. G. & Banks, C. E. *Understanding voltammetry* (Imperial College Press, London, 2010).

## 2. Theory

59. Bard, A. J. & Mirkin, M. V. *Scanning Electrochemical Microscopy* (CRC Press, Boca Raton, 2001).
60. Bard, A. J., Fan, F. R. F., Kwak, J. & Lev, O. Scanning electrochemical microscopy. *Anal. Chem.* **61**, 132-138 (1989).
61. Conzuelo, F., Schulte, A. & Schuhmann, W. Biological imaging with scanning electrochemical microscopy. *Proc. R. Soc. A* **474**, 20180409 (2018).
62. O'Connell, M. A. & Wain, A. J. Mapping Electroactivity at Individual Catalytic Nanostructures Using High-Resolution Scanning Electrochemical–Scanning Ion Conductance Microscopy. *Anal. Chem.* **86**, 12100-12107 (2014).
63. Sun, T., Yu, Y., Zacher, B. J. & Mirkin, M. V. Scanning Electrochemical Microscopy of Individual Catalytic Nanoparticles. *Angew. Chem. Int. Ed.* **53**, 14120-14123 (2014).
64. Ventosa, E. & Schuhmann, W. Scanning electrochemical microscopy of Li-ion batteries. *Phys. Chem. Chem. Phys.* **17**, 28441-28450 (2015).
65. Kumatani, A. & Matsue, T. Recent advances in scanning electrochemical microscopic analysis and visualization on lithium-ion battery electrodes. *Cur. Opin. Electrochem.* **22**, 228-233 (2020).
66. Sun, P., Laforge, F. O. & Mirkin, M. V. Scanning electrochemical microscopy in the 21st century. *Phys. Chem. Chem. Phys.* **9**, 802-823 (2007).
67. Macpherson, J. V. & Unwin, P. R. Combined Scanning Electrochemical–Atomic Force Microscopy. *Anal. Chem.* **72**, 276-285 (2000).
68. Dobson, P. S., Weaver, J. M. R., Holder, M. N., Unwin, P. R. & Macpherson, J. V. Characterization of Batch-Microfabricated Scanning Electrochemical-Atomic Force Microscopy Probes. *Anal. Chem.* **77**, 424-434 (2005).
69. Kranz, C. Recent advancements in nanoelectrodes and nanopipettes used in combined scanning electrochemical microscopy techniques. *The Analyst* **139**, 336-352 (2014).
70. Nellist, M. R. et al. Atomic force microscopy with nanoelectrode tips for high resolution electrochemical, nanoadhesion and nanoelectrical imaging. *Nanotechnology* **28**, 095711 (2017).
71. Mahankali, K., Thangavel, N. K. & Reddy Arava, L. M. In Situ Electrochemical Mapping of Lithium–Sulfur Battery Interfaces Using AFM–SECM. *Nano Letters* **19**, 5229-5236 (2019).
72. Shi, X., Qing, W., Marhaba, T. & Zhang, W. Atomic force microscopy - Scanning electrochemical microscopy (AFM-SECM) for nanoscale topographical and electrochemical characterization: Principles, applications and perspectives. *Electrochimica Acta* **332**, 135472 (2020).

## 3. Synopsis

### 3.1 Outline

In the framework of this thesis, several new approaches to performing electrochemistry on a local scale have been developed.

New measurement techniques like improved SECM and conductive colloidal probe measurements and their understanding are highly relevant, e.g., for the research of corrosion and energy storage.

Commercial cantilevers are adapted for this purpose through microfabrication, electrochemical deposition and screenprinting, and are also utilized for micromanipulation.

In the following, the content of all three publications is briefly summarized. The individual contributions of all co-authors have been summarized at the end of this chapter.

### 3.2 Content of Joint Publications

The force resolution of pN and lateral resolution of nm of an AFM allows for the measurement of a wide range of interaction types. Besides permitting for the measurement of adhesion and electrostatics the AFM allows assessing locally-defined electrochemical activity. Additionally, the precision of an AFM allows for the manipulation of  $\mu\text{m}$  and sub- $\mu\text{m}$ -sized objects into defined two-dimensional structures.

This dissertation is divided into three scientific projects that address different electrochemical problems. These are addressed by developing specific electrochemical active AFM-cantilevers that are subsequently used to investigate interfacial and physicochemical properties and processes and open new application fields for electrochemical AFM. The probes developed in the different projects in this thesis are summarized in figure 3.1, together with a short schematic showing the use case of these probes.

In the first scientific project of this thesis (cf. chapter 4), an electroactive AFM cantilever with defined spherical geometry has been developed, leading to an electrochemical colloidal probe (eCP). While eCPs have been reported previously<sup>1-3</sup>, here a simple

### 3. Synopsis

way to produce these eCPs that does not rely on sophisticated equipment like photolithography or focused ion beam milling has been developed. These eCPs were then used to measure the potential dependent surface interactions of a reference surface, namely a glass substrate, as well as applied to the characterization of electroactive polymer layers (**Paper 1**).

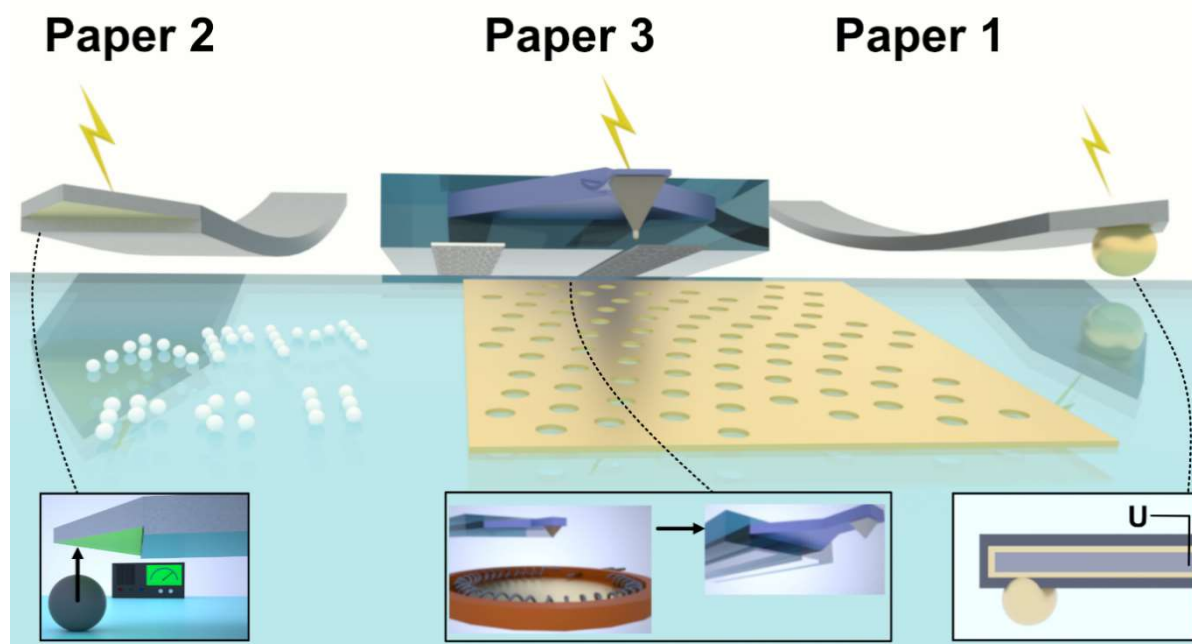


Figure 3.1: Overview of the different types of AFM-cantilevers developed in this work. **Paper 1**) Electrochemical colloidal probe, enabling the study of potential-dependent surface interactions because of its well-accessible geometric dimension. **Paper 2**) Electrochemical gripper allowing the manipulation of  $\mu\text{m}$  and sub- $\mu\text{m}$  objects by tuning the adhesion through external potentials. **Paper 3**) Integrated SECM cantilever, replacing an entire electrochemical cell with a 3-electrode setup incorporated into a cantilever.

In the second project of this thesis (cf. chapter 5), an electrochemical gripper for AFM was built by selectively removing a homemade insulation layer from a conductive cantilever. This gripper has no moveable parts but is based on tuning the adhesion forces between this modified AFM cantilever and the object to be manipulated by applying external potentials. This potential-dependent adhesion of a cantilever was studied against  $\mu\text{m}$ -sized colloidal silica beads. Furthermore, deploying these silica beads into complex structures showed the capabilities for manipulating  $\mu\text{m}$  and sub- $\mu\text{m}$  sized particles (**Paper 2**).

In the third part of this thesis (cf. chapter 6), the incorporation of a 3-electrode setup directly onto the cantilever and its carrier chip has been developed, thereby allowing to simultaneously measure topography and SECM without the need for an additional macroscopic electrochemical cell. This approach enables the analysis of locally resolved electrochemical activity without the necessity of further electrical connections, reducing the risk of dry electrodes. For this cantilever-based electrochemical cell, screen-printed electrodes were incorporated onto a commercial cantilever. The long-term stability was evaluated, and these integrated cantilevers were compared to a standard setup consisting of a cantilever and an electrochemical cell (**Paper 3**).

#### 3.2.1 Electrochemical Colloidal Probe for Direct Force Measurements

Recently, AFM-SECM became a valuable tool for analyzing local electrochemical properties of electrode materials in different application fields, such as energy storage and electrocatalysis research<sup>4-7</sup>. While AFM-SECM allows for the imaging of local electrochemical activity and topography, an AFM also enables the measurement of surface forces with pN resolution<sup>8</sup>. Therefore, a defined interaction geometry is required, which can be achieved by the colloidal probe technique, which relies on using a spherical particle with a highly defined geometry as a tip. The measurement of interaction forces with electrochemical colloidal probes (eCP) was reported only recently<sup>1</sup>. However, the production of these probes relies on non-standard equipment like focused ion beam lithography.

In order to prepare eCPs, commercial conductive cantilevers were electrically insulated utilizing an electrochemical deposition process, which is accessible using standard laboratory equipment. The insulating electropaint used as a coating provides excellent insulating properties, leading to a significantly lower current in a cyclic voltammetry measurement compared to non-insulated conductive cantilevers (cf. figure 3.2a). A masking process was used to achieve a bare hole at the end of the cantilever, which represented the electrochemically active area. This preparation was done by reversibly attaching colloidal polystyrene beads onto the cantilever. These were later removed by micromanipulation. Electrochemical colloidal probes were produced from these cantilevers by attaching gold colloids through a homemade

### 3. Synopsis

electrically conductive glue into the holes. SEM images of the thus-produced electrically colloidal probes are shown in figure 3.2b. Through gluing a conductive colloidal particle onto a hole-cantilever, the free electrode area increases, leading to an increase in current in the cyclic voltammetry (cf. figure 3.2c). Therefore, this behavior indicates successful contact between the cantilever and the particle.

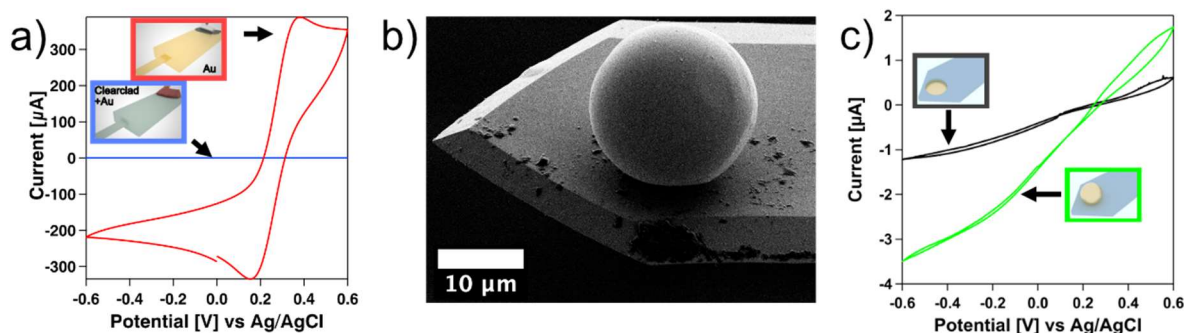


Figure 3.2: a) Cyclic voltammetry of a commercial conductive cantilever as bought and after modification by insulating electropaint. The measured current after the insulation was several magnitudes lower. b) SEM image of an electrochemical colloidal probe (eCP). c) Cyclic voltammetry measurement of an insulated cantilever with a defined hole in the insulation layer after removal of the sacrificial bead and the same cantilever after application of a gold particle with conductive glue.

To prove that the here prepared eCP-cantilevers were electrochemically active, force-distance curves on a soft conductive PEDOT:PSS substrate were measured in a two-electrode setup, resulting in a current flow when the conductive particle and the substrate were in contact (cf figure 3.3a).

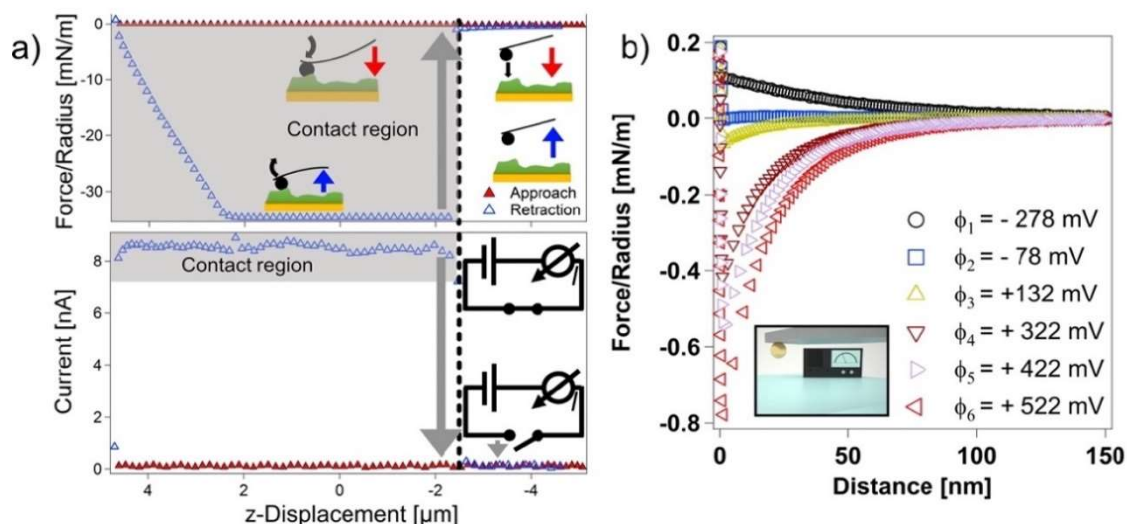


Figure 3.3: Force curves under potentiostatic control. a) Force measurements of an eCP against a PEDOT:PSS substrate in a 2-electrode setup with an applied potential. Upon contact between cantilever and substrate, a current flow is visible. b) Approach force curves of an eCP against a glass substrate in a three-electrode setup for different applied potentials. The more positive the applied potential, the more attractive the observed force curve, and vice-versa.

The eCP-cantilevers were then used to study the diffuse layer properties against glass surfaces for different applied potentials in a controlled aqueous environment (cf figure 3.3b). Here, for negative applied potential, repulsive behavior was observed as expected for negatively charged glass surfaces. By contrast, a more attractive behavior followed for positive applied potential. Using literature values for the surface properties of glass<sup>9,10</sup>, Poisson-Boltzmann fits accounting for charge regulation<sup>9,11</sup> were used to determine the effective potential of the eCP depending on the potential applied. These resulting potentials were in good agreement with the work on flat electrodes of Kuznetsov et al.<sup>12</sup>.

### 3.2.2 Electrochemical Grippers for Micro- and Nanorobotics: Manipulation by Tuning Surface Forces

There are many ways to manipulate macroscopic objects, ranging from grippers to suction cups. However, for objects at the nanoscale, defined gripping is severely inhibited by the dominance of surface forces like van der Waals and capillary forces<sup>13–17</sup>. Manipulation of micro- and nanosized objects using an atomic force microscope (AFM) has been described earlier in literature<sup>18–20</sup>. Nevertheless, AFM-based manipulation setups rely mainly on applying lateral forces and pushing an object with

### 3. Synopsis

---

the sharp cantilever tip. However, such approaches do not allow for a defined pick and place on a substrate.

Here, a so-called electrochemical gripper has been developed as a novel approach for manipulating micro- and nanometer-sized objects in a liquid environment. The working principle of these grippers solely relies on the electrochemical tuning of the adhesion forces between these home-built cantilevers and the colloidal particles and the substrate, respectively.

These special cantilevers were prepared from commercial gold-coated cantilevers, which were electrically contacted and insulated by an electrodeposition approach<sup>21</sup>. At a defined area at the free end of these cantilevers, the insulating coating was removed by focused ion beam milling, resulting in a defined electrode area at the cantilever apex. This free area is the essential part of the gripper since in this electrochemically active region, the adhesion can be switched on or off by applying a highly attractive or repulsive potential. Figure 3.4a shows an SEM image of the free electrode area of a microgripper produced in this work. To find a suitable substrate to manipulate on, the adhesion of colloidal particles on these substrates was measured by the so-called colloidal probe technique. For these measurements,  $\mu\text{m}$ -sized colloidal silica particles of the same sort that was later used for manipulation were glued onto the cantilever. The substrates examined in this work ranged from bare glass to different modified glass substrates. Modification has been carried out by chemical vapor deposition with varying densities of coverage of hydrophobic alkylsilanes. Afterwards, potential dependent force-curves were acquired with an electrochemical gripper against a particle glued to a substrate (cf figure 3.4b) to study the adhesion forces between the electrochemical gripper and the colloidal beads.

### 3. Synopsis

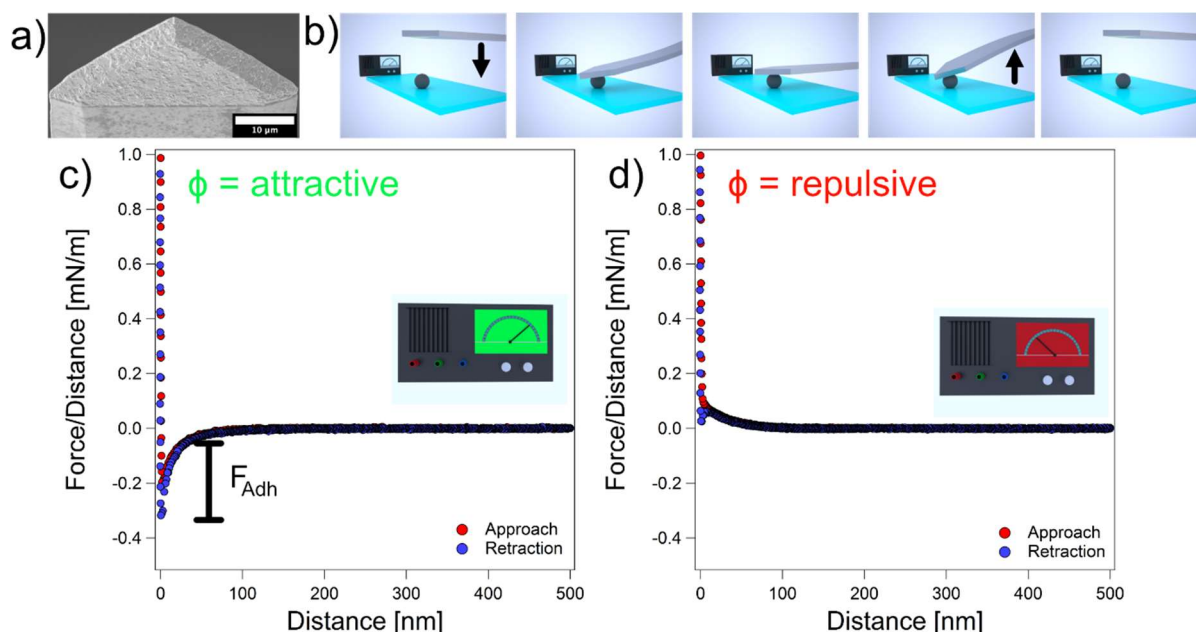


Figure 3.4: Potential dependent force-distance measurements of an electrochemical gripper produced in this work against a fixed colloidal particle. a) SEM-image showing the active electrode surface of an electrochemical gripper. b) Schematic illustrating the measurement. c) Force-distance curve while applying an attractive potential, showing attractive adhesion forces. d) Force-distance curve for repulsive applied potentials, showing only repulsive electrostatic forces.

The resulting adhesion forces for highly positive (+726 mV, attractive = grip, force curve cf. figure 3.4c) and negative (-474 mV, repulsive = release, force curve cf. 3.4d) applied potentials, which are later used for the grip- and release, were in the same order of magnitude as the adhesion forces between a particle and either a bare glass substrate or the silane-modified glass with the lowest examined packing density. As a result, these substrates were used for manipulation experiments. To follow the manipulation process easily under a light microscope, identical μm-sized silica particles were used for manipulation experiments. The pick-up probability of an electrochemical gripper with attractive applied potential was determined by measuring force-distance curves against silica particles sedimented on a silane-modified surface, where roughly 20% of the “pick-up”-experiments were successful. For a bare glass surface, practically all of the pick-up experiments succeeded. Figure 3.5a-d shows a “pick and place” – manipulation experiment schematically. To prove the capability of the electrogrippers, the silica particles were arranged into complex structures through several subsequent “grip” and “release” sequences. Namely, the words “AFM”(cf

figure 3.5e), the main technique used for manipulation, and “PC II” (cf. figure 3.5f), the chair the experiments were conducted in, were written by arranging these particles.

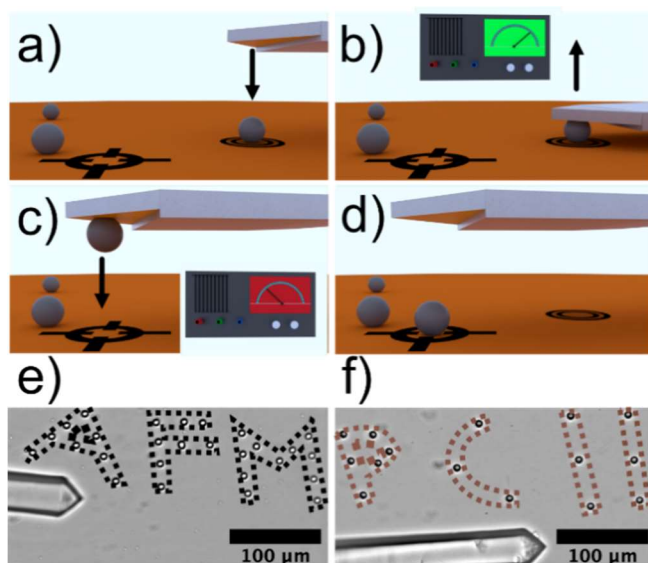


Figure 3.5: Overview of “pick and place” experiments with the electrochemical grippers developed in this work. a) Approach of an electrochemical gripper onto a colloidal particle while applying attractive potential. b) Due to the attractive potential, the particle sticks to the cantilever and can be manipulated in the  $xy$ -axis. c) Approach on the “place” location while applying repulsive potential after getting in contact with the surface. d) Due to the repulsive potential, the colloid stays in place on the substrate. e) Silica particles arranged into the word “AFM” on a glass surface. f) Silica particles arranged into the structure “PC II”, the chair this work was conducted in, on a silane-modified surface.

Additionally, the effective diffuse layer potential of the electrochemical grippers was determined as a function of the applied potential and compared with the literature.

#### 3.2.3 An integrated, exchangeable three-electrode electrochemical setup for AFM-based scanning electrochemical microscopy

Scanning electron microscopy (SECM) is a widely used tool for detecting in a laterally resolved manner electrochemical properties on a sample<sup>4,7,22</sup>. When combined with atomic force microscopy (AFM), SECM allows the direct simultaneous acquisition of position-dependent local electrochemistry and physical sample properties like topography, elasticity, and adhesion with a lateral resolution in the nm-range<sup>23–27</sup>. The commercial availability<sup>28</sup> of AFM-SECM cantilevers facilitated new application fields for the AFM-SECM<sup>3,29–31</sup>. However, for an AFM-SECM experiment, an elaborate fluid

### 3. Synopsis

cell with a three-electrode setup is required, making the AFM-SECM setup more complicated.

Here, we present a novel approach to integrating the electrode setup into the cantilever, thereby reducing the complexity of an AFM-SECM experiment, allowing the measurement in conventional fluid cells or even liquid droplets while improving the handling. A schematic of a thus-described experiment is shown in figure 3.6a.

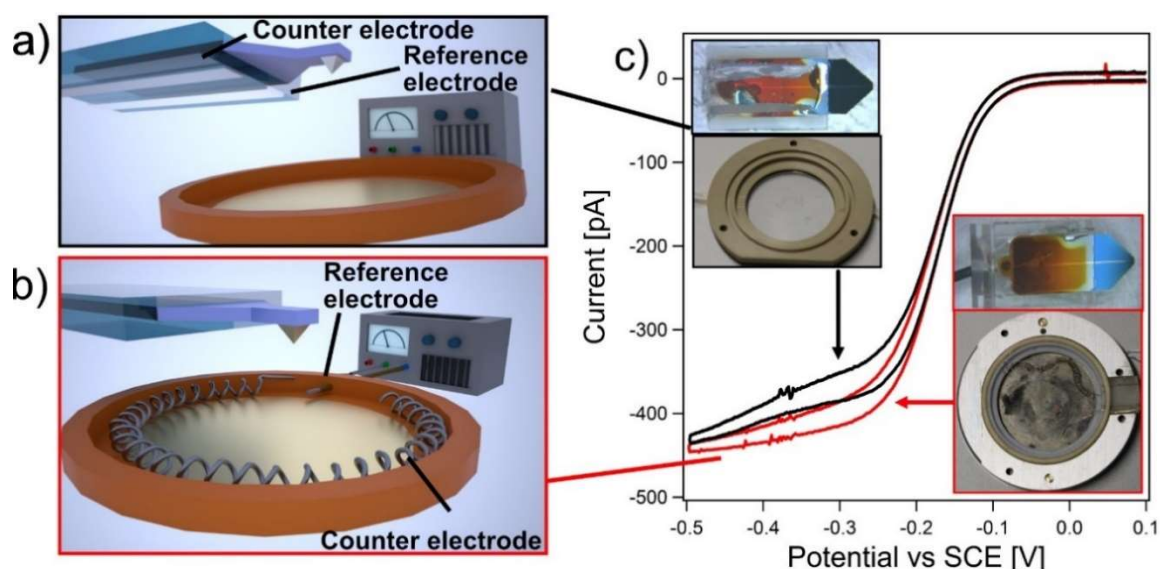


Figure 3.6: AFM-SECM setups used in this work a) Schematic of a 3-electrode setup integrated by screen-printing onto an AFM-SECM cantilever. b) Schematic of a traditional 3-electrode AFM-SECM setup with electrodes in the electrochemical cell. c) Cyclovoltammograms comparing the formerly mentioned setups, showing no significant difference in shape and current heights. Insets show photos of the used setups.

In a classical AFM-SECM setup, as shown in figure 3.6b, the cantilever tip acts as working electrode. By contrast, the rest of the electrode setup, consisting of a reference-electrode, typically an Ag/AgCl wire, and a counter electrode, e.g., a platinum wire or mesh, are integrated into the electrochemical fluid cell. A three-electrode setup has been integrated into a SECM cantilever. Paste electrodes were prepared on commercial AFM-SECM cantilevers by painting<sup>32</sup>. These electrodes were contacted and partially insulated as described elsewhere<sup>21</sup>.

To characterize the long-term stability of these screen-printed electrodes, cyclic voltammetry measurements were performed every 30 minutes for 3 hours using an analogous screen-printed electrode setup on a glass slide with a commercial Pt-macro-electrode acting as working electrode. The resulting cyclovoltammogram did

### 3. Synopsis

show the sigmoidal shape expected for a microelectrode and did not change significantly over a time of three hours. Furthermore, we compared the electrochemical behavior of a cantilever with integrated electrodes to the same cantilever in a standard electrochemical cell by measuring cyclic voltammetry with the cantilever tip as work electrode, and either the integrated electrodes or the electrochemical cell with Ag/AgCl and Pt-wire, as work- and reference electrodes, respectively. No significant differences in the shape of half-wave potential of the cyclic voltammograms could be observed (cf. figure 3.6c). As a test system for an AFM-SECM experiment with these integrated cantilevers, we chose gold nanomeshes, whose production is described elsewhere<sup>33</sup>.

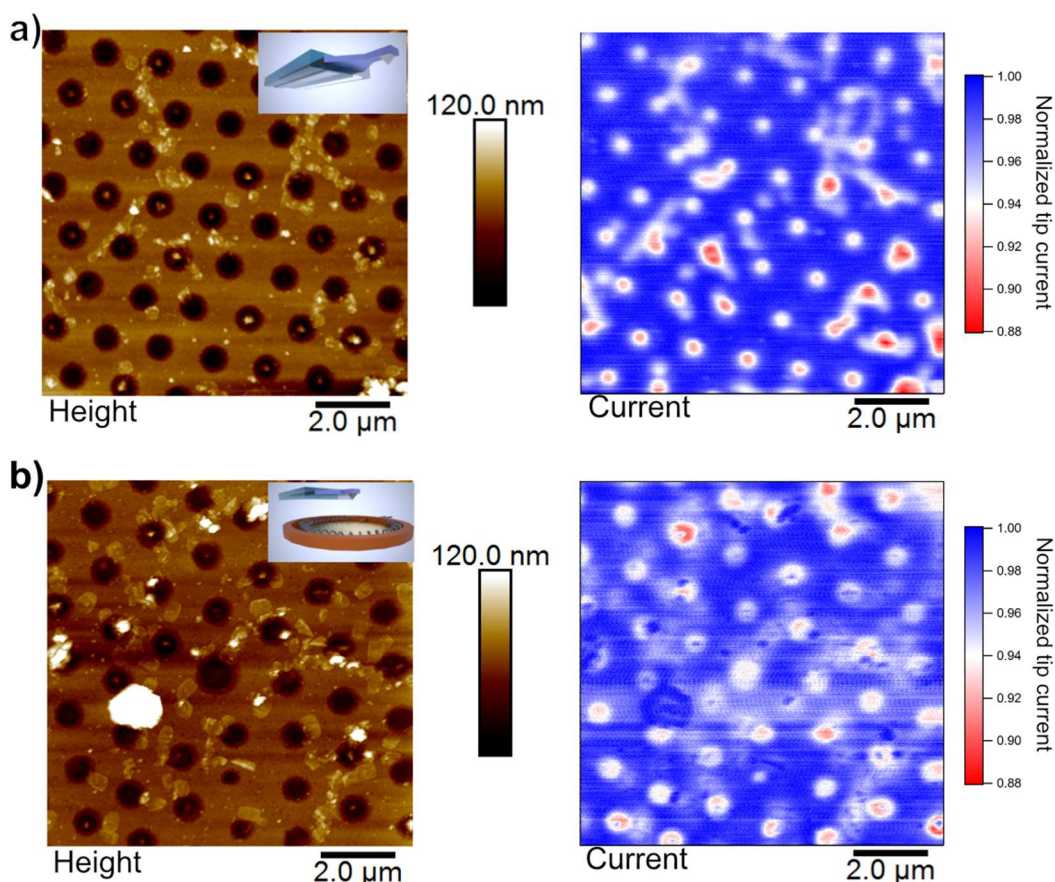


Figure 3.7: Topography and SECM-current images measured simultaneously on gold-nanomeshes for a) An integrated 3-electrode setup using a cantilever developed in this work. b) A traditional electrochemical AFM-SECM setup with electrodes in the electrochemical cell. Both show the same features, resolutions and similar currents.

Again, the integrated electrodes or the electrochemical cell's electrodes were connected as reference or counter electrode, while the cantilever tip always acted as working electrode. The gold nanomesh was connected as a second working electrode in a bipotentiostatic setup, allowing regeneration of the redox species near the gold

### 3. Synopsis

---

surface. As shown in figure 3.7, similar feedback and comparable currents were observed for both experiments, concluding that the integrated cantilever is a viable alternative to a standard electrochemical cell. This opens up further opportunities for AFM-SECM in easier handling, measurement in a smaller volume of test liquid, and no need for further wiring.

## 3.2 Individual Contributions to Joint Publications

In this thesis, the results of three scientific publications are presented. These publications result from collaborative research projects. Therefore, various authors participated in the experiments and the writing of these publications. The individual contributions have been as follows.

### **“A versatile and Simple Approach to Electrochemical Colloidal Probes for Direct Force Measurements”**

Andreas Karg, Tamino Rößler, Andreas Mark, Paul Markus, Tobias Lauster, Nicolas Helfricht, Georg Papastavrou\*

published in *Langmuir*, **2021**, 37 (46), 13537.

DOI: 10.1021/acs.langmuir.1c01557

---

I developed the production steps and prepared the electrochemical colloidal probes used in this work. Moreover, I performed the analytics and potential-dependent AFM force measurements, drew the schematics, and wrote a part of the manuscript.

Tamino Rößler prepared the PEDOT:PSS films and performed the corresponding AFM measurements on these films.

Dr. Andreas Mark assisted in developing the electrochemical colloidal probes and helped with AFM measurements.

Tobias Lauster developed the conductive glue used for the electrochemical colloidal probes.

Paul Markus helped with stability measurements of the electrochemical colloidal probes and lateral calibration.

Dr. Nicolas Helfricht was involved in scientific discussions and revised parts of the manuscript.

Prof. Dr. Georg Papastavrou supervised the project, was involved in scientific discussions, wrote a part of the manuscript, and revised the manuscript.

#### **“Electrochemical Grippers for Micro- and Nanorobotics: Manipulation by Tuning Surface Forces”**

Andreas Karg, Volodymyr Kuznetsov, Nicolas Helfricht, Markus Lippitz, Georg Papastavrou\*

published in *Scientific Reports*, **2023**, 13 (1), 7885.

DOI: 10.1038/s41598-023-33654-6

---

I prepared the fully insulated cantilevers, performed the cyclovoltammetric measurements and did the AFM measurements, performed the manipulation experiments, and evaluated the data. Furthermore, I drew the schematics and wrote parts of the manuscript.

Dr. Volodymyr Kuznetsov performed the initial experiments.

Dr. Nicolas Helfricht and Prof. Dr. Markus Lippitz were involved in scientific discussions and revised the manuscript

Prof. Dr. Georg Papastavrou supervised the project, was involved in scientific discussions, wrote a part of the manuscript, and revised the manuscript.

#### **“An integrated, exchangeable three-electrode electrochemical setup for AFM-based scanning electrochemical microscopy”**

Andreas Karg, Sebastian Gödrich, Philipp Dennstedt, Nicolas Helfricht, Markus Retsch, Georg Papastavrou\*

Published in *Sensors*, **2023**, 23 (11), 5228

DOI: 10.3390/s23115228

---

I produced the fully integrated cantilevers, performed the electrochemical analytics and SEM measurements, drew the schematics, and wrote a part of the manuscript.

Sebastian Gödrich helped with the initial screen-printing experiments.

Philipp Dennstedt helped with the experimental design of the measurement cells.

Dr. Nicolas Helfricht was involved in scientific discussions, wrote a part of the manuscript and revised the manuscript.

Prof. Dr. Markus Retsch supervised the production of the samples used for AFM-SECM measurements, participated in scientific discussions, and revised the manuscript.

Prof. Dr. Georg Papastavrou supervised the project, was involved in scientific discussions, wrote a part of the manuscript, and revised the manuscript.

## References

1. Knittel, P., Zhang, H., Kranz, C., Wallace, G. G. & Higgins, M. J. Probing the PEDOT:PSS/cell interface with conductive colloidal probe AFM-SECM. *Nanoscale* **8**, 4475-4481 (2016).
2. Daboss, S., Knittel, P., Nebel, C. E. & Kranz, C. Multifunctional Boron-Doped Diamond Colloidal AFM Probes. *Small* **1422**, 1902099-1902010 (2019).
3. Daboss, S., Lin, J., Godejohann, M. & Kranz, C. Redox Switchable Polydopamine-Modified AFM-SECM Probes: A Probe for Electrochemical Force Spectroscopy. *Anal. Chem.* **92**, 8404-8413 (2020).
4. Bard, A. J. & Mirkin, M. V. *Scanning Electrochemical Microscopy* (CRC Press, Boca Raton 2001).
5. Sun, P., Laforge, F. O. & Mirkin, M. V. Scanning electrochemical microscopy in the 21st century. *Phys. Chem. Chem. Phys.* **9**, 802-823 (2007).
6. Sun, T., Yu, Y., Zacher, B. J. & Mirkin, M. V. Scanning Electrochemical Microscopy of Individual Catalytic Nanoparticles. *Angew. Chem. Int. Ed.* **53**, 14120-14123 (2014).
7. Ventosa, E. & Schuhmann, W. Scanning electrochemical microscopy of Li-ion batteries. *Phys. Chem. Chem. Phys.* **17**, 28441-28450 (2015).
8. Butt, H.-J., Cappella, B. & Kappl, M. Force measurements with the atomic force microscope: Technique, interpretation and applications. *Surf. Sci. Rep.* **59**, 1-152 (2005).
9. Pericet-Camara, R., Papastavrou, G., Behrens, S. H. & Borkovec, M. Interaction between Charged Surfaces on the Poisson–Boltzmann Level: The Constant Regulation Approximation. *J. Phys. Chem. B* **108**, 19467-19475 (2004).
10. Behrens, S. H. & Grier, D. G. The charge of glass and silica surfaces. *J. Chem. Phys.* **115**, 6716-6721 (2001).
11. Behrens, S. H. & Borkovec, M. Electric double layer interaction of ionizable surfaces: Charge regulation for arbitrary potentials. *J. Chem. Phys.* **111**, 382-385 (1999).
12. Kuznetsov, V. & Papastavrou, G. Adhesion of Colloidal Particles on Modified Electrodes. *Langmuir* **28**, 16567-16579 (2012).
13. Sitti, M. Microscale and nanoscale robotic systems. *IEEE Robot. Autom. Mag.* **14**, 53-60 (2007).
14. Kim, S., Ratchford, D. C. & Li, X. Atomic Force Microscope Nanomanipulation with Simultaneous Visual Guidance. *ACS Nano* **3**, 2989-2994 (2009).
15. Mekid, S., Bashmal, S. & M Ouakad, H. Nanoscale manipulators: review of conceptual designs through recent patents. *Recent Patents on Nanotechnology* **10**, 44-58 (2016).
16. Dejeu, J., Bechelany, M., Rougeot, P., Philippe, L. & Gauthier, M. Adhesion control for micro- and nanomanipulation. *ACS Nano* **5**, 4648-4657 (2011).
17. Gauthier, M. et al. Analysis and specificities of adhesive forces between microscale and nanoscale. *IEEE Transactions on Automation Science and Engineering* **10**, 562-570 (2013).
18. Kim, S., Shafiei, F., Ratchford, D. & Li, X. Controlled AFM manipulation of small nanoparticles and assembly of hybrid nanostructures. *Nanotechnology* **22**, 115301 (2011).

19. Requicha, A. A. G. et al. Manipulation of nanoscale components with the AFM: principles and applications. **Proceedings of the 2001 1st IEEE Conference on Nanotechnology. IEEE-NANO 2001**, 81-86 (2001).
20. Ramachandran, T. R. et al. Direct and controlled manipulation of nanometer-sized particles using the non-contact atomic force microscope. *Nanotechnology* **9**, 237 (1998).
21. Karg, A. et al. A Versatile and Simple Approach to Electrochemical Colloidal Probes for Direct Force Measurements. *Langmuir* **37**, 13537-13547 (2021).
22. Bard, A. J., Fan, F. R. F., Kwak, J. & Lev, O. Scanning electrochemical microscopy. *Anal. Chem.* **61**, 132-138 (1989).
23. Wain, A. J., Pollard, A. J. & Richter, C. High-Resolution Electrochemical and Topographical Imaging Using Batch-Fabricated Cantilever Probes. *Anal. Chem.* **86**, 5143-5149 (2014).
24. Macpherson, J. V. & Unwin, P. R. Combined Scanning Electrochemical–Atomic Force Microscopy. *Anal. Chem.* **72**, 276-285 (2000).
25. Eifert, A., Mizaikoff, B. & Kranz, C. Advanced fabrication process for combined atomic force-scanning electrochemical microscopy (AFM-SECM) probes. *Micron* **68**, 27-35 (2015).
26. Abbou, J., Demaille, C., Druet, M. & Moiroux, J. Fabrication of Submicrometer-Sized Gold Electrodes of Controlled Geometry for Scanning Electrochemical-Atomic Force Microscopy. *Anal. Chem.* **74**, 6355-6363 (2002).
27. Jones, C. E., Macpherson, J. V., Barber, Z. H., Somekh, R. E. & Unwin, P. R. Simultaneous topographical and amperometric imaging of surfaces in air: towards a combined scanning force–scanning electrochemical microscope (SF–SECM). *Electrochem. com.* **1**, 55-60 (1999).
28. Nellist, M. R. et al. Atomic force microscopy with nanoelectrode tips for high resolution electrochemical, nanoadhesion and nanoelectrical imaging. *Nanotechnology* **28**, 095711 (2017).
29. Mahankali, K., Thangavel, N. K. & Reddy Arava, L. M. In Situ Electrochemical Mapping of Lithium–Sulfur Battery Interfaces Using AFM–SECM. *Nano Letters* **19**, 5229-5236 (2019).
30. Limani, N., Boudet, A., Blanchard, N., Jusselme, B. & Cornut, R. Local probe investigation of electrocatalytic activity. *Chemical Science* **12**, 71-98 (2021).
31. Shi, X., Qing, W., Marhaba, T. & Zhang, W. Atomic force microscopy - Scanning electrochemical microscopy (AFM-SECM) for nanoscale topographical and electrochemical characterization: Principles, applications and perspectives. *Electrochimica Acta* **332**, 135472 (2020).
32. Foster, C. W., Kadara, R. O. & Banks, C. E. in *Screen-printing electrochemical architectures* 13-23 (Springer, Heidelberg, Germany, 2016).
33. Stelling, C., Mark, A., Papastavrou, G. & Retsch, M. Showing particles their place: deterministic colloid immobilization by gold nanomeshes. *Nanoscale* **8**, 14556-14564 (2016).

# Manuscripts and Publications

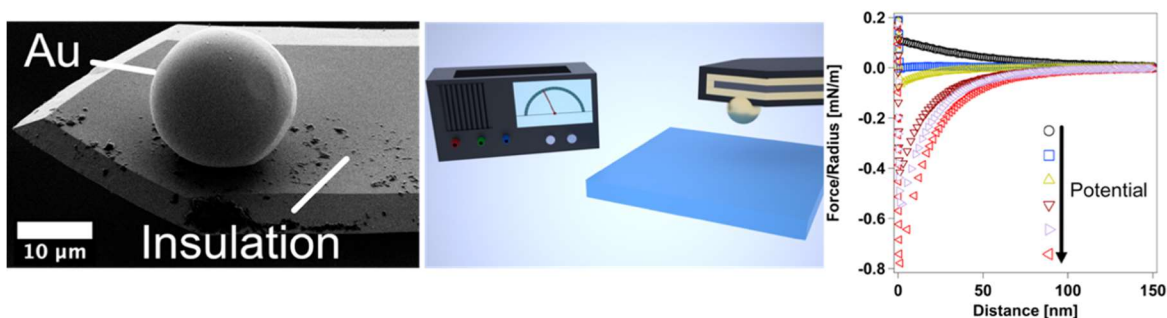
Chapters 4 - 6

## 4. A Versatile and Simple Approach to Electrochemical Colloidal Probes for Direct Force Measurements

Andreas Karg,<sup>1,2</sup> Tamino Rößler,<sup>1</sup> Andreas Mark,<sup>1</sup> Paul Markus,<sup>1</sup> Tobias Lauster,<sup>1</sup>  
Nicolas Helfricht,<sup>1</sup> Georg Papastavrou<sup>1,2\*</sup>

<sup>1</sup>Physical Chemistry II, University of Bayreuth, Universitätsstraße 30, 95447  
Bayreuth, Germany

<sup>2</sup>Bavarian Center for Battery Technology, Universitätsstraße 30, 95447 Bayreuth,  
Germany



Reprinted with permission from:

“A Versatile and Simple Approach to Electrochemical Colloidal Probes for Direct Force Measurements”, Andreas Karg, Tamino Rößler, Andreas Mark, Paul Markus, Tobias Lauster, Nicolas Helfricht, Georg Papastavrou\*, *Langmuir*, **2021**, 37 (46), 13537.

DOI: 10.1021/acs.langmuir.1c01557

© 2021, American Chemical Society

## 4. A Versatile and Simple Approach to Electrochemical Colloidal Probes for Direct Force Measurements

**Abstract:** *The colloidal probe technique, which is based on micrometer-sized colloidal particles that are attached to the end of a cantilever, revolutionized direct force measurements by atomic force microscopy (AFM). Its major advantages are a defined interaction geometry and a high force sensitivity. Here, we present a versatile and simple approach for preparing spherical electrodes in the micrometer range on an otherwise insulated AFM-cantilever. Thereby, it becomes possible to combine direct force measurements and potentiostatic control of the probe for various types of electrode materials. Two examples for the use of such electrochemical colloidal probes (eCP) are presented: Firstly, on soft, conductive films of poly(3,4-ethylenedioxythiophene) doped with polystyrene sulfonate (PEDOT:PSS) the adhesion behavior has been studied. The current through the contact area between probe and film remained constant until the jump-out of contact, indicating a constant geometrical contact area. Secondly, the long-range forces due to diffuse layer overlap between an eCP and a glass surface have been determined as function of the externally applied potential with a potentiostat. The resulting interaction force profiles are in good agreement with those calculated based on charge regulation and solutions of the full Poisson-Boltzmann equation.*

### Introduction

The study of electrode interfaces under *in-situ* conditions and on a local scale is of central importance for many application fields of electrochemistry such as batteries, fuel cells, electrocatalysis, and corrosion.<sup>1-6</sup> In particular, the combination of electrochemistry and atomic force microscopy allows to induce and monitor local electrochemical processes on a sub-micrometer scale and to image simultaneously surface topography as well as other sample properties, such as adhesion and elasticity.<sup>7-10</sup> Micropipette-based scanning electrochemical microscopy (SECM) has been implemented nearly half a century ago but it lacks the possibility for high-resolution imaging as well as the access to sample properties such as adhesion or elasticity. Unfortunately, AFM-based SECM remained an analytical niche technique as long as no suitable cantilevers with integrated electrochemical sensors were widely available. Recently, various approaches have been presented that lead to highly-defined and reproducible AFM-SECM cantilevers.<sup>11,12</sup>

#### 4. A Versatile and Simple Approach to Electrochemical Colloidal Probes for Direct Force Measurements

---

However, AFM is not only a technique that allows for acquiring surface topographies but it is also able to determine surface forces with pN resolution by direct force measurements.<sup>13</sup> In the past, direct force measurements under electrochemical control have been often based on the surface force apparatus (SFA). The SFA provides not only a defined interaction geometry but bears also large surfaces that can be directly converted to electrodes, which can be easily connected to a potentiostat.<sup>14–18</sup> However, defined interaction geometries can be also obtained for AFM by the so-called colloidal probe (CP) technique, where a micrometer-sized colloidal particle is attached to an AFM-cantilever.<sup>13,19–23</sup>

The combination of electrochemistry and direct force measurements by the colloidal probe technique has been reported previously.<sup>24–34</sup> However, in most cases only the sample has been potentiostatically controlled while a insulating colloidal particle, such as silica, has been used as probe.<sup>24–31</sup> However, the electrochemical control of a colloidal probe has been reported only recently.<sup>32–34</sup> Unfortunately, the preparation of these *electrochemical* colloidal probes (eCP) is rather complicated and makes use of instrumentation, namely focused ion beam (FIB) lithography that can only be accessed by few research groups. Here, we report a new approach for the preparation of eCPs. Our approach can be universally applied to micrometer-sized colloidal particles and requires 'standard' lab equipment only. The attached conductive particles are acting as electrodes and thus electrochemical probes. In order to characterize the probes, we performed besides cyclic voltammetry different AFM-based direct force measurements: Determining the adhesive properties on a conductive polymer layer and the long-range interaction forces as function of distance between a thiol-modified Au-eCP and an insulator surface due to diffuse layer overlap, respectively. The results of the latter experiments can be readily compared to measurements with an insulating CP against an electrode reported previously.<sup>28,31</sup>

## Experimental Section

No unexpected or unusually high safety hazards were encountered

**Materials.** All aqueous solutions were prepared from water of Milli-Q grade (resistivity  $> 18 \text{ M}\Omega \text{ cm}^{-1}$ , Merck Millipore, Darmstadt, Germany). The pH and ionic strength were adjusted by 1 M HCl (Titrisol, Merck, Darmstadt, Germany) to pH 4 and 0.1 mM. pH and ionic strength were verified with a pH meter (Metrohm 913, Metrohm, Filderstadt, Germany) and a conductometer (Metrohm 914, Metrohm, Filderstadt, Germany), respectively. 11-Mercapto-1-undecanol (97 %, Sigma Aldrich) was used for electrode modification. Solutions for cyclic voltammetric measurements were prepared from Potassium hexacyanoferrate(II) (99.95 %, Sigma Aldrich), Potassium hexacyanoferrate(III) (99.98 %, Sigma Aldrich) and potassium nitrate (99.7 %, abcr GmbH, Karlsruhe, Germany).

**Preparation of conductive glue.** An aqueous graphite dispersion (G303, Agar Scientific, Stansted, United Kingdom) was mixed with glycerol (99 %, Fisher Scientific) by a volume ratio of 2:1 and heated at 120 °C for 26 hours. Directly before application to the cantilever this solution is mixed in a ratio 4:1 (v/v) with a freshly prepared thermally curable two-component epoxy glue (Epo-Tek 377, Epoxy Technology Inc).

**Preparation of  $\mu\text{m}$ -sized gold particles.** Colloidal gold particles were produced by rapidly shortcircuiting two gold wires above a clean microscope glass slide positioned in a sealable glass vessel while applying an external voltage of 30 V with a power supply (TNG245, Voltcraft, Hirschau, Germany) and setting the current limiter to the maximum value. The particles originating from the evaporation in the spark have been collected on the glass slide. A similar procedure has been described previously.<sup>35</sup> The resulting particle size distribution is relatively broad ranging. We found particles in the size range of 2  $\mu\text{m}$  to 80  $\mu\text{m}$  by imaging with SEM (Hitachi TM 3030Plus).

**Preparation of Electrochemical Colloidal Probes (eCPs).** Tipless gold-coated cantilevers (CSC37, Cr/Au,  $\mu\text{masch}$ , Tallinn, Estonia) were cleaned in an air plasma (Zepto, Diener electronic, Ebhausen, Germany), and dipped in Ethanol (Analytical grade, Carl Roth GmbH & Co KG, Karlsruhe, Germany). Polystyrene beads with a nominal diameter of 20  $\mu\text{m}$  (Polybead, Polysciences Inc) were attached to the

#### 4. A Versatile and Simple Approach to Electrochemical Colloidal Probes for Direct Force Measurements

---

cantilever via micromanipulation using a tungsten wire under a dedicated optical microscope (Axio Examiner.D1, Zeiss, Oberkochen, Germany) with a micromanipulator (DC-3K, Märzhäuser, Wetzlar, Germany). Afterwards, the cantilevers were annealed at 200°C for 3 minutes in a reflow oven (Protoflow S, LKPF Laser & Electronics AG, Garbsen, Germany). In order to contact the cantilever, a silver wire insulated with PEI (Wire Diameter: 0.125 mm, Advent, Oxford, England) was connected to the cantilever's chip by means of conductive silver paint (G302, PLANO GmbH, Marburg, Germany). The silver paint contact has been insulated and mechanically stabilized with an UV-curable glue (NOA 63, Norland Optical Adhesives), which has been cured for 2 minutes with a UV lamp (Maxima 365 UV, Lohenstein, Stuttgart, Germany). An additional insulating resin (Red Insulating Varnish, GC Waldom) has been applied generously as further electrical insulation. It was dried at 80 °C for 30 minutes.

The primary electrical insulation of the cantilevers has been carried out by a cathodic electropaint (Clearclad HSR, Cleaclad Coatings Inc.), which was electrodeposited on the cantilever using a homebuilt electrochemical cell (2 electrode setup with a platinum mesh as counter electrode). We applied three times -3 V for 120 s. Between each deposition step, the cantilever was cleaned by immersing it three times into a beaker with Milli-Q water. Subsequently, the insulated cantilevers were annealed at 180°C for 1h.

The polystyrene particles acting as mask have been removed in a Tabletop-SEM (Hitachi TM 3030Plus) under low vacuum conditions without sputtering by means of a micromanipulator equipped with an etched tungsten wire as tip integrated in the SEM (MM3A-EM, Kleindiek Nanotechnik GmbH, Reutlingen, Germany). The SEM allowed in these experiments for a better control that the mask particle is indeed removed completely. In our opinion, the procedure can also be realized under optic control of light microscopy.

The freshly prepared conductive epoxy glue has been applied by means of an optical microscope (Examiner D1, Zeiss, Oberkochen, Germany) with a micromanipulator (DC-3K, Märzhäuser, Wetzlar, Germany). The amount of glue should be smaller than the dimensions of circular contact area in the insulation layer. This is directly followed by the application of a gold colloid using the micromanipulator. Afterwards, the colloidal probe cantilevers were cured at 180°C for 1h and cleaned with a UV/Ozone-

#### 4. A Versatile and Simple Approach to Electrochemical Colloidal Probes for Direct Force Measurements

---

cleaner (Model 18, Jelight Inc) for additional 10 minutes, followed by dipping in Milli-Q water and ethanol before the measurement.

The actual spring constants of the finished eCP-cantilevers have been calibrated by the thermal noise method according to Hutter-Bechhoefer.<sup>36</sup>

**Cyclic voltammetry.** Cyclic voltammetry measurements were done using a Chi750i (CH Instruments Inc) in aqueous solution of 5 mM Potassium hexacyanoferrate(II), 5mM Potassium hexacyanoferrate(III) and 0.1 M potassium nitrate. The scan rate was 40 mV/s for all data shown.

#### **Evaluation of the mechanical stability of the electrochemical colloidal probes.**

In order to address the mechanical stability of the eCPs, we performed experiments where a defined lateral force can be applied to the probe. These experiments have been implemented in a similar manner as reported by Kuznetsov and Papastavrou for sintered colloidal probes.<sup>30</sup> Shortly, the cantilever with the colloidal probe has been pressed towards the edge of a silicon in such a way that the probe particle is touching the side of the silicon wafer while the lever is situated above the edge of the substrate. By exerting a lateral force by moving the xy-scanner in direction of the silicon substrate, the cantilever bends in a torsional manner. Upon detachment of the probe the cantilever jumps back into the starting position. The linear relation between the movement of the scanner, the lateral photodetector signal and the applied force allows to extrapolate from the scanner positions at the moment of detachment the acting lateral force. Further details are given in the SI.

**Copper deposition on partially conductive cantilevers.** The insulated cantilever with a gold hole was cleaned with EtOH and Milli-Q water respectively. Afterward, copper was deposited electrochemically from an aqueous solution of 0.1 M H<sub>2</sub>SO<sub>4</sub> (99,99 %, Sigma Aldrich) and 10 mmol CuSO<sub>4</sub> (99 %, Grüssing GmbH, Filsum, Germany) by applying – 500 mV for 40 s using a potentiostat. The cantilevers were thoroughly rinsed with Milli-Q water and dried. All SEM-images and EDX measurements were done using a Zeiss LEO 1530.

**Preparation of PEDOT-PSS films.** Ultra-flat gold substrates were prepared with a modified template stripping method.<sup>37</sup> Here, gold was evaporated on a silicon wafer

#### 4. A Versatile and Simple Approach to Electrochemical Colloidal Probes for Direct Force Measurements

(CrysTec, Berlin, Germany) cleaned with a modified RCA-procedure<sup>38</sup>: First, the wafer was sonicated in a 2 vol-% solution of Hellmanex III (Hellma, Müllheim, Germany) in water for ten minutes at 40 °C. The wafer was then again sonicated in a solution of isopropanol 40 °C (99.7 %, Bernd Kraft GmbH, Duisburg, Germany) and Milli-Q water in a volumetric ratio of 3:1 for ten minutes at 40°C. The wafer was then placed in a mixture of Milli-Q water, hydrogen peroxide (30 % Fisher Chemical), and ammonia (25 % VWR chemicals) in a volumetric ratio of 5:1:1 for 20 minutes at 80 °C. On these cleaned wafers, a 100 nm layer gold (99,99%) was deposited via thermal evaporation. Hellmanex cleaned glass substrates were immobilized by means of an UV-curing adhesive (NOA63, Norland Adhesives) onto the gold. Before usage, the substrates were stripped off. They were treated with air plasma (Zepto, Diener electronic, Ebhausen, Germany) for five minutes. Thin films of PEDOT:PSS (0.1 wt%; CLEVIOS PH 1000; Heraeus, Hanau, Germany) on gold were prepared with spin-coating (100 µL; 90 s at 800 rpm and 2x 15 s at 2000 rpm and 15 min at 120 °C on a hot plate) from an aqueous dispersion of PEDOT:PSS. The film thickness after the spin coating has been verified by fixed-angle spectroscopic ellipsometry using a Cauchy fit (alpha-SE, J.A. Wollam). AFM images of the film were performed in Peakforce imaging mode on a Dimension Icon (Bruker Inc., Santa Barbara) equipped with a Nanoscope V Controller (Bruker Inc., Santa Barbara) with a OTESPA R3 cantilever with a nominal spring constant in the range of 26 – 57 N/m.

**Direct force measurements on PEDOT-PSS-films.** Direct force measurements in air were performed at a MFP-3D atomic force microscope (Asylum Research, Oxford Instruments, Abingdon, United Kingdom) with the colloidal probe AFM technique. Potential control was ensured by a potentiostat (PGU BI-1000, Jaisle Elektronik GmbH, Waiblingen, Germany). The eCP and the substrate were connected so that physical contact leads to a current flow. A potential of 100 mV was applied to the eCP. The recording of the currents was performed by the potentiostat and the ARC2 SPM controller (Asylum Research, Oxford Instruments plc, Abingdon, United Kingdom). The raw data of the direct force measurements was evaluated with a homemade Igor Pro procedure (WaveMetrics).

#### 4. A Versatile and Simple Approach to Electrochemical Colloidal Probes for Direct Force Measurements

---

**Direct force measurements under potentiostatic control of the eCP.** Gold eCPs were modified by means of a 5 mM ethanolic 11-Mercapto-1-undecanol solution in ethanol for 30 min and cleaned with pure ethanol.

Electrochemical colloidal probe cantilevers were connected to a MFP-3D in a 3-electrode electrochemical cell as the working electrode. A Pt-wire (diameter 0.125 mm, Alfa Aesar, Thermo Fisher Scientific) was connected as counter-electrode, a chlorinated silver wire (wire Diameter 0,25 mm, Advent, Oxford, England) was acting as a pseudo-reference electrode. The pseudo-reference was calibrated against a Baso saturated calomel electrode (RE2, BASi Inc) in an aqueous solution with ionic strength of 0.1 mM and pH 4.

The potential was applied by using a CH-750i potentiostat (CH Instruments). Direct force measurements in a nominal 0.1 mM electrolyte solution with pH 4 against RCA-cleaned glass substrates with external potential control were conducted. The actual ionic strength measured by the conductometer was 0.08 mM. The force vs. distance curves were evaluated using a homemade Igor Pro procedure. For the calculations of the theoretical force vs. distance curves, we used a regulation parameter  $p=0.67$  and an effective surface potential  $\phi=-13.4$  mV from the work of Pericet-Camara<sup>39</sup> for the glass surface. For the electrode surface we assumed a regulation parameter of  $p=0.6$  and used effective potentials from the work of Kuznetsov<sup>40</sup>. The ionic strength was fixed towards the actual ionic strength  $I=0.08$  mM. For the fitting of the effective potentials of the eCP, the same values were applied as fixed parameters, a fitting range of 15 nm – 60 nm was chosen while the potential of the eCP was the free fitting parameter.

## Results and Discussion

**Preparation of colloidal probes suitable for electrochemistry.** Figure 1 a) shows a scanning electron microscopy image (SEM) of an AFM-cantilever with an integrated electrochemical colloidal probe. To these electrochemical colloidal probes, we refer in the following as eCP. The gold colloidal particle acts as a microelectrode whose potential can be controlled by a potentiostat. For the here-prepared eCPs only the micrometer-sized particle at the apex of the cantilever represented an electrically conductive surface, while the rest of the cantilever was fully insulated. The debris on the SEM image resulted from the gluing procedure as well as from the fact that the cantilever has been used in an electrochemical experiment prior to imaging. Our approach to the preparation of eCPs is based on a masking technique: Shortly, a sacrificial organic particle has been placed on the cantilever before the cantilever was insulated by electrochemical deposition of a cathodic paint. Thereby, it was possible to prepare eCP cantilevers without the need for sophisticated instrumentation such as FIB. Figures 1b-g represent in a schematic manner the single steps of the preparation.

The electrochemical colloidal probes (eCPs) have been prepared on the base of conventional tipless cantilevers with a pre-coated layer of Cr/Au from both sides. Coating from both sides is advantageous in order to reduce thermal deflection by a type of bimorph-effect and allows here the deposition of an insulation layer on all sides of the cantilever. Figure 1h shows an optical microscopy image of such a cantilever before any further treatment (cf. schematic representation in Figure 1b). As first step (cf. Figure 1c) an electrical connection to the cantilever has been implemented by attaching an insulated silver wire to the Au-layer on the probe chip with high-quality silver paint. This electrical connection points have been mechanically 'stabilized' by an additional layer of an UV-curable glue (cf. Figure 1c). An additional insulating coating (cf. red paint in the optical microscopy image of Figure 1i) has been applied in the area where the wire has been attached in order to reduce any leak currents at points not directly accessible for the electro-paint. The next step (cf. Figure 1d) was the deposition of a sacrificial polystyrene bead with a nominal diameter of 20  $\mu\text{m}$  to the end of the cantilever by means of a micromanipulator. This particle served as a 'mask' during the electrochemical deposition of an insulation layer. In order to increase the contact area between bead and surface, the cantilever with bead has been heated

#### 4. A Versatile and Simple Approach to Electrochemical Colloidal Probes for Direct Force Measurements

up above the glass temperature of the PS bead (200° C for 3 min). A similar process has been proposed to increase the adhesive attachment of PS-beads in the preparation of ‘classical’ colloidal probes.<sup>41</sup> Then, the complete cantilever has been rendered insulating by coating the whole cantilever with a cathodic electro-paint (cf. Figure 1e). The electro-paint ‘ClearClad’ has well-known insulation properties for SECM-probes as well as STM-tips for electrochemical applications.<sup>42–44</sup> In order to promote a homogeneous distribution of the deposited electropaint, we introduced an additional annealing step at 180° C for 60 min.<sup>45</sup>

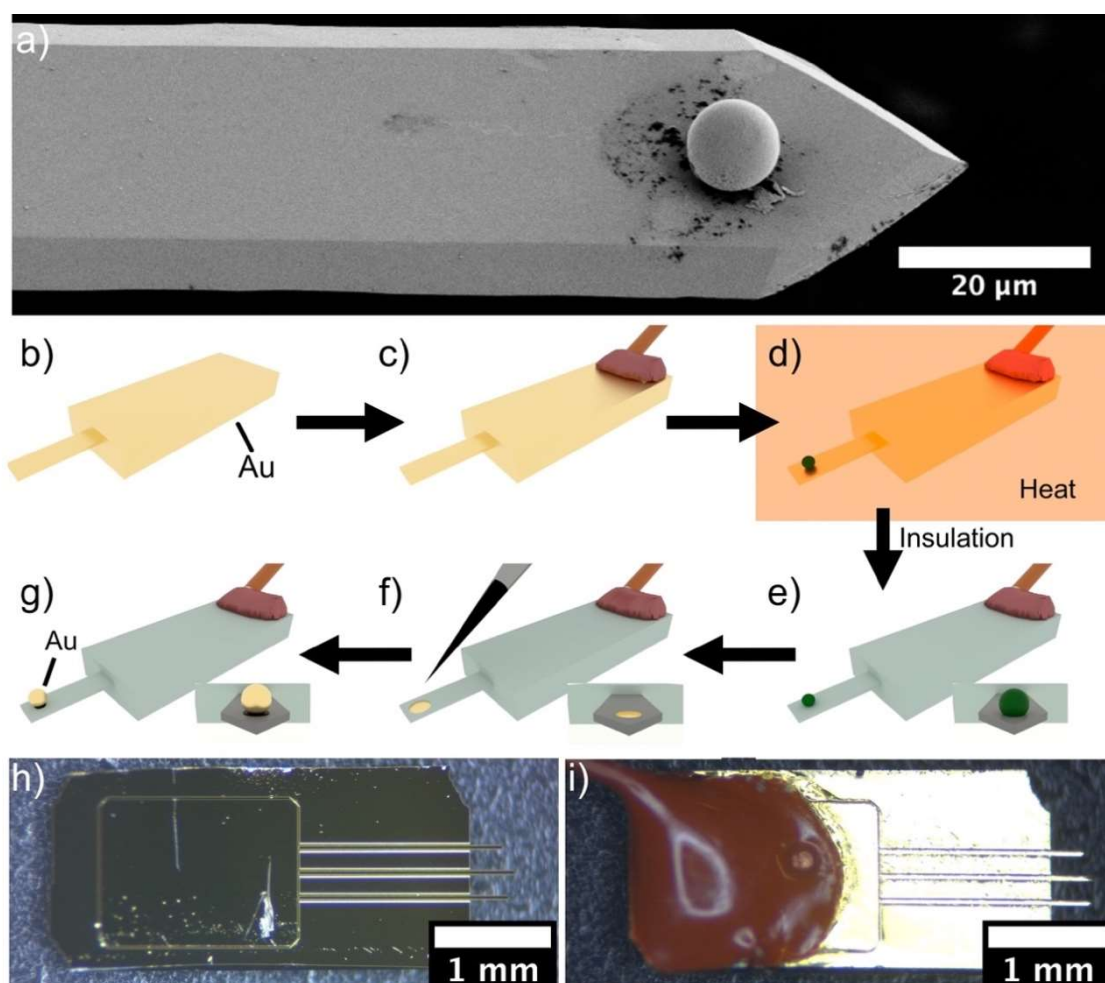


Figure 1. a) SEM image of an electrochemical colloidal probe (eCP). b-g) The preparation steps for the fabrication of eCPs. Light microscopy images of commercially available gold-coated cantilever, which represents the base for the preparation of eCP at the beginning the preparation (h) and the final eCP with the additional insulation at the contact point of the wire (i).

#### 4. A Versatile and Simple Approach to Electrochemical Colloidal Probes for Direct Force Measurements

Subsequently, the PS-bead, which acted as mask, has been removed from the cantilever by applying a lateral force with a dedicated micro-manipulator. In order to have a better control over this mechanical process, we used a micromanipulator placed in a SEM. However, it is also possible to perform this manipulation in a satisfactory manner by optical microscopy (cf. SI). The removal of the PS-bead has been observed in all cases as complete and left a hole in the insulation layer reaching down to the Au-layer (cf. Figure 1f). Thus, the cantilever can be considered already after this step as a flat circular  $\mu\text{m}$ -sized micro-electrode that could be addressed also electrochemically (see below). In order to prepare an electrochemical colloidal probe, we attached an additional spherical and conductive gold particle within this circular area that acts as electrode (cf. Figure 1g). The gold particles have been prepared by means of short-circuiting two gold wires and collecting the spherical particles that result from the evaporation in the spark and is thus applicable to practically all metals used for electrode materials. This colloidal particle has been immobilized by means of a home-made conductive glue that is based on a mixture of graphite and a commercial epoxy-glue (cf. experimental section). It is essential that this glue is applied only sparsely in order to minimize exposition of the gluing area in the electrochemical experiments. Here, we used Au-beads as  $\mu\text{m}$ -sized colloidal probes. These Au-beads have been obtained by evaporation from gold wires that have been short-circuited.<sup>35</sup> This method resulted in smooth, perfectly spherical Au-beads that are polydisperse but the dimensions can be selected under a microscope. After placing an Au-bead in the glue, the assembly has been cured at  $180^\circ\text{C}$  for 60 min (cf. Figure 1g). Figure 1i shows a light microscopy image of the final eCP assembly. The mechanical stability of the colloidal probes has been evaluated in an experiment, where defined lateral forces have been applied. By pressing the probe against a wedge structure and detecting the torsional deflection at which the detachment of probe particles takes place, the lateral force an eCP can sustain has been estimated. Details of the procedure are given in the SI and the experimental section. We could verify that a lateral force  $F_{detach}$  in the order of 3.5 mN was necessary in order to remove the Au-probe from an eCP (cf. SI). This force is much higher than forces commonly encountered in direct force measurements or even tribological studies. For comparison, the same type of experiments has been performed with 'standard' colloidal probes. For those probes a colloidal silica particle has been attached by

#### 4. A Versatile and Simple Approach to Electrochemical Colloidal Probes for Direct Force Measurements

---

means of a UV-curable glue. In this case an approximately 5× higher force has been necessary ( $F_{detach} = 16.0$  mN).

**Cyclic voltammetry.** The electrochemical behavior of microelectrode in general and of the eCP in particular can be directly examined by cyclic voltammetry. Figure 2 provides a summary of the various voltametric experiments performed on macroscopic electrodes and eCP cantilevers at different stages of preparation. All cyclic voltammograms (CVs) were obtained in a 5 mM solution of potassium hexacyanoferrate(II) and potassium hexacyanoferrate(III), respectively, with a background electrolyte concentration of 0.1 M potassium nitrate.<sup>46</sup> The scan rate was 40 mV/s for all data shown. Figure 2a shows the CV for a macroscopic electrode with an area of approximately 1 cm<sup>2</sup>. The electrode (cf. Figure 2a, red curve), has been prepared by the template stripped method, which results in an ultra-flat gold surface.<sup>37</sup> The macroscopic electrode has been contacted in an analogous manner as the cantilever (cf. Figure 1). We find pronounced oxidation and reduction peaks at 85 mV vs SCE and 350 mV vs SCE, respectively, which were clearly visible for the macroscopic electrode and correspond to the ones reported for this standard redox couple (120 mV and 330 mV vs SCE, respectively).<sup>47</sup> If such a macroscopic electrode has been insulated by the cathodic electro-paint, the current range shifts from the mA-range to the  $\mu$ A-range (cf. blue data vs. red data points in Figure 2a). This reduction by more than three orders of magnitude indicates that only a small number of defects were present in the insulation layer.

For an Au-coated cantilever without any insulation, the characteristic oxidation and reduction peaks were clearly visible and in their position comparable to the large flat electrode. However, these peaks were clearly reduced in magnitude as well as less pronounced, which we attribute to the smaller surface area of cantilever and chip, which we estimate to be 14 mm<sup>2</sup>. Also in this case, the electro-deposition of the insulation layer results in a drastic reduction of the current in the cyclic voltammetry experiments (cf. red vs blue data in Figure 2b). Figure 2c demonstrates that practically no leak-currents were detectable for a fully-insulated cantilever. The current is falling from high  $\mu$ A-range (not insulated) to the low nA-range when a complete insulation layer was present on the cantilever.

#### 4. A Versatile and Simple Approach to Electrochemical Colloidal Probes for Direct Force Measurements

---

Figure 2d shows finally the CVs for partially insulated cantilevers bearing microelectrodes, either of planar circular shape (i.e. directly after removal of the PS bead) or with spherical geometry (i.e. after attachment of a  $\mu\text{m}$ -sized Au-bead). The latter electrode geometry corresponds to the one of an eCP. As expected, the two different electrode geometries (black & green curve), resulted in significantly lower signals for the large electrodes. It also expected that the planar microelectrode (black curve) showed lower currents than the spherical microelectrode (green curve) due to the larger surface area and better diffusional transport. This behavior is in-line with the one expected for microelectrodes for planar and spherical shape, respectively.<sup>48,49</sup> The absence of pronounced reduction and oxidation peaks and their apparent shift in comparison to macroscopic electrodes, is as well expected for microelectrodes and in-line with the literature.<sup>48,49</sup> The same type of cyclic voltammograms as shown in Figure 4d) has been reported also for SECM-tips, which have an even smaller surface area.<sup>12</sup>

#### 4. A Versatile and Simple Approach to Electrochemical Colloidal Probes for Direct Force Measurements

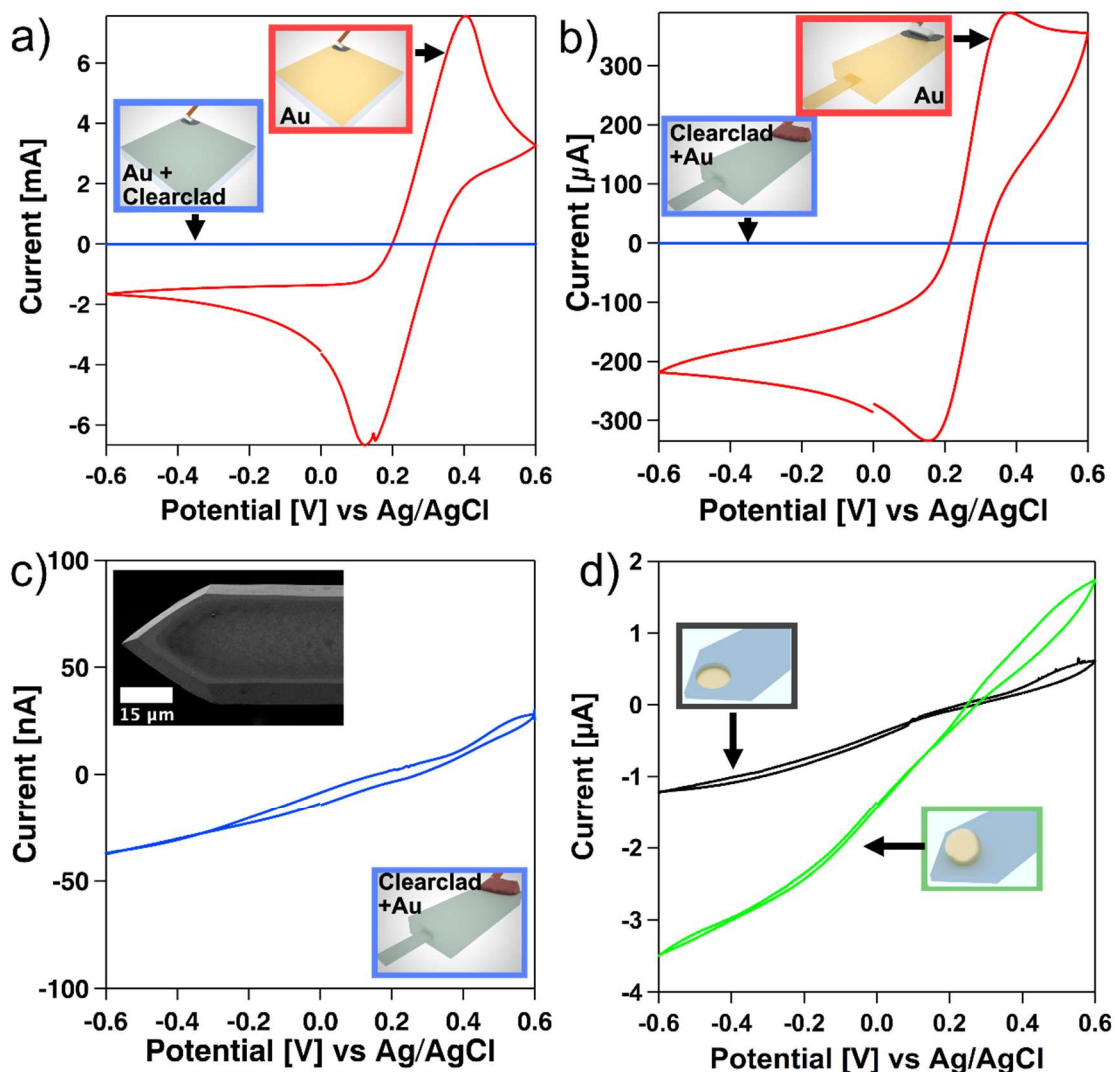


Figure 2. a) Cyclovoltammogram (CV) for an ultra-flat gold electrode (red) and an analogously prepared electrode that is completely covered with the same insulating electro-paint as used for the probes (blue), respectively. b) CV of gold-coated cantilever before deposition of electro-paint (red) and cantilever after complete insulation (blue), respectively. c) Differently scaled representation of data from b) for the fully insulated cantilever. d) CVs for insulated cantilever microelectrodes with circular hole in the insulation (black, cf. Figure 1f) and attached Au-particle (green, cf. Figure 1g), respectively.

**Analysis by electron microscopy and electrodeposition of copper.** Scanning electron microscopy (SEM) provides further insight in the state of the electrochemically active areas of the eCPs. The corresponding results are summarized in Figure 3. Figure 3a shows some representative gold particles, which have been produced by thermal evaporation (more examples are given in the SI).<sup>35</sup> By short-circuiting two gold wires the gold melts in the spark and forms perfectly spherical beads due to surface tension. The resulting beads are relatively polydisperse with dimensions in the  $\mu$ m-

#### 4. A Versatile and Simple Approach to Electrochemical Colloidal Probes for Direct Force Measurements

range. Thus, the possible size range for choosing the probe particles is large and the dimensions of the probe particles can be easily adapted for intended applications. Figure 3b shows an SEM-image of a PS-bead thermally attached to a tipless cantilever. This particle was acting as mask during the insulation procedure (cf. preparation step in Figure 1e). The pronounced neck particle and cantilever is caused by heating it above the glass transition temperature.<sup>41,50</sup> Figure 3c shows a cantilever with an insulation and after removal of the masking PS particle (cf. preparation step in Figure 1f). However, the probe particle has not yet been deposited. The area where the Au-coating of the cantilever has been masked by a PS-particle during insulation deposition can be clearly identified. The structures on the left and bottom of the hole in the film are present in the insulation layer only.

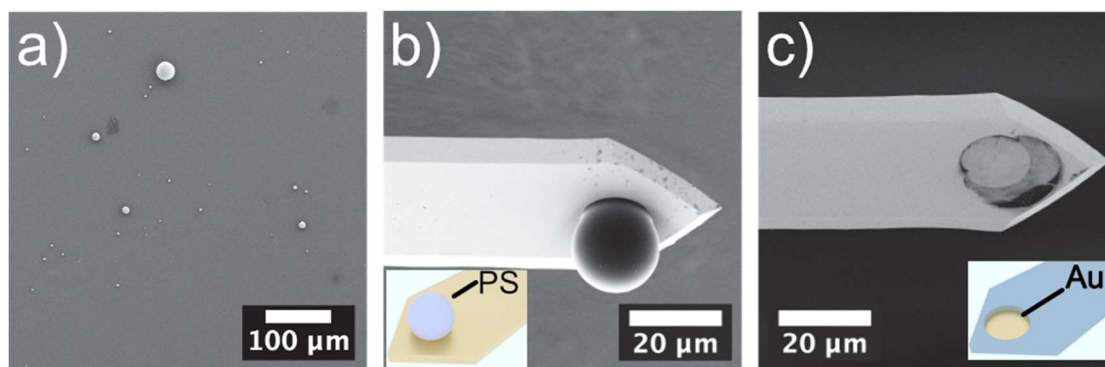


Figure 3. a) SEM image of representative gold particles obtained by thermal evaporation b) SEM image of sacrificial PS-bead attached to tipless gold cantilever before deposition of insulation electropaint. c) Hole in the insulated cantilever after removal of PS-bead.

In order to demonstrate further that the masking by the PS-particle did lead to a well-defined hole in the insulation layer, we performed electrodeposition of copper on partially prepared eCP-cantilever with a planar whole (cf. Figure 3c). Copper deposition on noble metal electrodes represents a classical test for an electrochemical setup.<sup>51</sup> Here, we applied a potential of -0.5 V (vs. SCE) to the cantilever while a reference and counter electrode have been placed in a 10 mM solution of  $\text{CuSO}_4$  in 0.1 M  $\text{H}_2\text{SO}_4$ . Figure 4a shows an SEM image after copper deposition for 40 s. The SEM image clearly shows that Cu has been deposited only in the circular area that has been masked before by the PS-bead. Moreover, the Cu-distribution has been verified by element specific energy-dispersive x-ray spectroscopy (EDX). Also, for EDX the Cu signal could be detected only in the circular area that was left free of the

#### 4. A Versatile and Simple Approach to Electrochemical Colloidal Probes for Direct Force Measurements

insulating coating. It is important to point out that no indication of Cu can be found on the insulating film; thus, confirming its insulation properties. The Au-signal that is present in the EDX spectra results from the original Au-coating of the cantilever, which is not sufficiently shielded by the organic electro-paint. This finding together with the CV-data provides a clear indication that the coating renders the rest of the cantilever electrochemically inactive and no larger defects are present in the insulation. Figure 4e shows for comparison an EDX gold map of a finished eCP with a gold bead. Here, EDX corroborates that the chemical composition of the probe particle and the absence of contaminations.

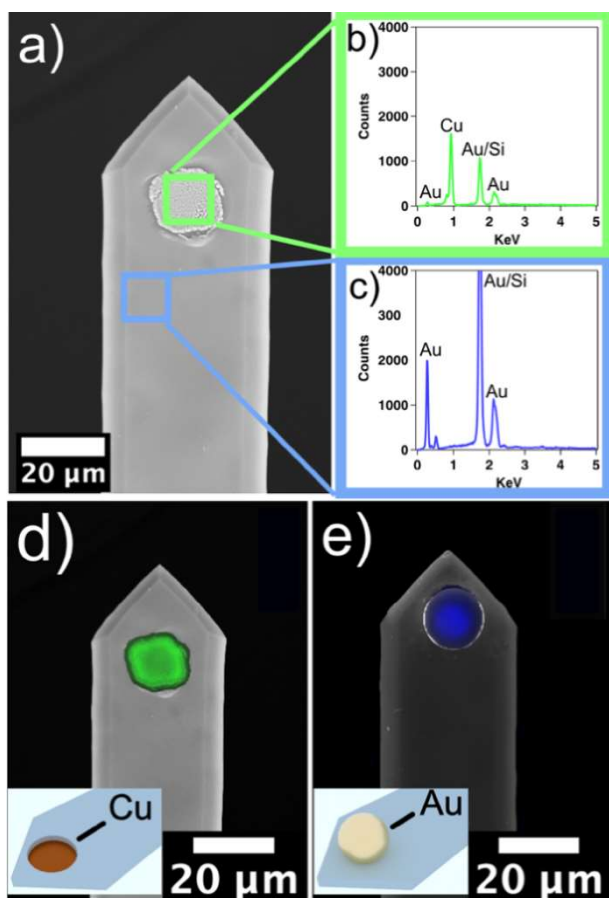


Figure 4. a) SEM image of Cu deposited in the non-insulated part of the cantilever after deposition of electro-paint and removal of the PS-particle. b, c) Corresponding EDX spectra for different parts of the cantilever. d) EDX map for Cu after Cu-deposition overlaid to the SEM image. e) EDX map for Au-signal for cantilever with contacted gold colloidal probe particle.

**Conductive measurements on PEDOT:PSS films.** Conductive AFM-cantilevers allow for probing the electrical properties of samples in a laterally resolved manner.<sup>52</sup> Direct force measurements with conductive AFM probes have been reported as well.<sup>53</sup>

#### 4. A Versatile and Simple Approach to Electrochemical Colloidal Probes for Direct Force Measurements

Conductive probes, either in form of sharp tips or colloidal probes, allow for simultaneous acquisition of interaction forces and electrical conductivity for adhesion or tribological experiments. Here, we probed a PEDOT:PSS-film with an eCP in a 2-electrode configuration under ambient conditions. PEDOT:PSS is widely used in organic electronics and as electrodes for organic solar cell technology.<sup>54, 55</sup> The PEDOT:PSS-film polymeric film has been deposited by spin coating on a gold substrate. We determined a thickness of ~100 nm by spectroscopic ellipsometry. Figure 5a demonstrates the smooth surface topography of the deposited film. Figure 5b shows a representative force-distance curve acquired with an eCP on the film. During the measurements, we applied an external potential of 100 mV between the two electrodes. Figure 5c shows the simultaneously acquired current between sample and eCP.

When the cantilever is far away from the surface; no current could be detected. Upon first contact between PEDOT:PSS-film and eCP, the current is increasing steadily until a plateau is reached at the maximum loading force of 7 nN. Subsequently, the piezo moves away from the surface, while the probe remains attached to the PEDOT:PSS-layer. Finally, the restoring force becomes so large that the probe separates with a jump-out of contact. The measured force corresponds to the so-called adhesion force. Exactly at the same moment the current drops instantaneously to zero, indicating the loss of contact. The PEDOT:PSS-layer is sufficiently soft in order to describe the indentation by the eCP probe in terms of the Johnson-Kendal-Roberts (JKR) theory, provided that no deep indentation is carried out and that the film behaves in a completely elastic manner. JKR-theory predicts a dependency of contact area, and thus the current, on the externally applied force and a finite contact radius upon separation.<sup>56</sup> The latter depends only on the surface forces and not on the previously applied indentation force. Due to the large forces acting between the eCP and the PEDOT:PSS film the photodetector signal for the deflection of the cantilever went into saturation during the retraction part of the force curve. The simultaneously acquired current increased upon initial contact but remains constant also upon reversal of the eCP. The jump-out of contact of the cantilever is in-line of JKR-type behavior and compatible with the presence surface forces in the contact area.<sup>21,56,57</sup> This interpretation is supported by sudden drop in the current taking place simultaneously and confirming an instantaneous separation of the two surfaces. However, variation

#### 4. A Versatile and Simple Approach to Electrochemical Colloidal Probes for Direct Force Measurements

---

of the maximum loading force did lead in all cases to an approximately constant current as long as the eCP remained in contact during the retraction part of the force curve. These data are shown in the SI. Hence, we assume that polymer remained attached to the surface of the eCP during the retraction, which would be not accounted for by the JKR theory and would be also compatible with plastic deformation in the contact area. Another explanation would be that the internal resistance of the probe (e.g. between particle and Au-coated cantilever) is much higher than the one between eCP and PEDOT:PSS film. We determined that the contact resistance between the eCP and a bare template-stripped gold surface was in the order of 2.1 k $\Omega$ . The high conductivity of PEDOT:PSS films has been verified additionally by macroscopic measurements but is nevertheless in the order of 100  $\Omega$  for a contact area several orders of magnitude larger than the one of eCP and film. Hence, it seems unlikely that constant current can be attributed to a high internal resistance of the eCP.

#### 4. A Versatile and Simple Approach to Electrochemical Colloidal Probes for Direct Force Measurements

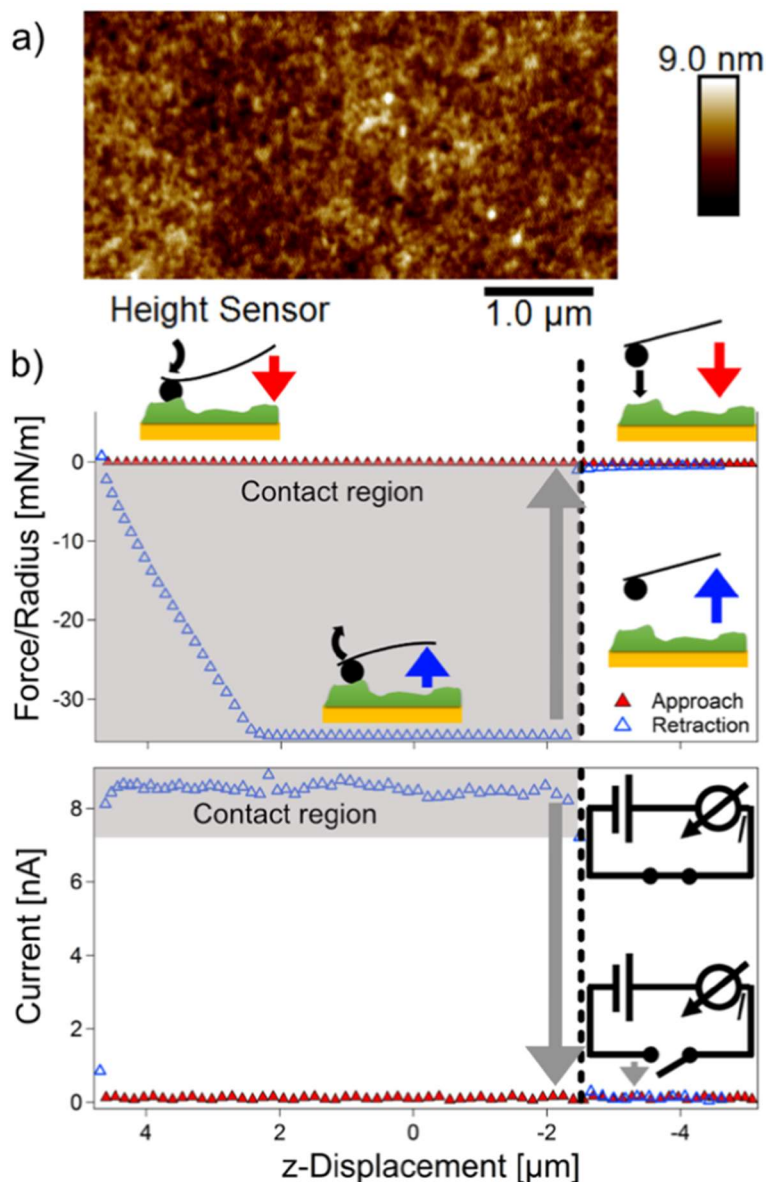


Figure 5. Adhesion measurements on PEDOT:PSS films with eCP. a) AFM- Peakforce image of PEDOT:PSS film. b) Force versus displacement curve upon approach and retraction of probe and simultaneously acquired data for the current. The contact region is highlighted in gray and jump-out of contact is indicated by an arrow.

**Direct force measurements in electrolyte solution.** Colloidal probes are ideally suited to determine interaction force profiles under highly-defined geometry by AFM.<sup>13,20,28,31,58,59</sup> eCPs allow to extend these capabilities to electrochemically controlled probes. In the past, such measurements have been mostly performed by the electrochemical surface force apparatus.<sup>14–18</sup> However, eCPs would allow for more flexibility in terms of the substrates involved, especially for asymmetric surface combinations or heterogeneous samples while still a defined interaction geometry

#### 4. A Versatile and Simple Approach to Electrochemical Colloidal Probes for Direct Force Measurements

combined with high force sensitivity could be ensured. Here, we will demonstrate a first proof of concept by determining the long-range interaction forces between a potentiostatically controlled eCP against an insulator surface, namely a borosilicate glass surface. Figure 6a shows a schematic representation of the experimental setup. The same type of experimental setup has been used previously, albeit for macroscopic electrodes at the place of the glass sample.<sup>28,31,40</sup> It should be noted that the position of the electrodes is in a circular manner around the working electrode has been chosen to ensure a homogeneous field distribution at the low ionic strength conditions used for the direct force measurements. However, recent evaluation for the electrode position in *in-situ* electrochemical cells for transmission electron microscopy (TEM) indicate that the electrode position should have only a minor influence.<sup>60</sup>

Here, the gold eCP has been modified by a self-assembled monolayer (SAM) of thiols terminating in OH-groups. A similar combination of surfaces has been studied previously, albeit in a different configuration: a potentiostatically-controlled SAM-modified electrode versus a silica colloidal probe.<sup>28,40</sup> Figure 6b shows the long-range interaction forces upon approach as a function of the applied potential. The interaction forces were normalized to the effective radius in order to allow for comparison with the theoretical curves based on full solutions of the non-linear Poisson-Boltzmann equation including charge regulation.<sup>39,61,62</sup>

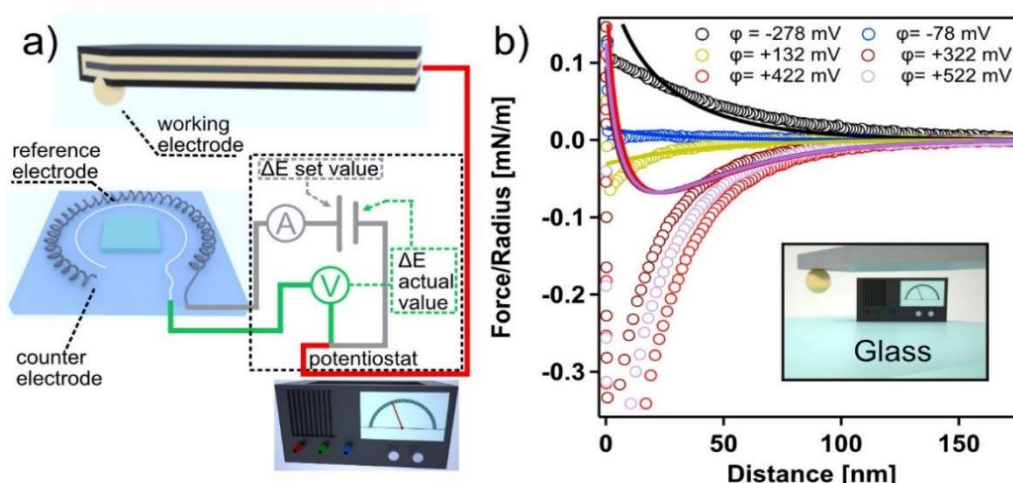


Figure 6. a) Schematic representation of the experimental setup for direct force measurements with eCPs. b) Averaged force profiles upon approach (eCP vs. glass) for different applied potentials.

#### 4. A Versatile and Simple Approach to Electrochemical Colloidal Probes for Direct Force Measurements

---

The force profiles shown in Figure 6b have been acquired at pH 4 and a nominal ionic strength of  $I=0.1$  mM. The actual ionic strength, as used in the quantitative evaluation of the experiments, has been determined additionally by conductivity measurements ( $I = 0.08$  mM). The potential  $\varphi$  applied to the eCP range from  $-278$  mV to  $+522$  mV vs. SCE. For low ionic strengths in the order of 1 mM, the interaction forces at large separations are dominated completely by the overlap of the diffuse layers and can be detected for separation distances of more than 100 nm. Figure 6b demonstrate that the interaction forces between the eCP and the glass surface depend critically on the external potential applied to the eCP. Glass shows a negative surface charge in an electrolyte solution of this pH-range.<sup>39,63</sup> In the following, assume a constant value of  $\psi = -13.4$  mV for the glass surface, which is in-line with various reports in the literature.<sup>39,63</sup> Thus, if highly negative potentials are applied to the eCP, a repulsive behavior due to double-layer repulsion is expected, while for highly positive applied potentials to the eCP an attractive interaction is expected. Figure 6b corroborates this expected behavior. The transition between repulsive and attractive interaction falls in the region of the potential of zero charge ( $pzc$ ) of the eCP. The  $pzc$  corresponds to the potential where the OH-modified eCP is practically non-charged. For comparable flat Au-electrodes with an OH-SAM under nearly identical conditions (pH 4.7 and  $I=0.12$  mM, here: pH 4.0 and  $I=0.08$  mM),<sup>40</sup> we reported a similar  $pzc$  as observed here as shown in Table 1, which will be discussed in more detail below.

#### 4. A Versatile and Simple Approach to Electrochemical Colloidal Probes for Direct Force Measurements

**Table 1.** Diffuse layer potentials from fits to experimental data and theoretical calculations as function of externally applied potentials.<sup>a</sup>

<i>Applied potential</i> $\phi$ (vs. SCE) [mV]	<i>Fitted diffuse layer potential</i> $\psi_{exp}$ [mV]	<i>Diffuse layer potential from literature</i> <sup>b</sup> $\psi_{Lit}$ [mV]
-278	-39	-40
-178	-3	-2
+132	+11	+37
+322	+75	+74
+422	+78	+93
+522	+84	+112

<sup>a</sup> Parameters fixed for the fitting procedure:  $\psi = -13.4$  mV and  $p = 0.67$  for the glass surface (in analogy to SiO<sub>2</sub> according to ref.<sup>39</sup>) and  $p = 0.6$  for the OH-terminated electrode (cf. ref.<sup>28</sup>)

<sup>b</sup> Reported values of the diffuse layer potential for flat electrode according to ref.<sup>40</sup>

In order to provide a more quantitative evaluation, we fitted the experimental force profiles to the full-solutions of the non-linear Poisson-Boltzmann (PB) equation including charge regulation.<sup>39,61,62</sup> Charge regulation has been accounted for by means of the constant regulation approximation that allows to summarize the charge regulation behavior by the so-called regulation parameter  $p$ .<sup>61</sup> We assumed here  $p = 0.6$  for the OH-terminated electrode. This value is based on direct force measurements on a flat OH-terminated Au electrode reported previously.<sup>28</sup> These measurements have been performed under similar electrolyte conditions of pH 4.7 and  $I = 1.2$  mM (in comparison here pH 4.0 and  $I = 0.08$  mM).<sup>31</sup> The diffuse layer potential  $\psi = -13.4$  mV and the regulation parameter  $p = 0.67$  for the glass surface have been approximated by the values for a silica substrate ( $p = 0.67$ ).<sup>39, 64</sup> Table 1 compares

## 4. A Versatile and Simple Approach to Electrochemical Colloidal Probes for Direct Force Measurements

diffuse layer potentials  $\psi_{exp}$  obtained from the fits of the interaction between an OH-terminated eCP (namely  $\psi_{exp}$ ) and a glass surface with previously reported values (namely  $\psi_{Lit}$ ) for interaction of a flat OH-terminated electrode and a silica colloidal probe under nearly identical conditions.<sup>40</sup> Despite the many approximations in the fitting procedure a surprisingly good agreement is found for a large range of potentials, in particular around the  $pzc$  (for an additional representation we refer to the SI). The significant deviations at very high applied positive potentials, especially at small separation distances, can be attributed to two factors: Firstly, the regulation parameter has been regarded as fixed in the fitting process as constant. In how far this approximation is valid has been to the best of our knowledge not been studied previously. Comparable regulation parameters (*i.e.*  $p=0.6$  and  $p=0.67$ ) for both surface would lead in the calculations a pronounced regulation behavior at small separations that might be not present in the physical reality. Moreover, hydrodynamic effects due to large attractive force and a small spring constant for eCP would render the data at small separation distances less reliable as the assumption of quasi-static deflection would be not only fulfilled under these conditions.<sup>39</sup>

### Conclusion

Direct force measurements by AFM have been largely profited from the versatility and defined interaction geometry of the colloidal probe technique. Here, we present a new approach that allows to extend the colloidal probe technique into the electrochemical domain. The preparation is versatile and allows for a vast selection of electrochemically active colloidal particles as probes. Moreover, the here-presented preparation technique does not require any special equipment besides a dedicated micromanipulation setup. The preparation of the colloidal particles allows for a large size range of probes (2– 80  $\mu\text{m}$ ). Due to the polydispersity resulting from the evaporation process in the spark a diameter suitable for the application can be chosen readily. Moreover, the size of the PS-particles as mask can be adapted accordingly in order to minimize the exposure of glue to the solution. Moreover, evaporation in the spark is a universal process that can be utilized for practically all metals suitable as electrodes, such as silver, platinum, or copper. Hence, eCPs can be also prepared from other metals.

#### 4. A Versatile and Simple Approach to Electrochemical Colloidal Probes for Direct Force Measurements

---

Colloidal probes under electrochemical control are of potential interest for various research fields, such as long-range interactions, adhesion science or tribology. The various recent implementations of SFA setups with electrochemical capabilities demonstrate impressively the need for direct force measurements under potentiostatic control.<sup>14–18</sup> In particular, the eCP combines the versatility of the CP-technique with electrochemistry. Hence, in difference to the SFA, one is relatively free in terms of the sample, which can be either under open circuit conditions, a second electrode under bi-potentiostatic control or an insulating surface. The eCPs might be also in the future of great interest for applications such as electrochemical impedance spectroscopy where ac-potentials are applied to the eCP. First tests in this respect have been promising. Most importantly, the eCPs are sufficiently stable to be used in electrochemically-controlled nanoindentation or tribology experiments. With these credentials, eCPs might of special interest in fields like battery research or bioelectronic applications.

#### **Acknowledgement**

The authors thank Samuel Rentsch, Volodymyr Kuznetsov, and Sebastian Gödrich for fruitful discussions and initial experiments that paved the way for this study. We thank the Keylab for electron microscopy of the Bavarian Polymer Institute. The generous gift of ClearClad by the company LHV Coatings is gratefully acknowledged.

## Supporting Information

### S1 Characterization of the Au-Particles by Scanning Electron Microscopy

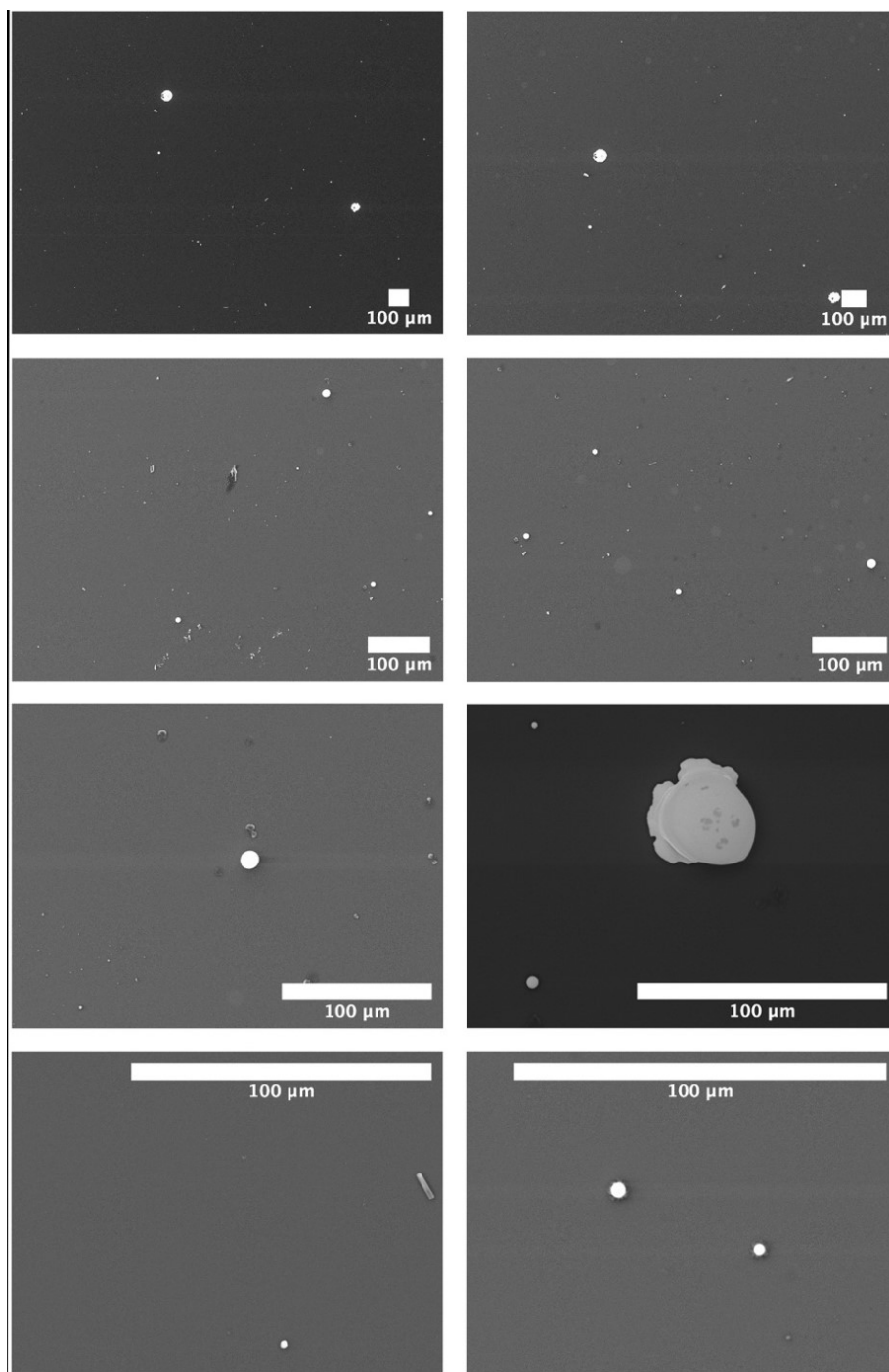


Figure S1-1: Scanning electron microscopy images of gold colloidal particles obtained by short-circuiting two gold wires and collecting the gold evaporated in the spark on a clean glass substrate. Due to this process the size distribution is very broad. We could identify particles in the size range from approximately 2  $\mu\text{m}$  – 80  $\mu\text{m}$ .

#### 4. A Versatile and Simple Approach to Electrochemical Colloidal Probes for Direct Force Measurements

##### S2 Micromanipulation of Masking Particles by Light Microscopy

The data shown in the manuscript have been acquired with eCPs prepared with the help of a high-precision electrical micromanipulator (MM3A-EM, Kleindiek Nanotechnik GmbH, Reutlingen, Germany) integrated into a Tabletop SEM (Hitachi TM 3030Plus). However, the process of removing a colloidal PS-particle that is serving as mask during the deposition of an insulation layer can be performed also with sufficient accuracy with a mechanical micromanipulator (DC-3K, Märzhäuser, Wetzlar, Germany) under an optical light microscope (Axio Examiner.D1, Zeiss, Oberkochen, Germany). Figure S2-1 is illustrating the process of removing the particle that served as mask for both types of setups.

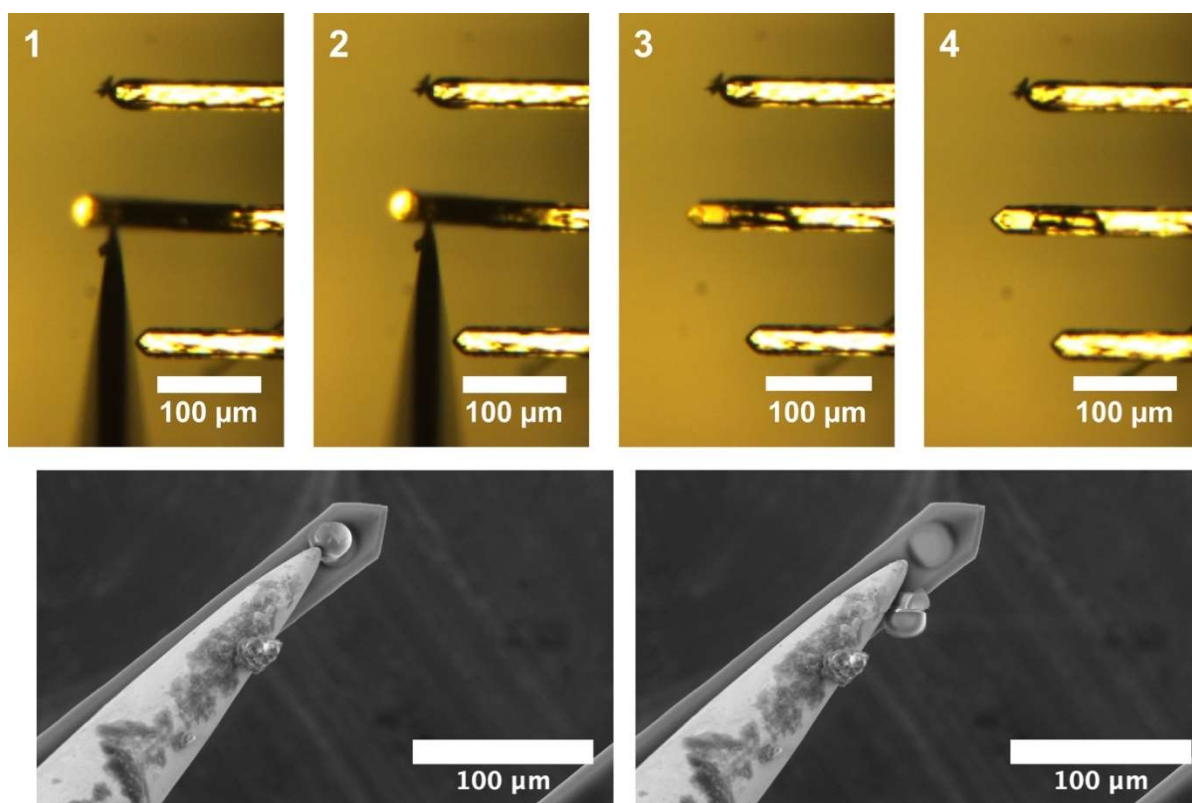


Figure S2-1: Top: The sequence of manipulation steps to remove the PS-particle from a cantilever after deposition of an insulation layer. The particle is removed with an etched Pt/Ir-wire. Bottom: For comparison the same process as observed within an electron microscope.

A movie showing the manipulation under a light microscope is available upon request

## 4. A Versatile and Simple Approach to Electrochemical Colloidal Probes for Direct Force Measurements

### S3 Mechanical Stability of the eCPs

The mechanical stability of the eCPs has been addressed here by means of the application of lateral forces similar to experiments reported for colloidal probes obtained by sintering.<sup>1</sup> In order to apply sufficiently large lateral shear forces we utilized a structure with a sharp edge (cf Fig S3-1).

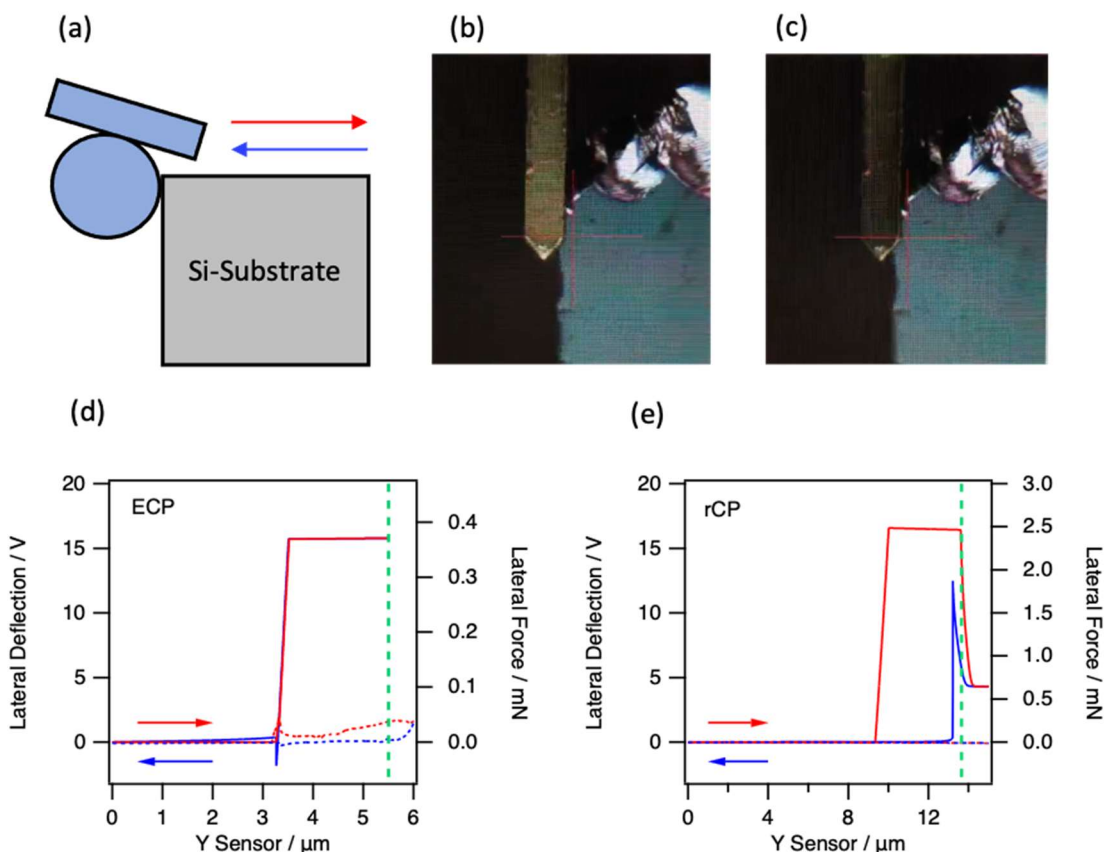


Figure S3-1: (a) Schematic representation for the setup to determine the lateral forces required to remove the colloidal particle from a colloidal probe assembly. (b) Light microscope image of an insulated cantilever with an eCP near the edge of a Si-substrate. (c) Light microscope image for the same probe while a lateral force is exerted. The torsion of the cantilever is directly visible by optical microscopy. (d) Lateral deflection signal for a typical lateral force experiment with an eCP. The solid lines correspond to the lateral deflection of a cantilever with an attached eCP, while for the dashed lines the probe particle disconnected due to the shear forces. (e) The same experiment for a 'conventional' colloidal probe (CP). Here a colloidal silica particle as been attached by UV-curable glue.

#### 4. A Versatile and Simple Approach to Electrochemical Colloidal Probes for Direct Force Measurements

In order to provide a quantitative estimation of the lateral force acting on the colloidal probe, the lateral force measurements had to be calibrated. First, the simple harmonic oscillator (SHO) model has been fit to the resonant frequencies for both thermal noise spectra (vertical and, torsional) <sup>65–67</sup>. Based on the calibration method of Sader et al., we retrieved the vertical  $k_{z, Sader}$  and, the torsional force constant  $k_{\phi, Sader}$ . The lateral spring constant  $k_{lat, Sader}$  has been calculated from  $k_{\phi, Sader}$  based on the CP dimensions according to Cannara et al.<sup>5</sup> The spring constants for an isolated cantilever with an eCP and a ‘regular’ colloidal probe (rCP) are summarized in Table S3-1.

**Table S3-1:** Cantilever spring constants and detachment forces.

Colloidal Probe	$k_{z, Sader}$ [N/m]	$k_{\phi, Sader}$ [nN/m]	$k_{lat, Sader}$ [N/m]	$F_{detach}$ [mN]
CP	0.08	0.73	3.77	16.0
ECP	0.21	0.52	1.62	3.5

Figures S6-1 d,e) show lateral the lateral force loops for eCP and rCP acquired at a velocity of 3  $\mu\text{m/s}$  in the case of attached (full lines) and removed colloidal particles (dashed lines), respectively. With attached probes, the lateral inverse optical lever sensitivity has been determined ( $InvOLS_{lat}$ ) while the lever twist with a torsional motion while being blocked in sliding over surface by the edge of the Si-substrate. We obtained values for  $InvOLS_{lat}$  of 39.8 nm/V and 14.5 nm/V for the rCP and the eCP, respectively. We attribute lower value for the latter to the reduction in reflection by the insulation coating. Further twist of the cantilever with for Y-travel larger than 2  $\mu\text{m}$  leads to saturation of the lateral signal for both probes. Thus, we cannot measure the actual detachment force but just determine the breaking point by means of the Y-travel at which it has been taken place (cf. dashed green lines in Figure S6-1d,e). However, reaching saturation values for the lateral force signals for eCP and eCP indicated already the robust adhesion of the eCPs to the cantilever.

Assuming, a linear deflection behavior also beyond the sensor saturation, we can estimate the detachment force of our CPs by linear extrapolation of the bending to the point where the lateral movement did lead to removal of the CP and thus a sudden drop in the lateral force signal. This point is indicated by the green dashed green lines

#### 4. A Versatile and Simple Approach to Electrochemical Colloidal Probes for Direct Force Measurements

---

in figures S5-1d) and e). By extrapolation, we calculated detachment forces of 16.0 and 3.5 mN for the rCP and ECP, respectively.

## 4. A Versatile and Simple Approach to Electrochemical Colloidal Probes for Direct Force Measurements

### S4 Current vs Applied Force for PEDOT:PSS Films

For the measurements on the PEDOT:PSS films, we applied an external potential between eCP and the electrode on which the film has been prepared. The measurements have been performed under ambient conditions. Figure S4-1 shows the current at maximum loading force. The latter quantity is expressed as 'setpoint' and measured in Volts. It corresponds to the trigger value at which the movement of the piezo-actuator. The relationship between setpoint and maximum force is linear. Thus, higher setpoint voltages correspond to higher applied forces. Figure S4-1 demonstrate that the maximum current through the contact area depends on the maximum external load. The linear relationship suggest by the guide through the eye is misleading as in absence of adhesive forces the relationship between contact radius  $a$  and applied force  $F$  is  $a^3 \propto F$ . Thus, we expect the current  $I_{max}$  to be proportional to the contact area  $I_{max} \propto a^2$  and thus  $I_{max} \propto F^{2/3}$ . Additional adhesive forces between probe and film lead to an offset for the contact area.

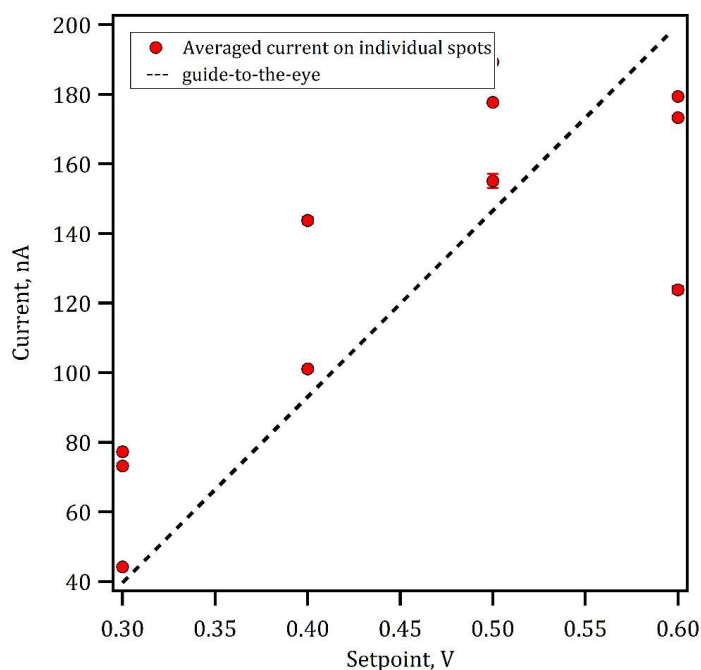


Figure S4-1: Current through the contact area for the maximum applied loading force as represented by the setpoint. The dashed line is only a guide to the eye and does not represent the envisaged functional dependence.

#### 4. A Versatile and Simple Approach to Electrochemical Colloidal Probes for Direct Force Measurements

While Figure S4-1 represents only the data for the current at maximum applied load, it is possible to record the current during a full force versus distance curve. Figure S4-2 shows a selection of data for different setpoints.

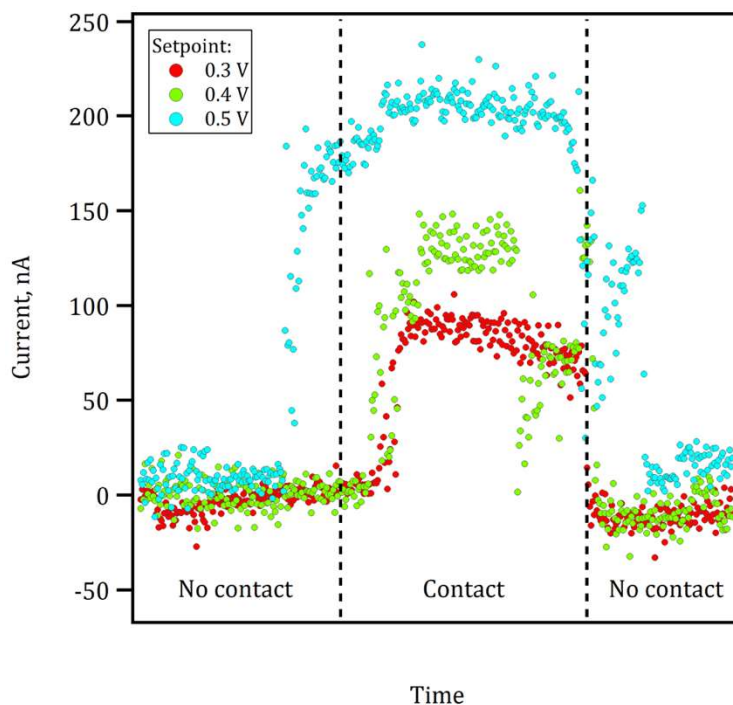


Figure S4-2: Current flow between eCP and PEDOT:PSS sample under ambient conditions. The data are shown as function of time during force versus distance cycles. Data sets of different colors indicate different setpoints. With increasing setpoint the maximum applied force increases.

#### 4. A Versatile and Simple Approach to Electrochemical Colloidal Probes for Direct Force Measurements

##### S5 Current Monitored during Direct Force Measurements

For the direct force measurements, the eCP was acting as working electrode, the current has been monitored while the direct force measurements have been performed. As the electrode has a surface modification by means of a self-assemble monolayer of OH-terminated thiols, the current serves as indicator that no desorption of the thiols has taken place.

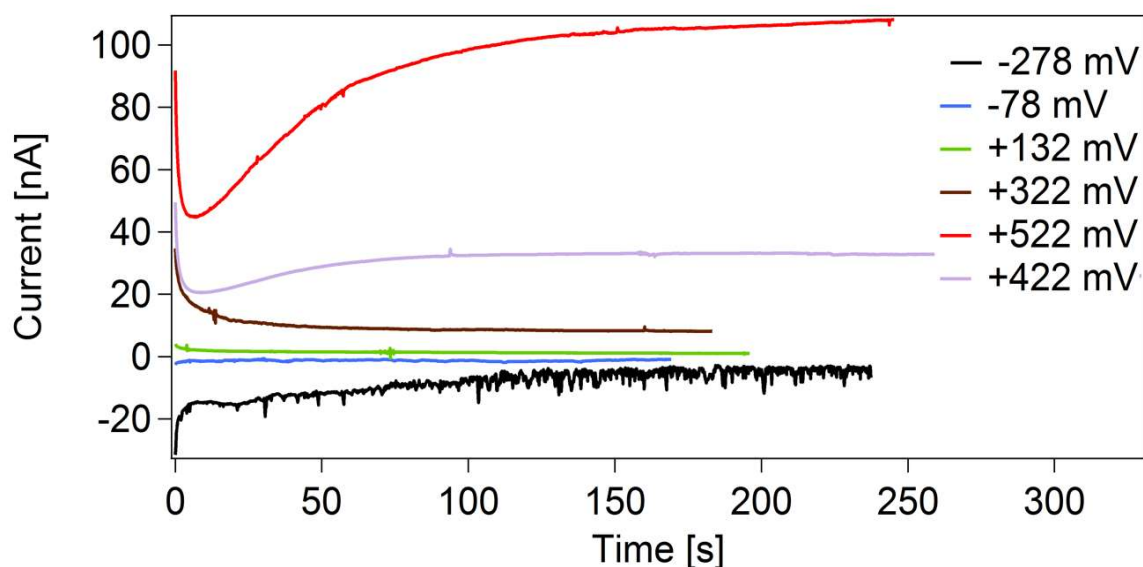


Figure S5-1: Current between eCP as working electrode and counter electrode for various applied potentials during a set of direct force measurements in 1 mM KCl solution. For practically all conditions a plateau in the current is observed on a timescale much shorter than the one required to perform the series of direct force measurements (< 100s vs. > 5min).

#### 4. A Versatile and Simple Approach to Electrochemical Colloidal Probes for Direct Force Measurements

##### S6 Fits to the full Poisson-Boltzmann Equation for Direct Force Measurements under Potentiostatic Control of the eCP - Comparison to Literature Data

In order to evaluate the direct force in quantitative manner the force versus distance profiles for the approach part have been fitted to the full-solutions of the Poisson-Boltzmann equation including charge regulation. Figure 6 of the manuscript shows the averaged force profiles with the corresponding fits.

The resulting potentials can be compared to diffuse layer potentials obtained for nearly analogous surfaces and similar conditions.<sup>1</sup> Figure S6-2 shows that for a large range of externally applied potentials comparable results have been obtained for the diffuse layer potential of an Au-electrode modified by an OH-terminated self-assembled monolayer; independently if the electrode was a flat, template stripped gold film or an eCP.

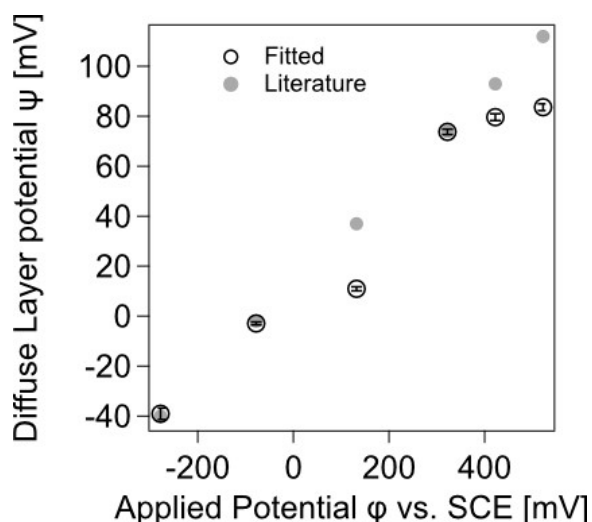


Figure S6-1: Comparison of the diffuse layer potentials obtained here for an eCP and the data reported in the literature for a flat, template-stripped Au-electrode<sup>40</sup>. Both electrodes have been modified by an OH-terminated SAM and the force profiles have been acquired under comparable conditions.

## References

1. Sun, P., Laforge, F. O. & Mirkin, M. V. Scanning electrochemical microscopy in the 21st century. *Physical Chemistry Chemical Physics* **9**, 802-823 (2007).
2. Amemiya, S., Bard, A. J., Fan, F.-R. F., Mirkin, M. V. & Unwin, P. R. Scanning electrochemical microscopy. *Annu. Rev. Anal. Chem.* **1**, 95-131 (2008).
3. Cortes-Salazar, F., Momotenko, D., Girault, H. H., Lesch, A. & Wittstock, G. Seeing big with scanning electrochemical microscopy. *Analytical Chemistry* **83**, 1493-1499 (2011).
4. Ventosa, E. & Schuhmann, W. Scanning electrochemical microscopy of Li-ion batteries. *Physical Chemistry Chemical Physics* **17**, 28441-28450 (2015).
5. Polcari, D., Dauphin-Ducharme, P. & Mauzeroll, J. Scanning electrochemical microscopy: a comprehensive review of experimental parameters from 1989 to 2015. *Chemical reviews* **116**, 13234-13278 (2016).
6. Izquierdo, J., Knittel, P. & Kranz, C. Scanning electrochemical microscopy: an analytical perspective. *Analytical and Bioanalytical Chemistry* **410**, 1-18 (2017).
7. Macpherson, J. V., Unwin, P. R., Hillier, A. C. & Bard, A. J. In-situ imaging of ionic crystal dissolution using an integrated electrochemical/AFM probe. *Journal of the American Chemical Society* **118**, 6445-6452 (1996).
8. Lugstein, A., Bertagnolli, E., Kranz, C. & Mizaikoff, B. Fabrication of a ring nanoelectrode in an AFM tip: novel approach towards simultaneous electrochemical and topographical imaging. *Surface and Interface Analysis* **33**, 146-150 (2002).
9. Kueng, A., Kranz, C., Lugstein, A., Bertagnolli, E. & Mizaikoff, B. Integrated AFM-SECM in tapping mode: simultaneous topographical and electrochemical imaging of enzyme activity. *Angewandte Chemie Internationale Edition* **42**, 3238-3240 (2003).
10. Dobson, P. S., Weaver, J. M. R., Holder, M. N., Unwin, P. R. & Macpherson, J. V. Characterization of Batch-Microfabricated Scanning Electrochemical-Atomic Force Microscopy Probes. *Analytical Chemistry* **77**, 424-434 (2005).
11. Eifert, A., Mizaikoff, B. & Kranz, C. Advanced fabrication process for combined atomic force-scanning electrochemical microscopy (AFM-SECM) probes. *Micron* **68**, 27-35 (2015).
12. Nellist, M. R. et al. Atomic force microscopy with nanoelectrode tips for high resolution electrochemical, nanoadhesion and nanoelectrical imaging. *Nanotechnology* **28**, 095711 (2017).
13. Butt, H.-J., Cappella, B. & Kappl, M. Force measurements with the atomic force microscope: Technique, interpretation and applications. *Surf. Sci. Rep.* **59**, 1-152 (2005).
14. Fréchette, J. & Vanderlick, T. K. Double Layer Forces over Large Potential Ranges as Measured in an Electrochemical Surface Forces Apparatus. *Langmuir* **17**, 7620-7627 (2001).
15. Kamijo, T., Kasuya, M., Mizukami, M. & Kurihara, K. Direct observation of double layer interactions between the potential-controlled gold electrode surfaces using the electrochemical surface forces apparatus. *Chemistry Letters* **40**, 674-675 (2011).
16. Tivony, R. & Klein, J. Probing the surface properties of gold at low electrolyte concentration. *Langmuir* **32**, 7346-7355 (2016).

#### 4. A Versatile and Simple Approach to Electrochemical Colloidal Probes for Direct Force Measurements

17. Gebbie, M. A. et al. Long range electrostatic forces in ionic liquids. *Chemical Communications* **53**, 1214-1224 (2017).
18. Wieser, V. et al. Novel in situ sensing surface forces apparatus for measuring gold versus gold, hydrophobic, and biophysical interactions. *Journal of Vacuum Science & Technology A* **39**, 023201 (2021).
19. Butt, H. J. Measuring electrostatic, van der Waals, and hydration forces in electrolyte solutions with an atomic force microscope. *Biophys. J.* **60**, 1438-1444 (1991).
20. Ducker, W. A., Senden, T. J. & Pashley, R. M. Direct measurement of colloidal forces using an atomic force microscope. *Nature* **353**, 239-241 (1991).
21. Kappl, M. & Butt, H. J. The colloidal probe technique and its application to adhesion force measurements. *Part. Part. Syst. Charact.* **19**, 129-143 (2002).
22. Gan, Y. A review of techniques for attaching micro- and nanoparticles to a probe's tip for surface force and near-field optical measurements. *Review of Scientific Instruments* **78**, 081101 (2007).
23. Yuan, C. C., Zhang, D. & Gan, Y. Invited Review Article: Tip modification methods for tip-enhanced Raman spectroscopy (TERS) and colloidal probe technique: A 10 year update (2006-2016) review. *Rev. Sci. Instrum.* **88**, 031101 (2017).
24. Hillier, A. C., Kim, S. & Bard, A. J. Measurement of double-layer forces at the electrode/electrolyte interface using the atomic force microscope: potential and anion dependent interactions. *J. Phys. Chem.* **100**, 18808-18817 (1996).
25. Campbell, S. D. & Hillier, A. C. Nanometer-scale probing of potential-dependent electrostatic forces, adhesion, and interfacial friction at the electrode/electrolyte interface. *Langmuir* **15**, 891-899 (1999).
26. Giesbers, M., Kleijn, J. M. & Cohen Stuart, M. A. The electrical double layer on gold probed by electrokinetic and surface force measurements. *Journal of Colloid and Interface Science* **248**, 88-95 (2002).
27. Barten, D. et al. Double Layer of a Gold Electrode Probed by AFM Force Measurements. *Langmuir* **19**, 1133-1139 (2003).
28. Rentsch, S., Siegenthaler, H. & Papastavrou, G. Diffuse Layer Properties of Thiol-Modified Gold Electrodes Probed by Direct Force Measurements. *Langmuir* **23**, 9083-9091 (2007).
29. Papastavrou, G. Combining electrochemistry and direct force measurements: from the control of surface properties towards applications. *Colloid Polym Sci.* **288**, 1201-1214 (2010).
30. Kuznetsov, V. & Papastavrou, G. Note: Mechanically and chemically stable colloidal probes from silica particles for atomic force microscopy. *Review of Scientific Instruments* **83**, 116103-116104 (2012).
31. Kuznetsov, V. & Papastavrou, G. Ion Adsorption on Modified Electrodes as Determined by Direct Force Measurements under Potentiostatic Control. *J. Phys. Chem. C* **118**, 2673-2685 (2014).
32. Knittel, P., Zhang, H., Kranz, C., Wallace, G. G. & Higgins, M. J. Probing the PEDOT:PSS/cell interface with conductive colloidal probe AFM-SECM. *Nanoscale* **8**, 4475-4481 (2016).
33. Daboss, S., Knittel, P., Nebel, C. E. & Kranz, C. Multifunctional Boron-Doped Diamond Colloidal AFM Probes. *Small* **1422**, 1902099-1902010 (2019).
34. Daboss, S., Lin, J., Godejohann, M. & Kranz, C. Redox Switchable Polydopamine-Modified AFM-SECM Probes: A Probe for Electrochemical Force Spectroscopy. *Analytical Chemistry* **92**, 8404-8413 (2020).

#### 4. A Versatile and Simple Approach to Electrochemical Colloidal Probes for Direct Force Measurements

35. Heim, L. O., Ecke, S., Preuss, M. & Butt, H.-J. Adhesion forces between individual gold and polystyrene particles. *J. Adh. Sci. Tech.* **16**, 829-843 (2002).
36. Hutter, J. L. & Bechhoefer, J. Calibration of atomic-force microscope tips. *Rev. Sci. Instrum.* **64**, 1868-1873 (1993).
37. Stamou, D. et al. Uniformly flat gold surfaces: Imaging the domain structure of organic monolayers using scanning force microscopy. *Langmuir* **13**, 2425-2428 (1997).
38. Kern, W. Cleaning solution based on hydrogen peroxide for use in silicon semiconductor technology. *RCA review* **31**, 187-205 (1970).
39. Pericet-Camara, R., Papastavrou, G., Behrens, S. H. & Borkovec, M. Interaction between Charged Surfaces on the Poisson-Boltzmann Level: The Constant Regulation Approximation. *J. Phys. Chem. B* **108**, 19467-19475 (2004).
40. Kuznetsov, V. & Papastavrou, G. Adhesion of Colloidal Particles on Modified Electrodes. *Langmuir* **28**, 16567-16579 (2012).
41. Ally, J. et al. Interaction of a microsphere with a solid-supported liquid film. *Langmuir* **26**, 11797-11803 (2010).
42. Thorgaard, S. N. & Bühlmann, P. Cathodic Electropaint Insulated Tips for Electrochemical Scanning Tunneling Microscopy. *Analytical Chemistry* **79**, 9224-9228 (2007).
43. Lindsay, A. E. & O'Hare, D. A comparative study of thin film insulation techniques for gold electrodes. *Electrochimica Acta* **51**, 6572-6579 (2006).
44. Sripirom, J., Kuhn, S., Jung, U., Magnussen, O. & Schulte, A. Pointed carbon fiber ultramicroelectrodes: a new probe option for electrochemical scanning tunneling microscopy. *Analytical Chemistry* **85**, 837-842 (2013).
45. Pobelov, I. V. et al. Electrochemical current-sensing atomic force microscopy in conductive solutions. *Nanotechnology* **24**, 115501-115511 (2013).
46. Petrovic, S. Cyclic Voltammetry of Hexachloroiridate(IV): An Alternative to the Electrochemical Study of the Ferricyanide Ion. *Chem. Educ.* **5**, 231-235 (2000).
47. Ji, X., Banks, C. E., Crossley, A. & Compton, R. G. Oxygenated edge plane sites slow the electron transfer of the ferro-/ferricyanide redox couple at graphite electrodes. *ChemPhysChem* **7**, 1337-1344 (2006).
48. Chen, R., Hu, K., Yu, Y., Mirkin, M. V. & Amemiya, S. Focused-ion-beam-milled carbon nanoelectrodes for scanning electrochemical microscopy. *J. Electrochem. Soc.* **163**, H3032 (2015).
49. Compton, R. G. & Banks, C. E. *Understanding voltammetry* (Imperial College Press, London, 2010).
50. Ecke, S. et al. Measuring normal and friction forces acting on individual fine particles. *Review of Scientific Instruments* **72**, 4164-4170 (2001).
51. Borges, G. L., Kanazawa, K. K., Gordon, J. G., Ashley, K. & Richer, J. An in-situ electrochemical quartz crystal microbalance study of the underpotential deposition of copper on Au(111) electrodes. *Journal of Electroanalytical Chemistry* **364**, 281-284 (1994).
52. Rumler, M. et al. Characterization of grain boundaries in multicrystalline silicon with high lateral resolution using conductive atomic force microscopy. *Journal of Applied Physics* **112**, 034909 (2012).
53. Hudson, J. E. & Abruña, H. D. Electrochemically Controlled Adhesion in Atomic Force Spectroscopy. *Journal of the American Chemical Society* **118**, 6303-6304 (1996).

#### 4. A Versatile and Simple Approach to Electrochemical Colloidal Probes for Direct Force Measurements

54. Kim, Y. H. et al. Highly Conductive PEDOT:PSS Electrode with Optimized Solvent and Thermal Post-Treatment for ITO-Free Organic Solar Cells. *Advanced Functional Materials* **21**, 1076-1081 (2011).
55. Du, J. et al. Pressure-assisted fabrication of organic light emitting diodes with MoO<sub>3</sub> hole-injection layer materials. *Journal of Applied Physics* **115**, 233703 (2014).
56. Israelachvili, J. N. *Intermolecular and surface forces* (American Press, New York, 1992).
57. Deruelle, M., Hervet, H., Jandeau, G. & Léger, L. Some remarks on JKR experiments. *Journal of Adhesion Science and Technology* **12**, 225-247 (1998).
58. Popa, I. et al. Importance of charge regulation in attractive double-layer forces between dissimilar surfaces. *Physical Review Letters* **104**, 228301 (2010).
59. Mark, A., Helfricht, N., Rauh, A., Karg, M. & Papastavrou, G. The Next Generation of Colloidal Probes: A Universal Approach for Soft and Ultra-Small Particles. *Small* **15**, 1902976 (2019).
60. Fahrenkrug, E., Alsem, D. H., Salmon, N. & Maldonado, S. Electrochemical measurements in in situ TEM experiments. *Journal of The Electrochemical Society* **164**, H358 (2017).
61. Behrens, S. H. & Borkovec, M. Electric double layer interaction of ionizable surfaces: Charge regulation for arbitrary potentials. *The Journal of Chemical Physics* **111**, 382-385 (1999).
62. Trefalt, G., Behrens, S. H. & Borkovec, M. Charge Regulation in the Electrical Double Layer: Ion Adsorption and Surface Interactions. *Langmuir* **32**, 380-400 (2016).
63. Behrens, S. H. & Grier, D. G. The charge of glass and silica surfaces. *J. Chem. Phys.* **115**, 6716-6721 (2001).
64. Pericet-Camara, R., Papastavrou, G. & Borkovec, M. Atomic Force Microscopy Study of the Adsorption and Electrostatic Self-Organization of Poly(amidoamine) Dendrimers on Mica. *Langmuir* **20**, 3264-3270 (2004).
65. Green, C. P. et al. Normal and torsional spring constants of atomic force microscope cantilevers. *Review of Scientific Instruments* **75**, 1988-1996 (2004).
66. Higgins, M. J. et al. Noninvasive determination of optical lever sensitivity in atomic force microscopy. *Review of Scientific Instruments* **77**, 013701 (2006).
67. Munz, M. Force calibration in lateral force microscopy: a review of the experimental methods. *Journal of Physics D: Applied Physics* **43**, 063001 (2010).

## 5. Electrochemical Grippers for Micro- and Nanorobotics: Manipulation by Tuning Surface Forces

*A. Karg<sup>1</sup>, V. Kuznetsov<sup>1</sup>, N. Helfricht<sup>1</sup>, M. Lippitz<sup>2</sup> & G. Papastavrou<sup>1\*</sup>*

<sup>1</sup>Physical Chemistry II; University of Bayreuth, Universitätsstraße 30, 95440  
Bayreuth, Germany.

<sup>2</sup>Experimental Physics III; University of Bayreuth, Universitätsstraße 30, 95440  
Bayreuth, Germany

Reprinted with permission from:

“Electrochemical Grippers for Micro- and Nanorobotics: Manipulation by Tuning  
Surface Forces”, Andreas Karg, Volodymyr Kuznetsov, Nicolas Helfricht,  
Markus Lippitz, Georg Papastavrou\*, *Scientific Reports*, **2023**, 13 (1), 7885.

DOI: 10.1038/s41598-023-33654-6

Under terms of the CC BY license

## 5. Electrochemical Grippers for Micro- and Nanorobotics: Manipulation by Tuning Surface Forces

**Abstract:** Existing approaches to robotic manipulation often rely on external mechanical devices, such as hydraulic and pneumatic devices or grippers. Both types of devices can be adapted to microrobots only with difficulties and for nanorobots not all. Here, we present a fundamentally different approach that is based on tuning the acting surface forces themselves rather than applying external forces by grippers. Tuning of forces is achieved by the electrochemical control of an electrode's diffuse layer. Such electrochemical grippers can be integrated directly into an atomic force microscope, allowing for 'pick and place' procedures typically used in macroscopic robotics. Due to the low potentials involved, small autonomous robots could as well be equipped with these electrochemical grippers that will be particularly useful in soft robotics as well as nanorobotics. Moreover, these grippers have no moving parts and can be incorporated in new concepts for actuators. The concept can easily be scaled down and applied to a wide range of objects, such as colloids, proteins, and macromolecules.

### Introduction

Robotics is a key technology for the twenty-first century. Currently, robots handle objects at length scales from meters down to a few micrometers. Decreasing the length scales, which are routinely accessible by robotic approaches would be of great importance for nanotechnology and medicine. To these means, various micro- and nanorobotic approaches have been pursued in the past years. When reaching the colloidal domain, i.e., few micrometers and smaller, surface forces are starting to become increasingly more important for robotics and well-established concepts of the macroscopic world cannot be applied anymore<sup>1-8</sup>. In particular, the process of 'pick and place', i.e., the complex process of gripping, picking-up, and subsequently releasing an object at a defined position becomes more and more difficult to implement<sup>9,10</sup>. Due to the ubiquitous attractive van der Waals (vdW) and capillary forces<sup>1,11</sup>, small objects adhere irreversibly to surfaces. Thus, grippers (cf. Fig. 1a,b), a tool common to macroscopic robotics, become severely limited in their function at small lengths, even when equipped with specifically designed surface modifications<sup>11-13</sup>. Despite recent advances in the development of novel actuator systems<sup>14,15</sup> that would allow in principle for a further miniaturization of grippers, the physical limits imposed by surface forces will remain in place. The introduction of novel approaches that rely on manipulating the surface forces themselves rather than optimizing tools from the macroscopic world represents an important step to extend robotic manipulation processes

## 5. Electrochemical Grippers for Micro- and Nanorobotics: Manipulation by Tuning Surface Forces

---

to the low micro- and nanometer scale. Thereby, it will be possible to preserve established manipulation processes like 'pick and place' for handling colloidal particles and macromolecules.

For the manipulation of micrometer-sized objects by means of grippers, approaches like increasing the surface roughness, and chemical surface modification of the gripper surfaces have been reported while the manipulation process itself can be followed by light microscopy or scanning electron microscopy (SEM)<sup>16</sup>. The necessity for surface modifications illustrates the increasing influence of surface forces, such as van der Waals and capillary forces, respectively, at decreasing length scales (cf. Fig. 1d,e)<sup>17,18</sup>. Without specifically designed surfaces, objects can be 'picked' and 'placed' but not subsequently released. Atomic force microscopy (AFM), where a sharp tip is attached to the end of a cantilever (cf. Fig. 1g), is not only a tool to image but also to manipulate objects on the micro- and nanoscale. The field of AFM-based nanorobotics progressed significantly in the last 20 years<sup>5,19,20</sup>. However, the dominating approach of applying lateral forces has remained largely unchallenged (Fig. 1h) and is by far the most-used technique for nanomanipulation by AFM. Nevertheless, by combining AFM with nanofluidics<sup>21,22</sup>, often also referred to as FluidFM-technique, a microscopic analog to suction caps (cf. Fig. 1c) became available at the colloidal scale. This technique allows to handle colloidal objects as small as 300 nm under force control, which allows to directly measure interaction forces (cf. Fig. 1f)<sup>23</sup>. However, a major disadvantage of this technique lies in the fact that microchanneled cantilevers in combination with an external pressure controller are required that do not allow for miniaturized autonomous robots.

## 5. Electrochemical Grippers for Micro- and Nanorobotics: Manipulation by Tuning Surface Forces

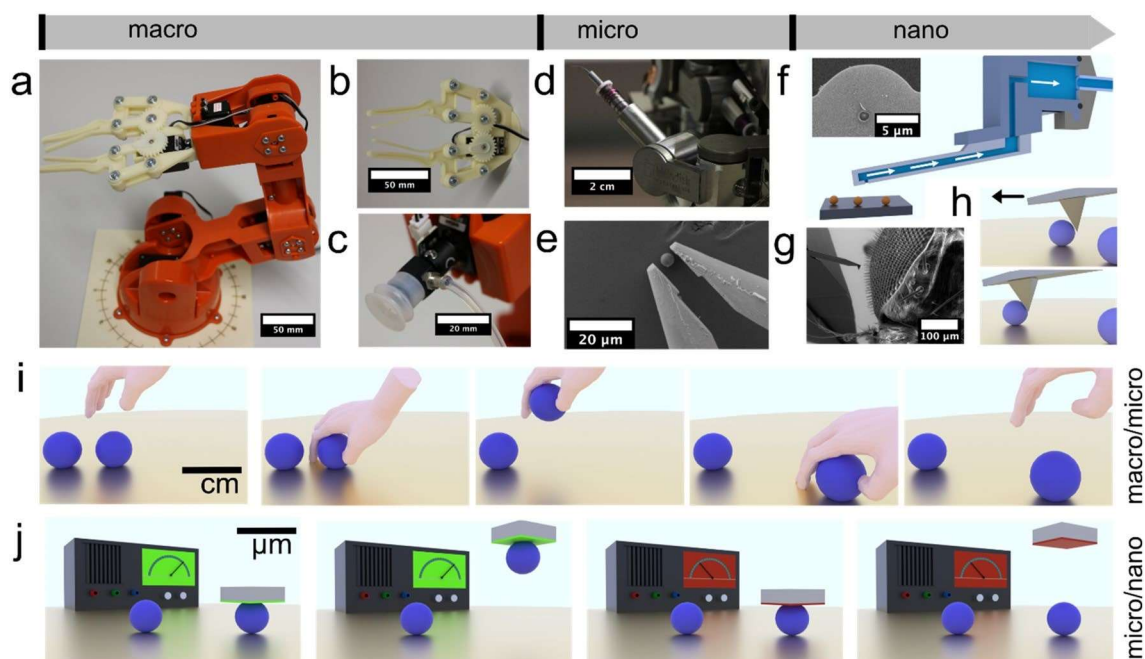


Figure 1. Robotic manipulation principles from macro- to nanoscale. (a) Macroscopic 6-axis robot in ‘classic’ design. (b) Gripper attachment for the macroscopic robot and (c) suction cap, respectively. (d) An analogous robotic platform for micromanipulation (here, in combination with a scanning electron microscope, SEM). (e) Gripper for the aforementioned micromanipulation platform, which allows for the handling of colloidal particles. (f) An equivalent of a suction cup that can be combined with an atomic force microscope (AFM). The inset shows a microfluidic hollow AFM cantilever with an aperture of  $2\ \mu\text{m}$  in diameter that can be directly connected to a nanofluidic controller. (g) The tip of an AFM-cantilever in comparison to the eye of a fly in SEM. (h) Example of nanomanipulation by applying shear forces by AFM to move particles to defined places on the sample. (i) Single manipulation steps for ‘pick’, ‘place’, and ‘release’, respectively, are illustrated by a human hand on the macroscopic scale. (j) Extending the ‘pick’ and ‘place’ concept to the colloidal domain and beyond: rather than applying mechanical pressure the interaction forces are tuned externally. Green indicates attractive interactions (i.e., equivalent to ‘grip’), and red indicates repulsive interactions (i.e., equivalent to ‘release’).

Here, we propose a novel approach for micro- and nanorobotic manipulation in liquid environment that is based on externally tuning the interaction forces rather than utilizing miniaturized tools such as grippers and suction caps (cf. Fig. 1b,c), or applying shear forces, respectively. Thus, the ‘pick and place’ process (cf. Fig. 1a) is based on controlling the surface forces themselves rather than exerting ‘external’ forces due to conventional grippers. The sequence in Fig. 1i illustrates the analogy to the manipulation process with grippers (or our hands): Instead of gripping an object one ‘switches on’ a strong attractive interaction force (cf. Fig. 1j), which is still applied during lifting and transferring. The object is

## 5. Electrochemical Grippers for Micro- and Nanorobotics: Manipulation by Tuning Surface Forces

released by 'switching-off' the strong attractive force and switching subsequently to a less strong interaction than acting between object and substrate. Tuning the adhesion force between an AFM-cantilever and a colloidal object provides thus a direct approach for the manipulation at colloidal length scales without elaborate mechanical devices. Previously, a small number of micromanipulation techniques have been reported based on electric fields in gaseous atmosphere<sup>24,25</sup>. However, the resulting image charges and required large field strengths render this approach not easy for manipulation in liquids<sup>26</sup>. To the best of our knowledge there are only few examples of micromanipulation by electrochemical control: One approach has been based on switching surface properties of a hydrogel by external potentials<sup>27</sup>. However, only objects with a suitable surface chemistry can be manipulated. Another approach has been reported for metallic objects only<sup>28</sup>. By contrast, a large number of electrochemically based actuation systems have been reported in the past<sup>29-32</sup>.

The interaction of colloidal objects is governed by various types of surface forces<sup>18,33</sup>. Which surface forces in liquid environment would be tunable, and strong enough? Van der Waals forces are ubiquitous but cannot be changed without replacing the materials themselves or the medium, respectively. Moreover, van der Waals forces are rather weak, especially in liquid environments. Capillary forces are only present under ambient conditions and are thus not of relevance here. Solvent exclusion can lead to rather strong adhesion forces<sup>34-36</sup>. However, these forces can only be tuned by changing the surface chemistry, which requires complex coatings and external stimuli such as temperature or light<sup>37,38</sup>. The only remaining force contribution in colloid science results from the overlap of the diffuse layers originating from charged surfaces in electrolyte solutions. The concept of diffuse layers (DLs) originates from electrochemistry and the extension of DLs strongly depends on the electrolyte solution composition and the potential applied to the electrode. Diffuse layer forces are known to influence the adhesion of colloidal particles on electrodes and these forces have been studied previously by the colloidal probe technique based on AFM<sup>39-42</sup>. Colloidal probes are force sensors that are prepared by attaching a single colloidal particle to the end of an AFM cantilever<sup>43-46</sup>. Here, we follow a different approach: By equipping an AFM-cantilever with a suitable, flat electrode, which is connected to an external potentiostat, we convert the AFM-cantilever to an 'electrochemical gripper' to handle colloidal objects in liquid environments by a 'pick and place' procedure.

### Results

**Combining AFM with electrochemistry.** A proof-of-principle for an AFM-based electrochemical gripper has been given in this study by the manipulation of colloidal silica particles with a diameter of a few microns. This choice of diameter allows to directly visualize the particles by light microscopy while they are still small enough to be dominated in their interaction by surface forces<sup>33</sup>. Figure 2a shows a schematic representation of the experimental setup (cf. also Supplementary Fig. 1): A commercial AFM was mounted on top of an inverted optical light microscope. A purposely made electrochemical cell allows for applying defined potentials to the working electrode, which was here integrated at the apex of a modified AFM-cantilever. Figure 2b shows a scanning electron microscopy (SEM) image of such a purposely made cantilever. These custom-made cantilevers were completely insulated except for their front part, which acted as electrode.

Figure 2c gives an overview on the preparation of these cantilevers, which will be referred to as *electrochemical grippers*. These grippers have been prepared from Au-coated tipless AFM-cantilevers (cf. Fig. 2c, left) that have been electrically contacted by means of thin insulated wires and silver paint. Then, these cantilevers were completely insulated by the deposition of a cathodic electro-paint (cf. Fig. 2c, center left). In the next preparation step, the insulation was removed only at the apex of the cantilever, which represents the later electrode area. The removal has been carried out by focused ion beam (FIB)-milling in the SEM. (Fig. 2c, center right, further details are also given in Supplementary Figs. 2 and 3). In terms of the insulation, this process is similar to the one presented recently for the preparation of electrochemical colloidal probes<sup>47</sup>. In order to confirm that only the front part of the cantilever was electrochemically active (cf. 2c, right), cyclic-voltammetry was performed (cf. Fig. 2d). In a cyclovoltammogram (CV), the applied potential is ramped, and the resulting current is acquired<sup>48</sup>. On macroscopic electrodes with dimensions larger  $\sim 25 \mu\text{m}$ , one finds isolated oxidation and reduction peaks that are specific for an electrochemical redox couple. By contrast for smaller dimensions, i.e., micro- and nano- electrodes, a sigmoidal shape is expected<sup>48</sup>. Here, the redox couple has been potassium ferrocyanide and potassium ferricyanide<sup>49</sup>. The corresponding peaks for analogous conditions as used in our experiments have been reported to be 0.120 V and 0.240 V (vs SCE), respectively<sup>50</sup>. The electrode area on the apex of the here-prepared cantilever has an area of  $A = 645 \mu\text{m}^2$  (approximation as a triangle). Hence, its critical dimension falls just in the transition region between macro- and micro-electrodes. In consequence, small oxidation and reduction peaks

## 5. Electrochemical Grippers for Micro- and Nanorobotics: Manipulation by Tuning Surface Forces

at the expected potentials that are superimposed to an overall sigmoidal shape have been observed (cf. Fig. 2b). In order to verify the insulation properties of the coating, we performed additional experiments acquiring CVs for cantilevers before the FIB-treatment and thus a complete insulation layer. No significant electrochemical activity could be observed in the CV. Further details for the electrochemical experiments (cf. Supplementary Fig. 4) as well as for the preparation of the cantilever (cf. Supplementary Figs. 2 and 3) are given in the SI.

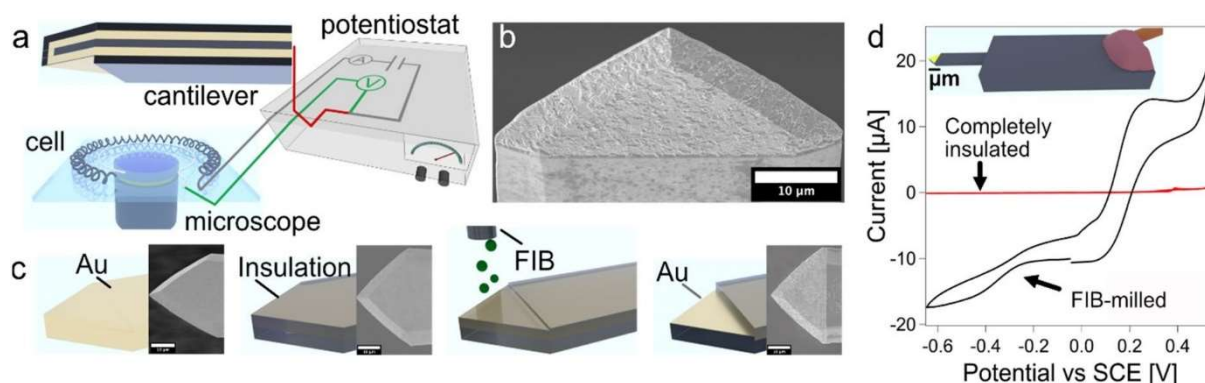


Figure 2. Preparation and characterization of an electrochemical gripper on an AFM-cantilever. (a) Schematic representation of the electrochemical setup to control the electrode at the end of an AFM-cantilever by a potentiostat. The electrochemical cell was placed on top of an inverted optical microscope. (b) SEM image of a cantilever with an insulation layer, which has been selectively removed at the front. (c) Schematic representation of the preparation steps: an insulation layer of electropaint has been deposited onto an AFM-cantilever that has been coated from both sides with gold. Then, this insulation layer has been partially removed from the apex of the cantilever by FIB-milling. (d) Cyclic voltammogram (CV) for the thereby formed electrode on the cantilever that acts then as electrochemical gripper. The CV confirms that the electrode is electrochemically active (black) in comparison to a completely insulated cantilever (red).

**Interaction forces between colloidal particles and substrates.** To establish micromanipulation based on tuning the surface forces in a defined manner, we first had to quantify the acting force contributions. Two sets of interaction forces are of interest here: First, the forces between silica particles and the substrate. The latter were microscopy slides made from borosilicate glass. Second, the forces between the particles and the electrode of the electrochemical gripper. This electrode has been incorporated in an AFM-cantilever (cf. Fig. 2), and its potential has been externally controlled by means of a potentiostat.

Figure 3 shows how the interaction forces between the silica particles and substrates have been determined: We prepared so-called ‘colloidal probes’ by attaching a particle permanently to an AFM-cantilever<sup>43,44</sup>. Such ‘classical’ colloidal probes allow for the

## 5. Electrochemical Grippers for Micro- and Nanorobotics: Manipulation by Tuning Surface Forces

---

acquisition of interaction force profiles between the colloidal particles and the flat substrate in well-defined sphere/plane geometry<sup>51</sup>. The interaction force profiles were acquired by ramping the z-piezo in direction of the substrate and detecting simultaneously the force acting on the colloidal probe as function of the piezo-displacement and separation distance, respectively. A schematic representation of the measurement principle is shown in Fig. 3a and an exemplary force versus distance curve is shown in Fig. 3b. Starting at large separations, no interaction forces were detectable initially. With decreasing distance, the forces due to the overlap of the diffuse layers started to act. In Fig. 3b the diffuse layer force was repulsive, as expected, since both, the glass surface as well as silica colloid are charged negatively<sup>52,53</sup>. An exponential force law could be recuperated as expected for the diffuse layer overlap. A quantitative analysis of the interaction force profiles based on full solutions of the Poisson-Boltzmann equation including charge regulation is given in the SI (cf. Supplementary Fig. 6). Furthermore, no attractive forces are detected, which can be attributed to the substantial surface roughness on the colloidal particle as well as on the electrode<sup>54,55</sup>. Upon contact of the colloidal probe and the substrate, the interaction is governed additionally by contact mechanics<sup>33,51</sup>. With increasing piezo-displacement the particle was pressed increasingly against the substrate until a pre-defined maximum loading force was reached, where the movement of the z-piezo was reversed. Due to adhesive forces in the contact area, the two surfaces remain in contact. At a certain point, finally a jump-out-of-contact took place when the cantilever's restoring force overcomes the adhesion forces. Contributions to the adhesion forces are not only given by long-ranged contributions, i.e., diffuse layer overlap and van der Waals forces, but also by contributions within the contact area, such as chemical bonds and solvent exclusion. Stronger adhesion force can be observed on hydrophobized glass substrates, an example is given in Fig. 3c.

## 5. Electrochemical Grippers for Micro- and Nanorobotics: Manipulation by Tuning Surface Forces

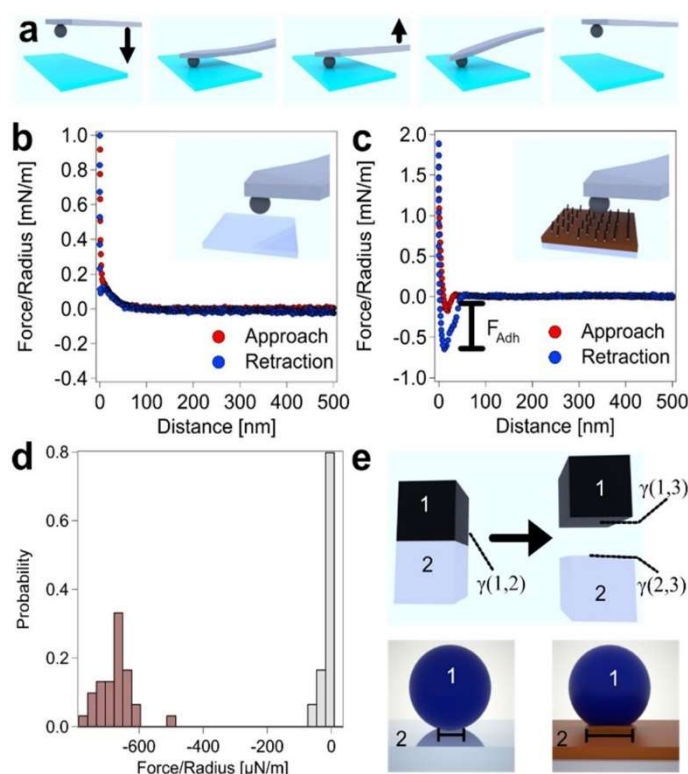


Figure 3. Substrate vs. particle interaction. (a) Schematic representation of direct force measurements by conventional colloidal probe AFM in sphere/plane geometry. A silica particle (i.e., the colloidal probe) has been permanently attached to the cantilever and has been approached to the sample surface while the acting force has been sensed simultaneously. Thus, the long-range forces can be determined. Upon reversal of the movement, additionally the adhesive forces ( $F_{Adh}$ ) can be determined. (b) Exemplary force versus distance curve for a silica particle interacting with a bare glass surface in electrolyte solution (pH = 4.0,  $I = 0.1$  mM). No adhesion could be detected in most cases. (c) Exemplary force versus distance curve for the interaction of a silica particle with a silane-modified glass surface (contact angle  $\theta = 48^\circ$ ) under the same conditions. Here, strong adhesive behavior has been present, which can be attributed to solvent exclusion. (d) Distributions of the adhesion forces acquired on both substrates. For each substrate, at least 30 force curves have been measured (e) Schematic representation of how solvent exclusion controls the adhesion behavior due to the ‘creation’ and ‘destruction’ of interfaces with the liquid phase. Each interface is by its respective interfacial energy  $\gamma$  (top).

The interfacial properties of the substrates can be varied in a defined manner by means of gas-phase silanization with methoxy(dimethyl)octylsilane (MDOS)<sup>56,57</sup>, which forms hydrophobic self-assembled monolayers (SAMs). The degree of hydrophobicity has been verified by static measurement of the contact angle  $\theta$  (cf. Supplementary Table 1). Besides the hydrophilic, bare glass surfaces ( $\theta < 15^\circ$ ), we studied here the interaction between silica particles and SAMs obtained by gas phase silanization with different exposition times. The

## 5. Electrochemical Grippers for Micro- and Nanorobotics: Manipulation by Tuning Surface Forces

resulting contact angles were:  $\theta = 48^\circ \pm 1^\circ$ ,  $\theta = 77^\circ \pm 6^\circ$ , and  $\theta = 101^\circ \pm 3^\circ$  (cf. Fig. 4f and Supplementary Table 1), respectively. Figure 3d compares the distribution of the adhesion forces for the exemplary force profiles acquired with a silica colloidal probe and a bare glass surface (cf. Fig. 3b) and a substrate with  $\theta = 48^\circ$  (cf. Fig. 3c). The adhesion force was significantly different for these two substrates. In the case of the silane-modified sample the adhesion forces ( $F_{Adh}/R = 675 \pm 52 \mu\text{N/m}$ ) were much larger than for the bare glass surface ( $F_{Adh}/R = 10 \pm 19 \mu\text{N/m}$ ). The corresponding adhesion force distributions show a broad distribution. The reasons are manifold but can be mostly attributed to surface roughness and variation on the single molecule level<sup>58-60</sup>. In the framework of the Johnson-Kendall-Roberts (JKR)-theory, which only takes acting forces in the contact area into account, the adhesion force is given by  $F_{Adh}/R = 1.5\pi W_{adh}$  in the sphere-plane interaction geometry<sup>33</sup>. The JKR-theory is commonly applied for gold surfaces<sup>34-36</sup> and has also been utilized here for the interpretation of the adhesion forces due to solvent exclusion only (i.e., without electrostatic contributions due to the potentiostatic control). The work of adhesion  $W_{adh} = \gamma_{13} + \gamma_{23} - \gamma_{12}$  is given by the interfacial energies  $\gamma$  of the interfaces created ( $\gamma_{(1,3)}$  and  $\gamma_{(2,3)}$ ) and destroyed ( $\gamma_{(1,2)}$ ) (cf. Fig. 3e). The hydrophilicity and surface chemistry of bare glass surfaces and silica particles is similar ( $\gamma_{(1,3)}, \gamma_{(2,3)} \approx 1.6 \text{ mN/m}$ )<sup>41</sup> and leads only to small contributions to the adhesion by solvent exclusion. Thus, the interaction of the diffuse layers, which is repulsive and drives the two surfaces away from each other, dominates and leads to no adhesive behavior. The silica particles stick only in a few cases on the glass surface. On the other hand, with additional hydrophobic entities on the glass, the value of  $\gamma_{(1,3)}$  increases up to the point where solvent exclusion dominates the diffuse layer repulsion. This finding has been corroborated by the adhesion forces on the substrates with higher contact angles (cf. Fig. 4).

**Interaction forces between colloidal particles and the electrode of the electrochemical gripper.** Figure 4a shows in a schematic manner how the interaction forces between the silica colloidal particles and the electrode of the electrochemical gripper have been determined. We introduced a special interaction geometry, in which the colloidal particle has been immobilized by glue on a solid substrate while the potentiostatically controlled cantilever with the electrochemical gripper is positioned directly above the particle. This interaction geometry is practically 'inverted' in respect to the conventional sphere/plane configuration present in a colloidal probe (cf. Figs. 3a, 4a). The gold electrode on the cantilever has been modified by a thiol-based SAM terminating in OH-groups in order

## 5. Electrochemical Grippers for Micro- and Nanorobotics: Manipulation by Tuning Surface Forces

to render the electrode hydrophilic in a defined manner. Thus, solvent exclusion is not expected to contribute significantly to the adhesion behavior with the modified electrode as for glass and silica, respectively<sup>41</sup>. Figure 4b,c represent two exemplary force profiles for a cantilever under potentiostatic control at different applied potentials. These exemplary force profiles have been selected from the series ( $n=30$ ) of force versus distance curves acquired for each potential. Figure 4b shows a force profile, which was acquired at a highly positive potential ( $\phi_{gripping} = +726$  mV). In this case, the surfaces of the colloid and electrode are oppositely charged. In consequence, the long-ranged electrostatic forces upon approach between the particle and the gripper are attractive. The same is valid for the adhesion forces, where the electrostatic attraction superimposes to the solvent exclusion. By contrast, Fig. 4c shows a force profile acquired at a highly negative applied potential ( $\phi_{release} = -474$  mV). Upon approach the long-range forces are repulsive over the whole distance range, as expected for the interaction between two negatively charged surfaces. Moreover, no adhesion between the surfaces can be detected. Figure 4d shows the corresponding distributions for the adhesion forces at these two applied potentials as determined from all force profiles ( $n=30$ ) acquired at each potential. Due to the hydrophilic nature of the two surfaces involved, the adhesion forces reflect the long-ranged interaction forces due to the diffuse layer overlap primarily. The latter is also acting upon approach before the two surfaces were in contact. We noticed that no adhesion was taking place for the negative potential, and the interaction remained completely repulsive even when the surfaces were in contact. It should be noted that attractive contributions due to van der Waals forces are strongly reduced due to the surface roughness<sup>58,59</sup>.

The variation of adhesion forces as a function of the external potential has been reported previously, albeit on flat electrodes. It has been probed in sphere/plane geometry by colloidal probes<sup>41,61,62</sup>. We could recently demonstrate<sup>41</sup> that the contribution of the long-range interaction forces due to diffuse layer overlap is essential for the modulation of the adhesion forces<sup>41</sup>. Figure 4e illustrates the influence of the forces due to diffuse layer overlap in a schematic manner and shows how the diffuse layer on the electrode changes in function of the potential applied by the potentiostat: For highly negative potentials, the diffuse layer is composed of cations as counter ions while for highly positive potentials the anions form the counter ions. The diffuse layer decays exponentially from the surface of the electrode until the ion composition reaches the bulk concentration again. At an ionic strength of 0.1 mM, the exponential decay takes place with a Debye-length of 30 nm<sup>33</sup>. The measurements have been performed at pH 4.0, therefore, the silica colloidal particles have a slightly negative

## 5. Electrochemical Grippers for Micro- and Nanorobotics: Manipulation by Tuning Surface Forces

diffuse layer charge. Silica as insulator does not change its diffuse layer properties in function of the externally applied potential to the electrode<sup>41,63,64</sup>. The overlap of silica's diffuse layer with the one of the electrodes leads thus to a repulsive force in the case of a negative potential. (cf. Fig. 4e Bottom). By contrast, a highly positive potential does lead to an attractive interaction force (cf. Fig. 4e Top).

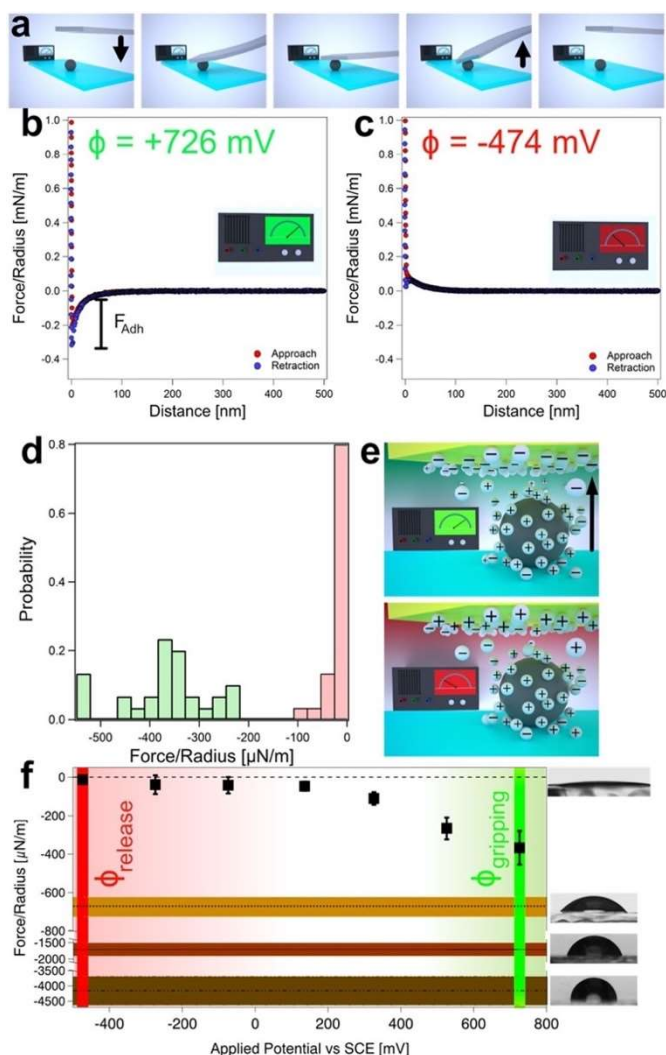


Figure 4. Interaction of the particles with the electrochemical gripper. (a) Schematic representation how interaction force profiles between silica particles and the 'electrochemical gripper' (i.e., cantilever with an integrated electrode) have been determined: the silica particle has been glued to a flat substrate and remains immobile. (b) Exemplary force versus distance curve for an applied potential of  $\phi_{gripping} = +726$  mV. At this potential the long-range forces are attractive and large adhesion forces can be observed. (c) Exemplary force versus distance curve for an applied potential of  $\phi_{release} = -474$  mV. The long-range forces are completely repulsive, and no adhesion can be observed. (d) Distribution of adhesion forces  $F_{Adh}$  for  $\phi_{gripping} = +726$  mV and  $\phi_{release} = -474$  mV. For both potentials, at least 30 force curves have been measured (e) Schematic representation of how diffuse layer overlap dominates the interaction force and thus also adhesion of non-

## 5. Electrochemical Grippers for Micro- and Nanorobotics: Manipulation by Tuning Surface Forces

hydrophobic electrode surfaces. The overlap of the diffuse ion layers of electrode and particle leads to an osmotic pressure and the resulting force can be repulsive (likewise charged counterions) or attractive (differently charged counterions). (f) Adhesion forces as a function of the externally applied potential are summarized. For comparison also, the adhesion forces on the differently modified glass surfaces ( $\theta < 15^\circ$ ,  $\theta = 48^\circ$ ,  $\theta = 77^\circ$ , and  $\theta = 101^\circ$ ) are shown together with images of the corresponding contact angle measurements. The externally applied potential allowed to switch the adhesive behavior from highly adhesive (green, 'gripping') to highly repulsive (red, 'release').

**Particle manipulation by potentiostatic control.** Tuning the adhesion in a defined manner by an external signal represents the key to our approach of nanomanipulation by AFM. Figure 4f summarizes the data of adhesion forces for a range of applied potentials ( $\phi = -474$  mV to  $\phi = +726$  mV vs. SCE). Each data point originates from a distribution analogous to the data shown in Fig. 4d. In the potential range  $\phi = -474$  mV to  $+136$  mV no adhesion between the particle and the electrode of the gripper has been observed. Due to the lack of adhesive forces, i.e., 'non-sticking' of the particle to the electrode, a 'gripped' particle would be released to the substrate in this case. To this process, we will refer in the following as '*placing*' a particle. Instead, for potentials  $\phi > +136$  mV, the adhesion force increased monotonically with increasing the applied potential. Thus, the adhesion force between the particle and the electrode on the gripper becomes larger than the ones between the particle and the substrate. Therefore, these potentials allow for '*gripping*' or '*picking*' a particle from the substrate as the particle will 'stick' to the gripper. The transition coincides with the potential of zero charge (pzc), where the electrode is practically uncharged and the long-range forces are minimal<sup>41,64</sup>. For external potentials smaller than the pzc, the diffuse layer interaction is repulsive as particle and electrode are likewise charged. For potentials above the pzc the electrode is reversing its charge to positive. In consequence the long-range forces upon approach are becoming attractive and the adhesion forces are monotonically increasing with increasing the applied potentials. A similar adhesion behavior has been reported previously for studies on flat electrodes with an analogous surface modification<sup>41</sup>. However, a direct comparison of the pzc for the electrodes prepared by FIB and flat electrodes is not possible as the different crystal surfaces of the former are leading to a shift of the pzc<sup>65,66</sup>. In particular, for surfaces subject to a FIB-treatment, this effect is highly pronounced and leads to an increased roughness<sup>67</sup>. A more detailed comparison between the two types of electrodes is given in the SI (cf. Supplementary Fig. 7). The data in Fig. 4f can be divided into a region where the external potentials are leading to a repulsive behavior and thus the

## 5. Electrochemical Grippers for Micro- and Nanorobotics: Manipulation by Tuning Surface Forces

'placing' of a particle and a region of potential that corresponds to attractive interaction forces and thus a 'gripping' of particles from a substrate.

The '*pick and place*' procedure implemented with the electrochemical gripper makes use of the principle that a particle will transfer most likely to the surface on which a higher adhesion is present. In the following, we illustrate that this process takes place with a high probability, provided that the right potentials are applied to the electrochemical gripper. Thus, if an electrochemical gripper is placed on a particle sitting on a glass substrate, an attractive potential  $\phi$  (e.g.,  $\phi_{gripping}$ , cf. adhesion force in Fig. 4b in comparison to the one in Fig. 3b) applied to the gripper electrode leads to greater adhesive forces between particle and electrochemical gripper in comparison to the glass. Upon retraction of the cantilever (i.e., the electrochemical gripper), the particle has then been 'gripped' (or 'picked') as it attaches to the gripper due to the higher adhesive forces. Nonetheless, it can be 'released' again to the substrate when a highly negative potential (e.g.,  $\phi_{release}$ ) is applied to the electrode of the electrochemical gripper. In this case, the interaction becomes now more repulsive with the electrode than with the substrate.

The transfer process by applying  $\phi_{gripping}$  and subsequently  $\phi_{release}$  takes place only with a certain probability. The probability depends on the applied potential and the interfacial energy of the substrate, which combined give the total adhesion force. The different parameters influencing the total adhesion forces, in particular the dependence from the externally applied potential (cf. Fig. 4f) has been studied in detail elsewhere, albeit in an inverse geometry<sup>41</sup>. In summary, the the adhesion force depends approximately linearly from the externally applied potential (cf. Fig. 4f) while the interfacial energy (hydrophilic to hydrophobic) leads to an offset in the adhesion forces<sup>41</sup>. In order to demonstrate that highly positive potentials, i.e., of  $\phi_{gripping} = +726$  mV vs. SCE, provide a reliable means to remove particles from the substrates, we performed experiments with different substrates at this potential: For bare glass substrate, a transfer of the particle from the substrate to the cantilever was practically always taking place, thus a success rate of  $\xi \approx 1$  ( $n > 30$ ) has been attributed. However, for the slightly hydrophobic silane-modified substrate ( $\theta = 77^\circ$ , cf. Fig. 4f) a success rate of about  $\xi = 0.2$  ( $n=45$ ) for successful picking of the particles from the substrate has been observed by optical microscopy. The corresponding sequence is shown in Fig. 5a. Thus, even on hydrophobic substrates, gripping of particles is possible, despite a more unfavorable partition of forces due to solvent exclusion and to diffuse layer overlap. Figure 5b–f show how the implementation of an electrochemical gripper has been utilized for the defined manipulation of single colloidal particles on a bare glass substrate. The

## 5. Electrochemical Grippers for Micro- and Nanorobotics: Manipulation by Tuning Surface Forces

---

process has been followed by optical microscopy. By applying a high positive potential ( $\phi_{gripping} = +726$  mV) to the gripper electrode the adhesion with the particle has been rendered favorable compared to the particle's adhesion with the substrate (cf. Fig. 5b). Consequently, the particle remained on the electrode when the cantilever has been retracted from the substrate (cf. Fig. 5c). Thus, the particle has been 'gripped' solely by tuning the surface forces. After being about 10  $\mu\text{m}$  separated from the surface, the cantilever with the gripper was moved to a new position (cf. Fig. 5d) where the cantilever is again approached to the surface (cf. Fig. 5e). A negative potential ( $\phi_{release} = -474$  mV) has been applied (cf. Fig. 5f), which leads to a highly repulsive interaction between the electrochemical gripper and particle. In consequence, the transferred particle is 'released' on the substrate on the new position at the substrate upon retraction of the cantilever (cf. Fig. 5g). It must be noted, that the interaction between bare glass and the particle is slightly repulsive as both surfaces are negatively charged. The movement of the electrochemical gripper, i.e., AFM-cantilever, is connected with hydrodynamic movement of the liquid in the vicinity of the particles on the substrate and leads also to slight lateral movements of these particles when the piezoelectric actuator of the AFM has been moved too fast. However, such unintentional lateral movements can be clearly distinguished from the gripping of a particle as in the latter case the particle remains attached to the cantilever.

## 5. Electrochemical Grippers for Micro- and Nanorobotics: Manipulation by Tuning Surface Forces

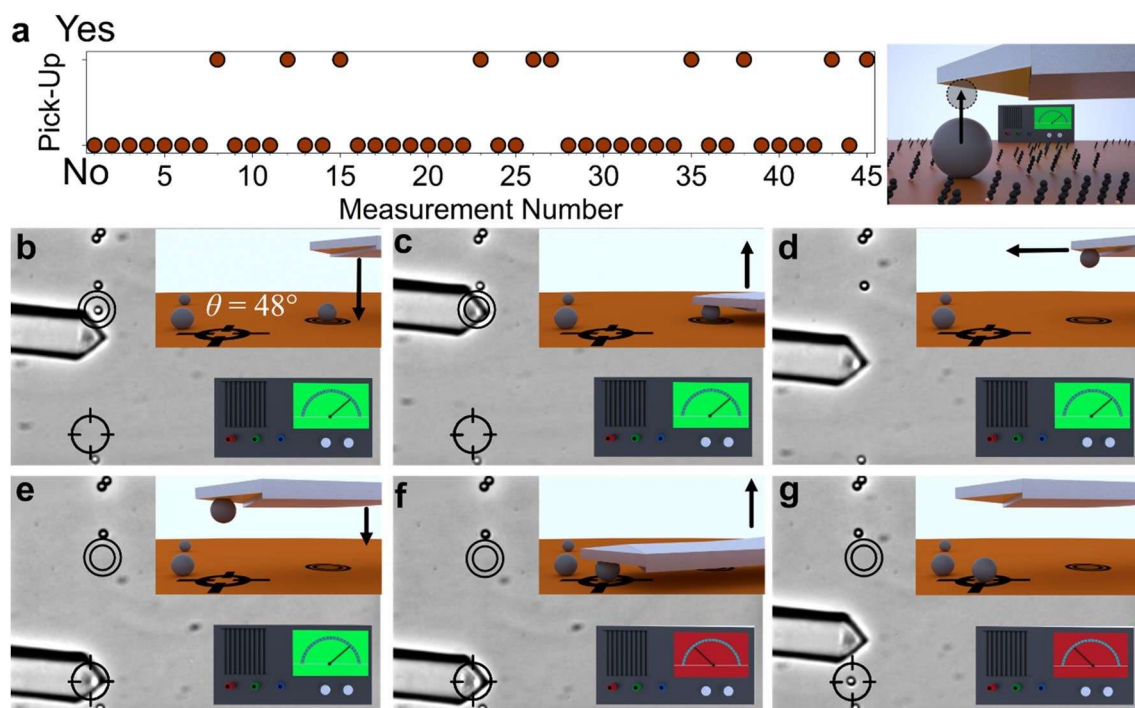


Figure 5. Particle manipulation by an electrochemical gripper. (a) Time series for successful events of ‘gripping’ of colloidal silica particles from a silane-modified glass substrate ( $\theta = 77^\circ$ ). As shown in the schematic representation on the right, the particle is now not immobilized. A success probability of 0.2 has been observed, while practically all pick-up events have been successful for the bare glass ( $\theta < 15^\circ$ ). (b-g) Sequence for the different manipulation steps of a single particle by an ‘electrochemical gripper’. The cantilever is set to an attractive ‘gripping’ potential (green) (b) and placed over the particle (c). Upon retraction of the cantilever the particle remains attached to it (d). The cantilever is moved to a new position and placed on the surface (e). The interaction is switched to ‘repulsive’ (red) (f). Then the cantilever is moved away from the surface and the transferred particle resting on the substrate has been ‘released’ (g).

**Electrochemical gripper for nano- and microrobotics.** Sequential manipulation of single particles allows to perform more complex tasks common in robotics. As proof-of-principle, we prepared the two structures shown in Fig. 6. Our examples of particle arrangements represent the abbreviations ‘AFM’ and ‘PC II’, which stand for ‘atomic force microscopy’ and ‘Physical Chemistry II’. The manipulation processes required about 120 min and 60 min, respectively. To assemble these structures, single particles have been manipulated by the ‘pick and place’ or, more specifically, the ‘gripping and release’ process in a sequential manner. Here, also individual particles were manipulated more than once. A time-lapse movie showing the whole process for writing ‘AFM’ (cf. Fig. 6a) is available in Supplementary Movie 1. We prepared the structures on two different substrates, namely a bare glass slide (‘AFM’, cf. Fig. 6a) and a partially silane-modified glass slide ( $\theta \approx 48^\circ$ , PC II,

## 5. Electrochemical Grippers for Micro- and Nanorobotics: Manipulation by Tuning Surface Forces

cf. Fig. 6c). The different substrates allowed to demonstrate that manipulation can be performed on a large range of surface chemistries. Additionally, the size of the accessible working area is in this approach only limited by the size of the used liquid cell. The latter substrate has the advantage that the manufactured structures remain much more stable due to the stronger adhesion forces between deposited particles and the substrate.

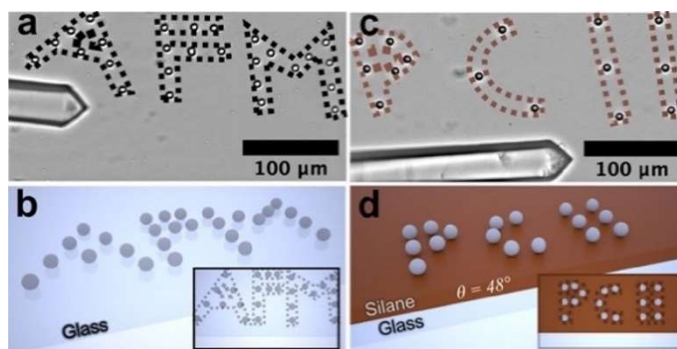


Figure 6. Creating complex structures by electrochemical manipulation. (a) Particle structure on a bare glass substrate; the dashed lines serve only to highlight the text 'AFM'. (b) Schematic representation of the structure shown above. (c) Another structure but formed on a silane-modified glass slide ( $\theta = 48^\circ$ ). The adhesion forces are higher, leading to more stable structures with a lower gripping probability. The abbreviation 'PC II' stands for 'Physical Chemistry II'. (d) Schematic representation for structure in (c).

### Discussion

Tuning surface forces by electrochemistry is a highly universal approach for micro- as well as nanorobotics as it does not require complicated grippers or nanofluidic probes. Most importantly, it can be easily scaled down. The here-presented electrochemical approach can be directly integrated into existing commercial AFMs. Tuning of surface forces by applying potentials is much more direct and faster compared to stimuli-responsive layers that change their surface properties in terms of pH-value or illumination. In particular, the electrochemical grippers can be coupled to a computer in a very direct manner, as most commercial potentiostats can be directly interfaced. Simple electrical signals can then be used as triggers to 'pick' and 'release' objects. Thereby, it will be easily possible to 'mimic' handling algorithms common for macroscopic robotics, in particular 'pick and place' (cf. Fig. 1). The general idea of the electrochemical approach is somehow related to the application of electrostatic forces in air<sup>6,24,38,68</sup>. However, long-ranged electrostatic forces are only working in air or vacuum and requires large potentials and objects with sufficient intrinsic charge. By

## 5. Electrochemical Grippers for Micro- and Nanorobotics: Manipulation by Tuning Surface Forces

---

contrast, the electrochemical gripper represents also an 'electrical' approach, but operates with small currents and potentials and, most importantly: Working in liquids, and in particular electrolytes, represents the native environment for this electrochemical approach. As there are no mechanical parts, it is open to miniaturization and does not need external hydraulic or pneumatic pumps. Thus, it can be incorporated in autonomous micro- and nanorobotic approaches presented so far<sup>69</sup>. It should be noted that the potential applied here is sufficiently small compared to the potentials where electrolysis of water is taking place ( $E = + 1.23 \text{ V vs SHE}$  cf. ref.<sup>70</sup>) Hence, no development of gas bubbles is observed, neither for the flat electrodes nor for electrochemical grippers.

Currently, micro- and nanomanipulation by AFM is based practically exclusively on applying lateral forces with the tip and 'pushing' or 'dragging' the objects over the substrate<sup>3</sup>. The limitations of this established approach are evident: On the one hand the danger of mechanical damage and on the other hand the restriction to two-dimensional structures. By contrast, the electrochemical gripper allows not only for overcoming these limitations but is also a much more universal approach; It can be scaled down easily and could be also merged with other approaches from robotics, such as autonomous robots or soft robots. By 'grabbing' an object, placing it at a defined position, and then 'releasing' it, no shear forces are applied. Such forces are known to destroy samples, in particular soft, biological ones. Additionally, 'gripping' evades the central problem of push-manipulation: During the process, the object, which has to be manipulated must remain in contact with the substrate. Hence, extending structures into the third dimension or manipulation on rough substrates is intrinsically problematic to impossible. Moreover, the technique does not allow to separate objects that are attached to each other by van der Waals forces, e.g. colloidal particles. The same would be valid if adhesive forces between particles are too strong to be overcome by a repulsive force due to the externally applied potential. However, we did not encounter these situations normally in our manipulation experiments that concentrated on the preparation of 2D-structures. In the case of 3D-structures these situation would be encountered to a much higher degree.

Another important advantage of the electrochemical grippers is the possibility of merging them with existing algorithms from AFM-based nanomanipulation and macro/micro-robotics<sup>20,71-73</sup>. Commonly, AFM-based nanomanipulation is founded on laterally pushing a particle or object by applying shear forces. Imaging and manipulation are both based on AFM<sup>8</sup>. By applying different potentials it would be possible to pick and place the particle directly, while imaging would still be possible with the potentials leading to repulsive

## 5. Electrochemical Grippers for Micro- and Nanorobotics: Manipulation by Tuning Surface Forces

interactions. In the case of coupling electrochemical grippers with an AFM, the accuracy of the positioning is given by the lateral resolution of the piezo-scanners, which is on the Angstrom level. However, in combination with coarse positioning by stepper motors the range is practically limited only by the dimension of the liquid cell. If the particles are large enough to be identified by optical microscopy, algorithms utilized by automated micromanipulation in combination with optical or electron microscopy can be applied directly<sup>74-77</sup>.

What are the fundamental limitations of electrochemical grippers? Firstly, such grippers will only work in liquid media, mainly electrolytes, in order to guarantee potentiostatic control and suppress capillary forces. However, for biomedical applications and most cases of nanofabrication, especially with soft materials or nanoparticles, the liquid phase is not a limitation but a requirement. One limiting factor for biological samples would be surface fouling. To prevent this, especially in high ionic strength solutions, an antifouling agent, like an amphifunctional thiol-SAM, could be incorporated into the gripper<sup>78-80</sup>. Additionally, the gripper electrode could be cleaned by cyclic voltammetry as it can be performed for flat electrodes<sup>81</sup>. High ionic strengths of electrolyte solution will lead to smaller forces due to reduced diffuse layer overlap<sup>41,63,64</sup>. However, increased viscosity would not represent a problem<sup>36</sup>. Hence, also manipulation in ionic liquids would be possible, provided that an electrochemical control of the gripper electrode can be ensured. Secondly, there is only a certain size range for the objects that can be handled: Too small, then the van der Waals forces would dominate; too big, the surface forces cannot compensate for gravitational effects. Essentially, the diffuse layer overlap should allow for tuning the overall interaction, which is possible for a wide range of adhesion forces due to hydrophobicity. For hard colloidal particles the size range starts approximately at 50–100 nm and goes up to 5–8  $\mu\text{m}$ , also depending on their surface charge, roughness, and density, respectively. However, for larger particles conventional mechanical grippers would be most-likely a more convenient method for manipulation. Thus, the here-presented approach of electrochemical grippers allows to bridge the gap between objects of the micro- and the nanoscale for two-dimensional manipulations. Objects smaller than 100 nm might be handled, but low van der Waals forces would be necessary, which requires small Hamaker constants. Luckily, materials that fulfill these requirements would be the most interesting for robotics at this length scale: macromolecules, like proteins or lipids. For both, it has been reported that their adhesion to electrodes can be tuned and adsorption as well as desorption can be controlled depending on the externally applied potential<sup>82,83</sup>. However, with decreasing size of the objects, the

## 5. Electrochemical Grippers for Micro- and Nanorobotics: Manipulation by Tuning Surface Forces

---

geometry and dimensions of the tip become more important and would have to be adapted specifically<sup>84,85</sup>. In particular, as an AFM tip might be needed for manipulation as well as for imaging. In summary, a size range of colloidal particles of 0.7–8  $\mu\text{m}$  would be readily accessible by the here-presented grippers. Most likely also very soft objects, such as hydrogel particles<sup>86</sup> can be handled provided that the adhesion hysteresis is not too large. In this respect, the possibility to ‘switch’ the charging state and thus the interaction forces may become very helpful to tune the tip for imaging without unintentionally disturbing and thus manipulating the objects. Moreover, the surface modification of the electrode and its roughness allow additional tuning of the interaction forces by tuning the contribution of solvent exclusion and the extent of diffuse layer overlap during contact as reported previously<sup>41</sup>. In difference to previously reported robotic grippers that are based on the electrochemical switching of a hydrogel coating<sup>27</sup>, the electrochemical grippers developed here are based on a direct manipulation of the interaction forces without an intermediate electrochemically active layer<sup>27</sup>. This additional layer provides the advantage of large adhesion forces and is, therefore, highly appropriate for macroscopic surfaces but is limited at smaller length scales due to the film morphology and thickness. At small length scales, the surface forces due to the diffuse layer are sufficient for manipulation. The lateral resolution of the positioning with electrochemical grippers is in principle only limited by the actuators. Here, the grippers have been implemented on an AFM- cantilever, thus the positioning resolution is in the sub-nanometre regime. Therefore, the main limitation is given by the dimension of the AFM-cantilever and the resolution of the optical microscope used to control the manipulation process. However, the here-presented grippers can also be used in combination with alternative actuation systems that are more suitable for soft robotics<sup>14,15</sup>.

### Methods

**Materials.** Tipless gold-coated AFM-cantilevers used for the preparation of colloidal probes and electrochemical grippers were obtained commercially (CSC-37, Cr–Au coated from both sides,  $\mu$ masch, Tallinn, Estonia). Cathodic insulating paint (Clearclad HSR, Clearclad Coatings Inc.) was used for the insulation of the electrochemical grippers. Silica particles with a nominal average diameter of 6.8  $\mu$ m (Bangs Laboratories Inc.) were used to prepare colloidal probes for direct force measurements and for manipulation. UV curing adhesive (NOA63) was purchased from Norland products. Red insulating resist was purchased from GC Waldom. All aqueous solutions have been prepared with deionized water of Milli-Q grade (resistivity  $> 18 \text{ m}\Omega \text{ cm}^{-1}$ , Merck Millipore, Darmstadt, Germany). Ionic strength and pH of the solutions were adjusted to pH 4 and ionic strength of 0.1 mM using 1 M HCl (Titrisol, Merck, Darmstadt, Germany). All solutions were degassed for at least 60 min before the experiments and filtered using a syringe filter with a pore size of 0.22  $\mu$ m (Rotilabo, Carl Roth, Karlsruhe, Germany). Methoxy(dimethyl)octylsilane, ferrocyanide, ferricyanide, 11-mercapto-1-undecanol, chloroform, potassium nitrate were purchased from Sigma Aldrich. Hellmanex III was purchased from Hellma (Mühlheim, Germany). Silver wires insulated with polyimide and a diameter of 0.125 mm were purchased from Advent (Advent research materials, Oxford, England). Ethanol of HPLC grade was purchased from Carl Roth (Carl Roth, Karlsruhe, Germany).

**Preparation of electrochemical grippers and cyclic voltammetry.** Gold-coated AFM-cantilevers were cleaned by dipping in ethanol and chloroform, followed by subsequent air plasma treatment (Zepto, Diener electronic, Ebhausen, Germany) for 30 min. An additional gold layer (99.99%) with a thickness of at least 100 nm was evaporated onto the cantilevers using a tectra minicoater (tectra, Frankfurt, Germany) to prevent complete removal of the gold in the focused ion beam (FIB) treatment. In order to contact the cantilever, a polyimide-insulated silver wire was connected to the cantilever chip by silver paint (G302, PLANO, Germany), fixated, and insulated using an UV-curing adhesive. Cathodic insulating paint was electrodeposited onto the cantilevers by applying  $-3 \text{ V}$  for 120 s in a 1:5 solution (v/v) of Clearclad-HSR and water. The electrodeposition was performed three times for each cantilever, with a rinsing step (water and ethanol) between each cycle. The insulated cantilevers were annealed at  $180 \text{ }^\circ\text{C}$  for 1 h. The wire's contact was insulated further using insulating resist. For FIB-milling, a FEI SCIOS-FIB was used with a milling

## 5. Electrochemical Grippers for Micro- and Nanorobotics: Manipulation by Tuning Surface Forces

---

depth of 50 nm. All SEM images shown were also acquired at the same SEM.

FIB-milled cantilevers were cleaned afterwards by dipping them in ethanol and water, followed by UV-cleaning (Model 18, Jelight Inc.) for 10 min and subsequent dipping in ethanol. The FIB-milled cantilevers were then immersed into a 5 mM 11-mercapto-1-undecanol solution in ethanol for 1 h and rinsed with ethanol afterwards. The spring constants have been determined by fitting the thermal noise spectra (Hutter-Bechhoefer method)<sup>87</sup>.

Cyclovoltammetric measurements were conducted in an aqueous solution of 5 mM ferrocyanide, 5 mM ferricyanide, and 100 mM KNO<sub>3</sub> using a potentiostat (CH 750i, CH-Instruments)<sup>49</sup>. The scan rate used was 0.01 V/s.

**Surface modification.** First, glass slides were cleaned using a 2% aqueous Hellmanex solution in an ultrasonic bath for 40 min at 40 °C, followed by 10 min air plasma treatment. The silane modification has been carried out by chemical vapor deposition with methoxy(dimethyl)octylsilane. The glass slides were put in a desiccator together with 30  $\mu$ L methoxy(dimethyl)octylsilane. The desiccator was evaporated and placed in an oven at 90 °C for 20 min, 35 min, or 60 min, respectively. Static water contact angles for all substrates were determined by the sitting drop method (OCA-20, Dataphysics, Filderstadt, Germany).

**Colloidal probe measurements on glass surfaces.** Silica beads were glued onto tiplless AFM cantilevers using UV-curable glue (NOA 63, Norland Adhesives) by means of a micromanipulator (DC-3 KS, Märzhäuser, Wetzlar, Germany). The micromanipulator was mounted on a fixed-stage microscope (Examiner, Zeiss, Oberkochen, Germany). The cantilever was cleaned beforehand by rinsing with ethanol and MQ-water, followed by 10 min plasma cleaning. For the gluing first, a small drop of glue with a diameter slightly less than the ones of colloidal particles has been placed on the cantilever. Then a freshly etched tungsten wire has been used to place a colloidal particle in the glue drop. Curing was carried out with the mercury lamp attached to the optical microscope. The procedure was similar to the one reported previously<sup>41</sup>. All force measurements were performed with a dedicated atomic force microscope (MFP 3D, Asylum Research, Abingdon, United Kingdom) mounted on an inverse optical microscope (Observer, Zeiss, Oberkochen, Germany). For determining the effective potential and regulation parameter  $p$  of the silica beads, 30 consecutive force curves were measured with a silica colloidal probe against silica beads glued to a glass substrate. The force curves were fitted using a homemade algorithm taking charge regulation into account<sup>53</sup>. For the measurement of substrate adhesion 30 force curves were

## 5. Electrochemical Grippers for Micro- and Nanorobotics: Manipulation by Tuning Surface Forces

---

measured with colloidal probes against the silane covered glass slides and bare glass slides, respectively. Adhesion forces were determined from the force-curves based on a custom written procedure in IGOR PRO (Wavemetrics) that determined the absolute minima in the force-curves upon retraction.

**Direct force measurements under potentiostatic control.** For the potentiostatically controlled direct force measurements, silica-particles were glued onto a Hellmanex-clean glass slide using NOA 63 and a micromanipulator attached to an optical microscope (Examiner, Zeiss, Oberkochen, Germany). For the preparation of colloidal probes, first a small drop of UV-curing NOA 63 glue was picked up with an etched tungsten wire, and placed on the substrate. A silica particle, dried from aqueous solution onto a clean glass slide, was placed onto the drop with a clean micromanipulator needle. The placed bead was cured for 1 min with UV light. For the force measurements, 30 force curves were performed in an aqueous solution (ionic strength of 0.1 mM and pH 4). The working electrode was the electrochemical gripper electrode, a Pt-wire was used as counter electrode and a chlorinated Ag/AgCl wire was used as a pseudo reference electrode. The electrochemical cell has been controlled by the same potentiostat also used for CV-measurements. The half-cell potential of the pseudo-reference was controlled against a calomel electrode (RE2, BASi Inc.) in an aqueous solution with ionic strength of 0.1 mM and pH 4. Force deflection curves were averaged and evaluated using a homemade procedure. Approach and retraction curves have been baseline corrected individually.

**Particle manipulation by electrochemical grippers.** Silica particles were sedimented on a plasma- clean glass slide in aqueous solution with ionic strength of 0.1 mM and pH 4. The electrochemical cell and potentiostat were the same as described for the potential dependent force measurements. After alignment using the optical microscope, a potential of  $\phi = +726$  mV vs. SCE was applied to the cantilever, and the cantilever was approached toward the bead using the z-piezo. After withdrawal, the particle stuck to the cantilever. XY-movement was done using micrometer screws. For particle placement, a potential of  $\phi = -474$  mV vs. SCE was applied to the cantilever, and the cantilever was approached to the substrate using the z-piezo movement.

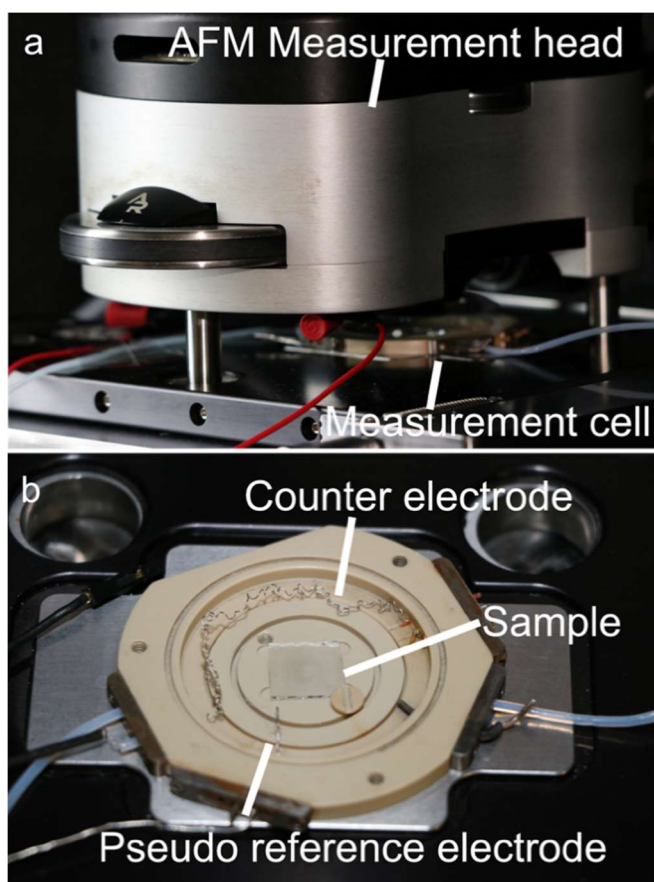
## **Acknowledgements**

The authors are very grateful to LHV Coatings Ltd for providing the electro-paint that has been used for isolating the cantilevers. The authors thank Patrick Knödler for the preparation of probes by FIB and Philipp Dennstedt for his support with the macroscopic robot. Andreas Mark helped with direct force measurements. Publication was funded by the Deutsche Forschungsgemeinschaft (DFG, German Research Foundation) – 491183248 and by the Open Access Publishing Fund of the University of Bayreuth.

## Supplementary Materials

### S.1 Setup for electrochemical control

For direct force measurements under potentiostatic control, an electrochemical cell consisting of a pseudo Ag/AgCl reference electrode fabricated by electrochemically covering an PTFE-insulated Ag wire with an AgCl layer (AC1-01 Automatic Chlorider, NPI electronic GmbH) and a coiled Pt-wire as counter electrode were used. Supplementary Fig. 1 shows photographic images of the AFM setup and the electrochemical cell.

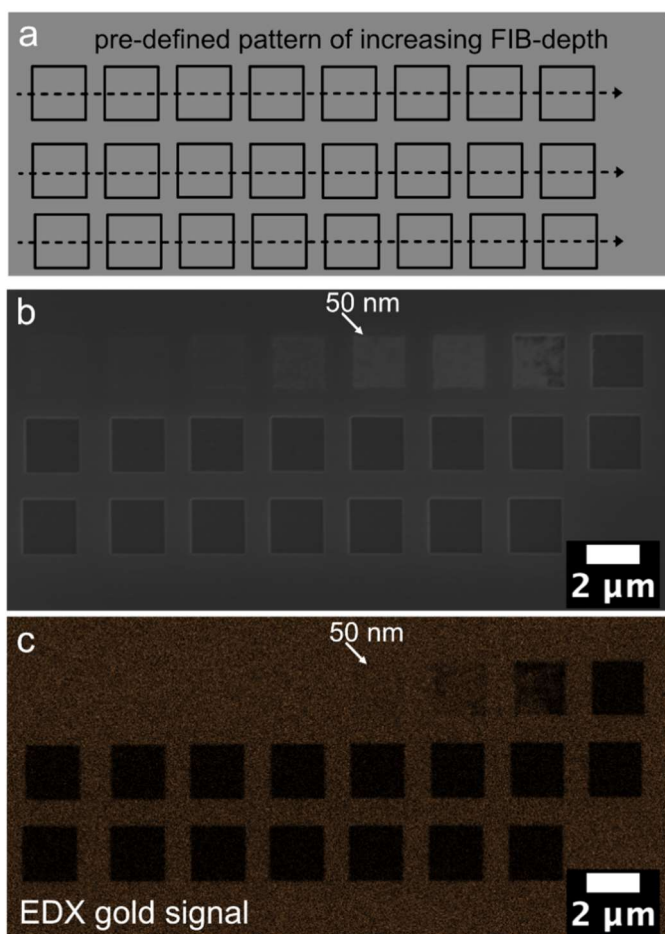


Supplementary Figure 1. Setup for direct force measurements under potentiostatic control and manipulation with an electrochemical gripper. (a) AFM head used for measurements in this work, with connected electrochemical measurement cell. (b) Electrochemistry cell for AFM measurements in liquid, with a chlorinated silver wire as pseudo reference and a Pt-wire as counter electrode. Here, a glass substrate is installed as sample.

## 5. Electrochemical Grippers for Micro- and Nanorobotics: Manipulation by Tuning Surface Forces

### S.2 Focused ion beam (FIB) milling depth

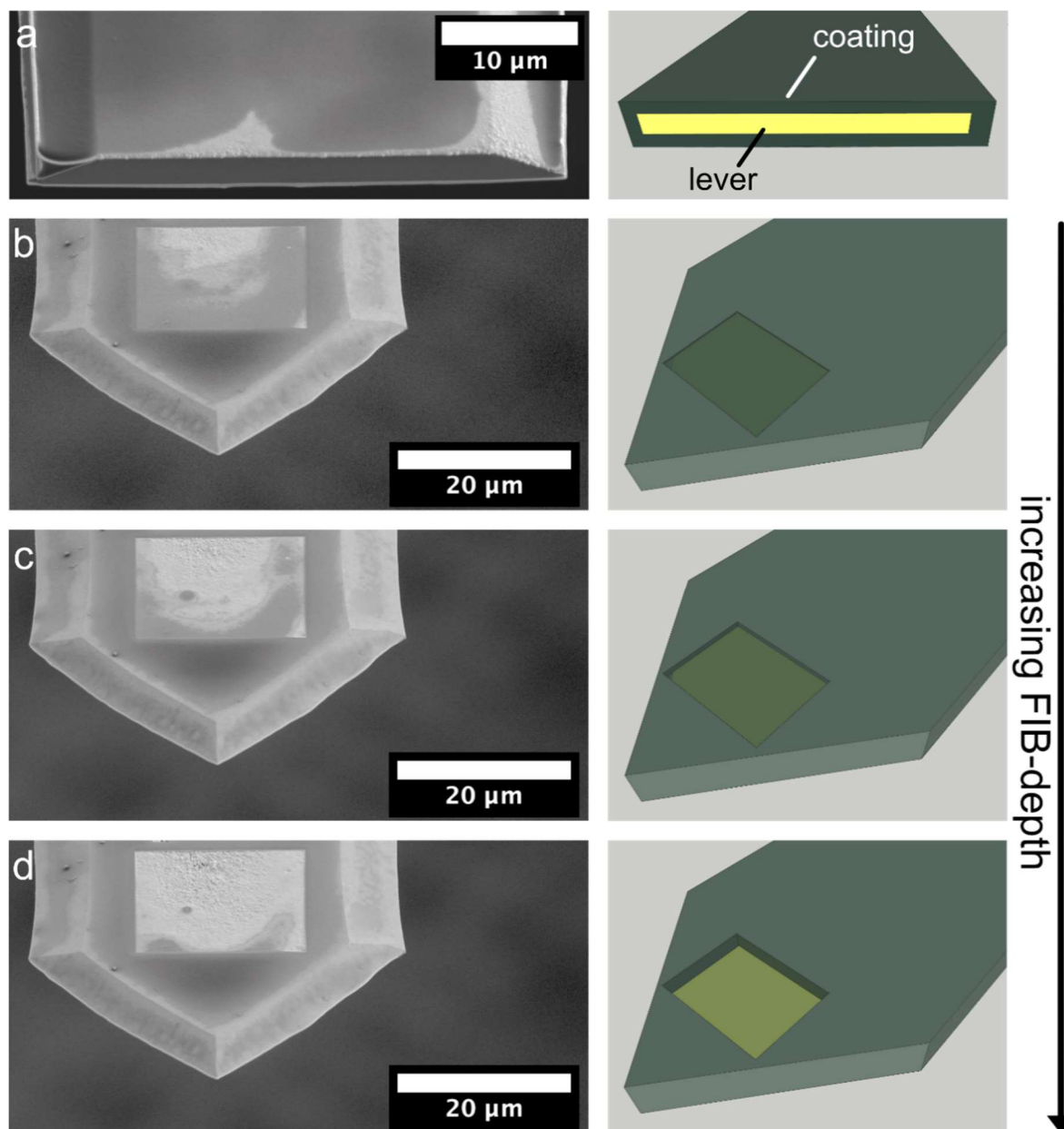
FIB-milling parameters for production of electrochemical grippers were determined experimentally by writing patterns with increasing FIB milling depth into the chip of an insulated cantilever. To determine the correct milling depth, namely just uncovering the gold surface while circumventing residual insulating film on the surface and preventing a complete removal of the gold, EDX and BSD images were used. As a result of this experiments, we chose a milling depth of 50 nm for preparation of electrochemical grippers.



Supplementary Figure 2. Focused ion beam (FIB) milling of an insulating film on a flat substrate. (a) Schematic of a preliminary FIB-milling experiment. A pattern with FIB-milling depth increasing in 10 nm steps was milled into an insulated cantilever to find the ideal milling-depth. (b) SEM-image of FIB-milling tests. (c) Corresponding gold-EDX map. While the removal of insulating film is not visible because of the low thickness of the insulation film, a damaging of the gold is visible for FIB-depths that were too deep, like 70 nm in this case. The milling-depth that did not show any damaging of the gold layer, marked as "50 nm", was chosen for electrochemical gripper preparation.

### S.3 FIB-milling on AFM-cantilever

Using the parameters determined in S.2, a rectangular pattern was milled onto the free end of an insulated cantilever in several steps to exclude different behavior of insulating film on the chip and at the cantilever free end. An overview over a completely milled insulated cantilever and individual milling steps is shown in Supplementary Figure 3.



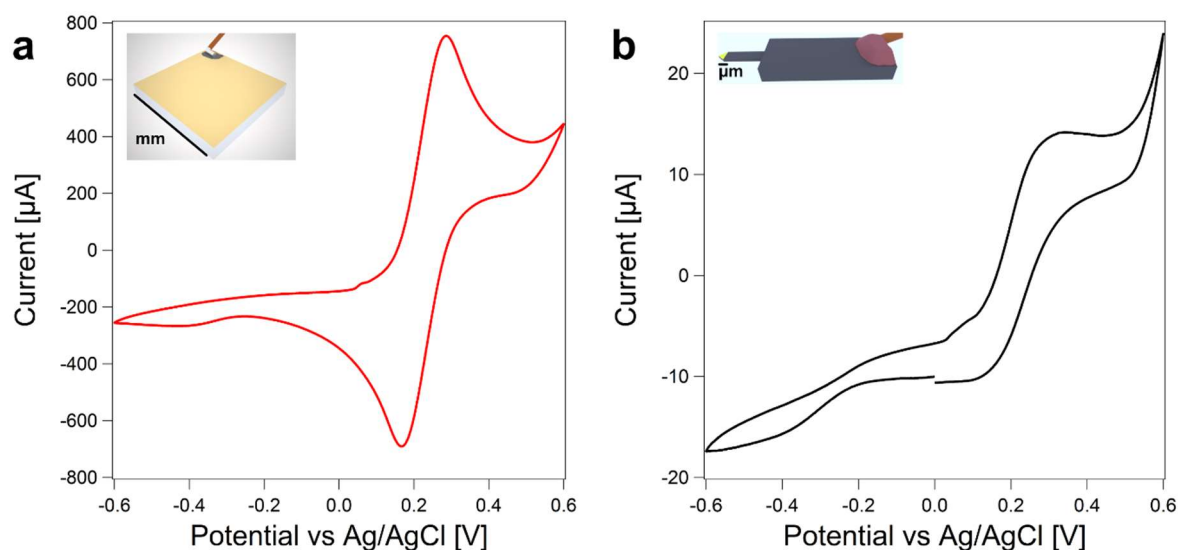
Supplementary Figure 3. FIB milling of an electrode on an insulated cantilever. (a) A cantilever that was cut through by FIB-milling to image the structure of the insulating film. (b) an initial FIB-milling depth of 30 nm in a rectangular shape. The non-insulated gold surface is visible brighter than the insulating film. (c) SEM image after another 10

## 5. Electrochemical Grippers for Micro- and Nanorobotics: Manipulation by Tuning Surface Forces

nm FIB-milling step. (d) SEM-image after another subsequent 10 nm FIB-milling step, amounting to 50 nm total FIB milling depth.

### S.4 Electrochemical characterization

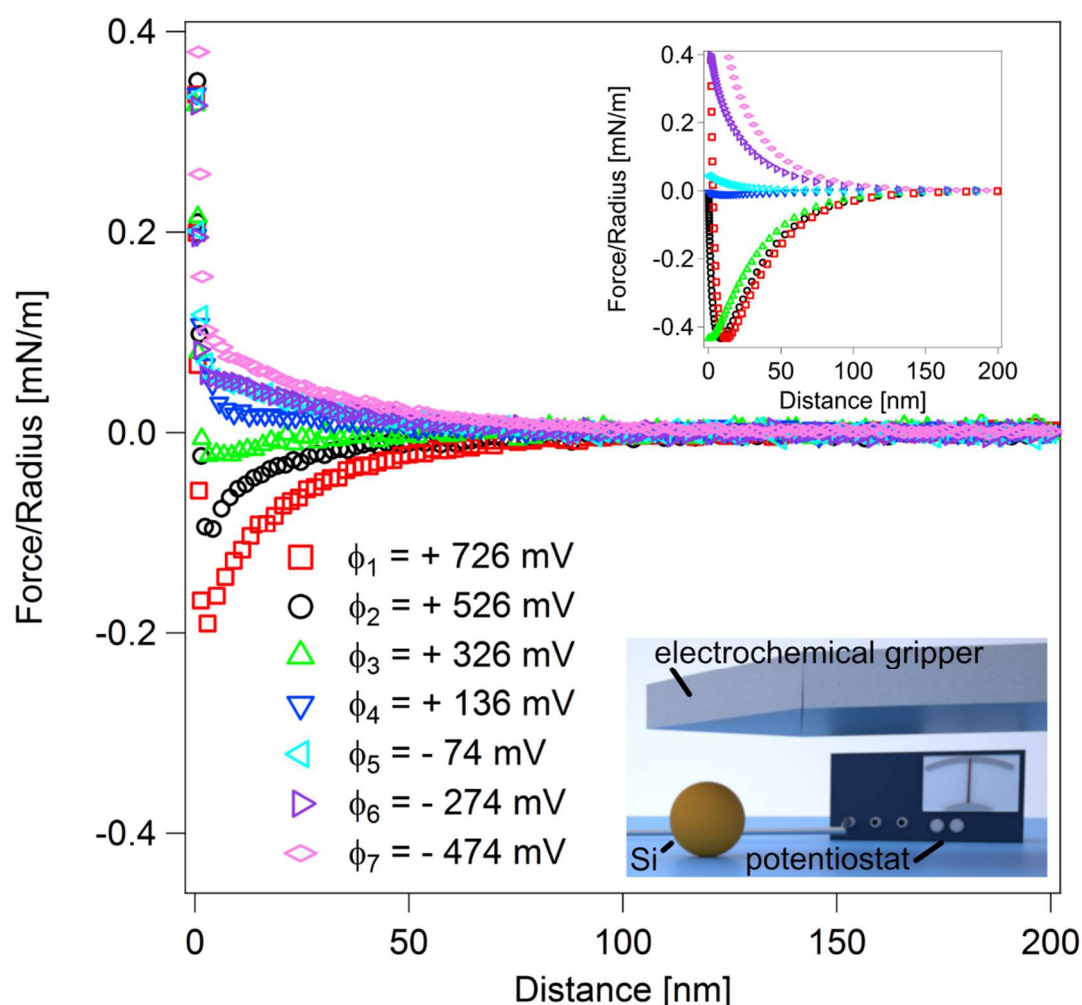
To examine the electrochemical activity of electrochemical grippers, cyclic voltammetric experiments were done with both macroscopic electrodes and electrochemical grippers. The resulting cyclic voltammograms are shown in Supplementary Fig. 4.



Supplementary Figure 4. Electrochemical characterization by cyclic voltammetry (a) Cyclovoltammetric measurement of a macroelectrode (11 mm x 11 mm) in aqueous solution of ferrocyanide (5 mM) /ferrocyanide (5 mM) and 0.1 M  $\text{KNO}_3$  obtained at scanning speeds of 0.01 V/s. The current signal shows the isolated shapes at 0.3 V and 0.18 V expected for a macroelectrode. (b) Cyclovoltammetric measurement of a FIB- Cantilever electrode with an area in the  $\mu\text{m}$ -range. A superposition of isolated reduction and oxidation peaks onto the sigmoidal shape that is typical for the cyclovoltammogramm of a ultramicroelectrode is visible.

### S.5 Potential-dependent force measurements

To determine the behavior of electrochemical grippers under potentiostatic control during force-measurements, Force-Distance curves on immobilized silica particles were measured using a potentiostatic controlled electrochemically gripper while applying different potentials on the free electrode at the cantilever end. The resulting force curves are shown in Supplementary Fig. 4. For all potentials higher than +136 mV, attractive behavior was visible, while for the more negative potentials repulsive behavior can be observed.



Supplementary Figure 5. Force versus distance profiles for different applied potentials. Measured force vs distance curves of a cantilever electrode against an immobilized silica bead depending on the applied potential in aqueous solution (pH = 4, I = 0.1 mM). All potentials shown were normalized against a SCE electrode. For a high negative potential, the curve is completely repulsive. The more positive the applied potential gets, the less repulsive is the force curve. From +326 mV vs SCE, an attractive interaction can be observed, that gets more attractive for more positive

## 5. Electrochemical Grippers for Micro- and Nanorobotics: Manipulation by Tuning Surface Forces

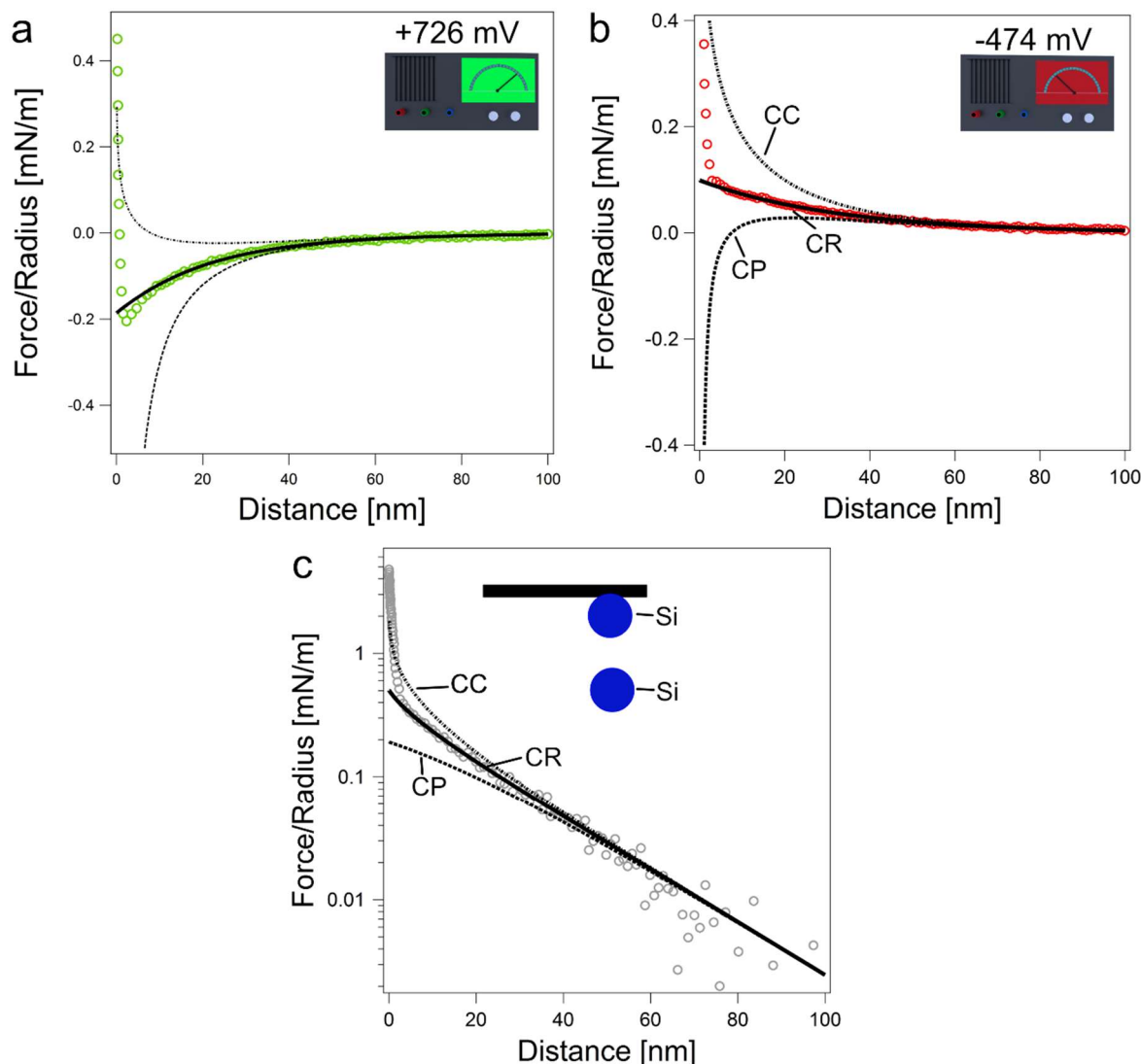
---

applied potentials. The inset shows force curves that were calculated using the Poisson-Boltzmann equation and consideration of charge regulation. As values for the effective potentials of the electrode, literature values were used <sup>41</sup>. The effective potential and regulation parameter for the silica beads was determined by symmetric measurements (cf. Fig. S6).

## 5. Electrochemical Grippers for Micro- and Nanorobotics: Manipulation by Tuning Surface Forces

### S.6 Poisson-Boltzmann theory

To further analyze the behavior of the electrochemical grippers at the potentials used for manipulation, their force profiles were fitted to the full Poisson-Boltzmann equation while taking into account charge regulation. The resulting fits are shown in Supplementary Fig. 6.



Supplementary Figure 6. Fitting the force profiles to the full solutions of the Poisson-Boltzmann equation including charge regulation. (a) PB-fit with consideration of charge regulation of a force curve of a cantilever electrode against an immobilized bead while applying a potential of 726 mV vs SCE, the potential that was also used for manipulation experiments in aqueous solution (pH = 4, I = 0.1 mM) Charge regulation takes into account the charge regulation parameter  $p$ , which assumes values in a range between  $p=0$  and  $p=1$ . The dashed lines indicate the classical boundary conditions needed for a solution of the Poisson-Boltzmann equation. The boundary condition for  $p=0$  is the constant potential (CP) condition, indicating a constant diffuse layer potential for all separations. Meanwhile,  $p=1$  corresponds to the constant charge (CC) condition, indicating a layer of ions is adhering to the surface, and therefore

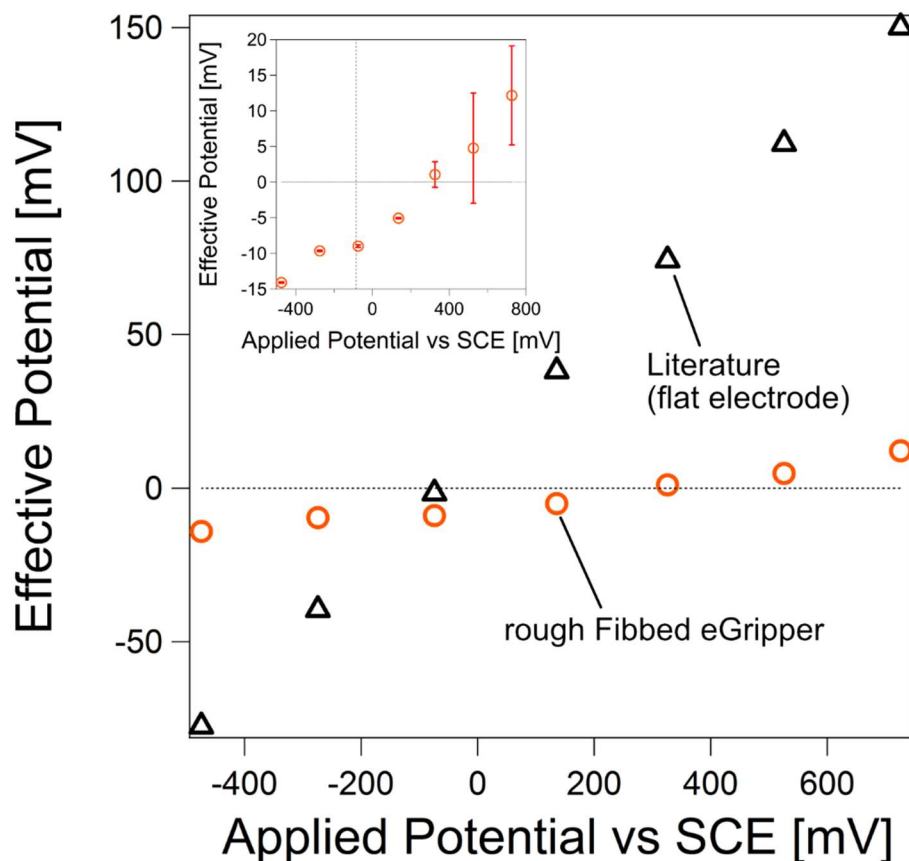
## 5. Electrochemical Grippers for Micro- and Nanorobotics: Manipulation by Tuning Surface Forces

---

leading to a constant charge density over all separations. The solid line represents fits to the constant regulation (CR) approximation, which accounts for charge regulation between two surfaces. For small distances, the CR approximation allows for a good description of interaction forces.<sup>53,64</sup> (b) PB Fit of a force curve with an applied potential of -474 mV vs SCE for the analogous experiment. (c) PB-Fit for the measurement of a colloidal probe against an immobilized silica particle to determine the effective potential  $\Psi$  and regulation parameter  $p$  of a silica colloidal probe. The effective potential was determined to be  $\Psi = -24$  mV, while the regulation parameter was determined to  $p=0.92$

### S.7 Comparison of electrochemical gripper and flat electrode

The effective potentials for the electrochemical grippers used in this work were determined by PB-fitting as shown in Supplementary Fig. 6 for all potentials used in S.5. Supplementary Fig. 7 shows a comparison of these potentials with the potentials on a flat electrode determined by Kuznetsov et al. <sup>41</sup>.



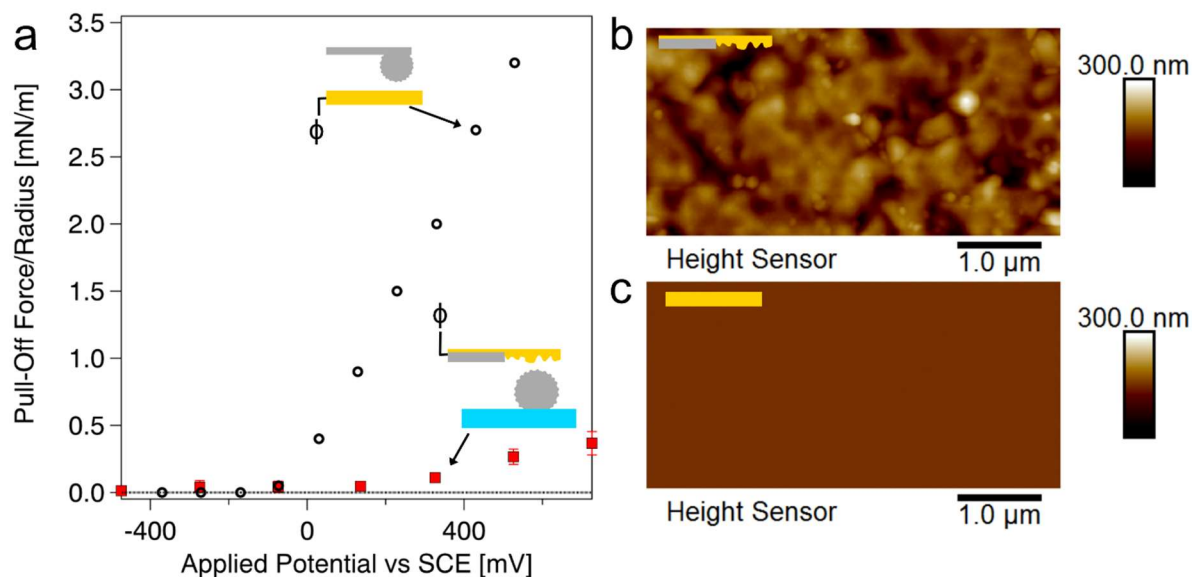
Supplementary Figure 7. Diffuse layer potentials as function of the applied potential to the electrochemical gripper.

The effective potentials determined by PB fitting (cf. Fig. S6) are shown as a function of the applied potentials. The inset shows a close-up of the data obtained in this work. The dotted line shows the potential of zero charge from Kuznetsov et al.. The effective potentials from this work for FIB-milled electrochemical grippers are compared with literature values of Kuznetsov et al. <sup>41</sup>, who did a similar experiment for colloidal probe vs ultraflat gold electrodes with applied potential. The slope of the values is lower for the electrode cantilevers. We blame this disparity on the roughness of the electrode (cf. Fig. S9), since during the measurement parts of the silica colloids could not have been in contact with the electrode of the electrochemical gripper as a result of the high roughness.

## 5. Electrochemical Grippers for Micro- and Nanorobotics: Manipulation by Tuning Surface Forces

### S.8 Adhesion on electrochemical gripper

The pull-off force of electrochemical grippers against immobilised silica particles were determined for various applied potentials from force-distance curves (cf. Supplementary Fig. 5). Supplementary Fig. 8 shows a comparison with an inverted setup- a standard colloidal probe against a flat electrode under potentiostatic control and their respective surface topography.

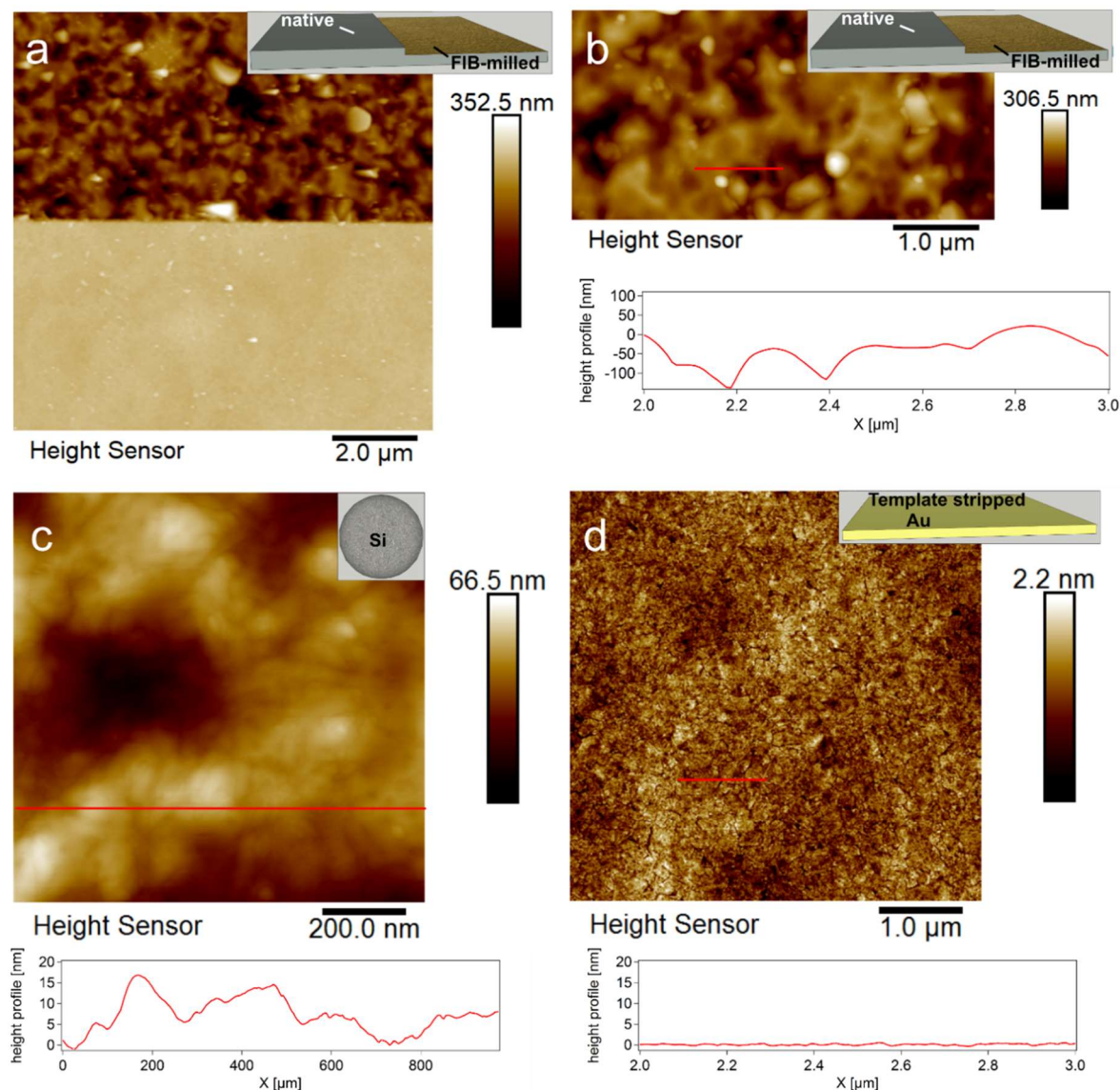


Supplementary Figure 8. Adhesion between silica particles and the electrochemical gripper. (a) The pull-off force (the absolute value of the adhesion force  $F_{\text{Adh}}$ ) with a OH-terminated microelectrode cantilever against an immobilized silica bead is shown depending on the applied potential (red). For comparison, the pull-off force from for an inverse system, where the cantilever is immobilized on the cantilever as colloidal probe and measured against a ultraflat gold lectrode modified with OH-silane. The microelectrode cantilever shows a much lower pull-off force even for high attractive applied potentials. A possible reason for this is the high roughness of the microelectrode cantilever (cf. Fig. S9). (b) AFM topography image of electrochemical gripper (top) and ultraflat gold electrode (bottom), indicating the higher roughness of the FIB-milled electrochemical gripper.

## 5. Electrochemical Grippers for Micro- and Nanorobotics: Manipulation by Tuning Surface Forces

### S.9 Surface roughness comparison

We compared the surface roughnesses of FIB-milled electrodes, silica particles used in this study and template stripped gold electrodes used for adhesion experiments (cf. Supplementary Fig. 8). The resulting AFM topography images and profiles are shown in Supplementary Fig. 9.



Supplementary Figure 9. Comparison of surface roughness. (a) Height image of the microelectrode cantilever as measured using a Bruker Icon AFM equipped with a OTESPA R3 cantilever in tapping mode. The smooth area on the bottom is the insulating film. The rough part on top is the FIB-milled gold area. (b) Topography of FIB-milled gold area and section through the height image. The position of the section is marked in the topography image. A roughness with valleys as low as 100 nm can be observed as result of the FIB-milling process. (c) Topography image of the silica beads used in this work, and section through the topography, showing the microroughness caused by Stöber-synthesis. These roughness decreases the adhesion compared to JKR theory.<sup>88</sup> (d). Topography of ultraflat gold electrode, as

## 5. Electrochemical Grippers for Micro- and Nanorobotics: Manipulation by Tuning Surface Forces

---

used in the work of Kuznetsov et al.<sup>41</sup> (cf. Fig S7). The same flat electrodes have been used to determine the pull-off forces for the inverse system (cf. Fig S8). An almost ideal flat surface is present.

While microroughness is most critical during adhesion<sup>88</sup>, the high roughness of the electrochemical grippers could lead to a nonuniform part between the gripper and the particle, explaining in part the inferior pull-off force compared to the inverse system (cf. Fig. 8), as well as the lower effective potential compared to literature (cf. Fig. 6).

## 5. Electrochemical Grippers for Micro- and Nanorobotics: Manipulation by Tuning Surface Forces

### S.10 Contact angle of silanized substrates

To determine the wettability of the silanized glass substrates used for adhesion experiment (cf. Fig. 4f), their contact angle was measured using sitting-drop method. The results are shown in Supplementary Table 1.

**Supplementary Table 1.** Contact angle measurements of methoxy(dimethyl)octylsilane (MDOS) -modified substrates.

Silanization duration [min]	20 min	35 min	60 min
Pos. 1l	49.3°	84.7°	104.9°
Pos. 1r	48.5°	84.5°	104.9°
Pos. 2l	48.4°	71.3°	97.6°
Pos. 2r	48.3°	69°	97.6°
Pos. 3l	46.6°	76.8°	100.5°
Pos. 3r	46.4°	76°	100.2°
Avg. $\theta \pm$ s.d.	47.9° $\pm$ 1.2°	77.1° $\pm$ 6.5°	101,0° $\pm$ 3.3°

### S.11 Movie of Manipulation experiments

We provide a sped-up movie (Supplementary Movie 1) showing the process of manipulating silica particles into complex structures by use of the electrochemical grippers presented in this work.

#### Link To Movie:

<https://www.nature.com/articles/s41598-023-33654-6#Sec16>

## References

1. Li, J. et al. Optical nanomanipulation on solid substrates via optothermally-gated photon nudging. *Nat. Commun.* **10**, 5672 (2019).
2. Min, Y., Akbulut, M., Kristiansen, K., Golan, Y. & Israelachvili, J. The role of interparticle and external forces in nanoparticle assembly. *Nature materials* **7**, 527-538 (2008).
3. Xie, H., Onal, C., Régnier, S. & Sitti, M. *Atomic Force Microscopy Based Nanorobotics* (Springer, Berlin Heidelberg, 2011).
4. Mavroidis, C. & Ferreira, A. *Nanorobotics: Current Approaches and Techniques* (Springer, New York, 2013).
5. Sitti, M. *Mobile Microrobotics* (MIT Press, Cambridge, 2017).
6. Li, J., de Ávila, B. E.-F., Gao, W., Zhang, L. & Wang, J. Micro/nanorobots for biomedicine: Delivery, surgery, sensing, and detoxification. *Sci. Rob.* **2**, (2017).
7. Sitti, M. Microscale and nanoscale robotic systems. *IEEE Robot. Autom. Mag.* **14**, 53-60 (2007).
8. Kim, S., Ratchford, D. C. & Li, X. Atomic Force Microscope Nanomanipulation with Simultaneous Visual Guidance. *ACS Nano* **3**, 2989-2994 (2009).
9. Bøggild, P. et al. Microfabricated tools for pick-and-place of nanoscale components. *IFAC Proceedings Volumes* **39**, 120-126 (2006).
10. Møhlhave, K., Wich, T., Kortschack, A. & Bøggild, P. Pick-and-place nanomanipulation using microfabricated grippers. *Nanotechnology* **17**, 2434-2441 (2006).
11. Dejeu, J., Bechelany, M., Rougeot, P., Philippe, L. & Gauthier, M. Adhesion control for micro- and nanomanipulation. *ACS Nano* **5**, 4648-4657 (2011).
12. Zubir, M. N. M., Shirinzadeh, B. & Tian, Y. Development of a novel flexure-based microgripper for high precision micro-object manipulation. *Sens. Actuator A Phys.* **150**, 257-266 (2009).
13. Huang, V. M. et al. Local electrochemical impedance spectroscopy: A review and some recent developments. *Electrochim. Acta* **56**, 8048-8057 (2011).
14. Shu, J. et al. A liquid metal artificial muscle. *Adv. Mater.* **33**, 2103062 (2021).
15. Liao, J. & Majidi, C. Muscle-Inspired Linear Actuators by Electrochemical Oxidation of Liquid Metal Bridges. *Adv. Sci.* **9**, 2201963 (2022).
16. Shi, C. et al. Recent advances in nanorobotic manipulation inside scanning electron microscopes. *Microsyst. Nanoeng.* **2**, 16024 (2016).
17. Dejeu, J. B., M., Philippe, L., Rougeot, P. & Michler, J. G., M. Reducing the adhesion between surfaces using surface structuring with PS latex particle. *ACS Appl. Mater. Interfaces* **2**, 1630-1636 (2010).
18. Gauthier, M., Régnier, S. & Rougeot, P. Analysis of forces for micromanipulations in dry and liquid media. *J. Micromechatron.* **3**, 389-413 (2006).
19. Garza, H., Ghatkesar, M., Basak, S., Löthman, P. & Staufer, U. Nano-Workbench: A Combined Hollow AFM Cantilever and Robotic Manipulator. *Micromachines* **6**, 600-610 (2015).
20. Yuan, S., Liu, L., Wang, Z. & Xi, N. *AFM-based Observation and Robotic Nanomanipulation* (Springer, Singapore, 2020).
21. Meister, A. et al. FluidFM: combining atomic force microscopy and nanofluidics in a universal liquid delivery system for single cell applications and beyond. *Nano Lett.* **9**, 2501-2507 (2009).

## 5. Electrochemical Grippers for Micro- and Nanorobotics: Manipulation by Tuning Surface Forces

22. Helfricht, N., Mark, A., Dorwling-Carter, L., Zambelli, T. & Papastavrou, G. Extending the limits of direct force measurements: colloidal probes from sub-micron particles. *Nanoscale* **9**, 9491-9501 (2017).
23. Mark, A., Helfricht, N., Rauh, A., Karg, M. & Papastavrou, G. The Next Generation of Colloidal Probes: A Universal Approach for Soft and Ultra-Small Particles. *Small* **15**, 1902976 (2019).
24. Lhernould, M. S., Delchambre, A., Régnier, S. & Lambert, P. Electrostatic forces in micromanipulations: Review of analytical models and simulations including roughness. *Appl. Surf. Sci.* **253**, 6203-6210 (2007).
25. Li, W. et al. Honeybee-inspired electrostatic microparticle manipulation system based on triboelectric nanogenerator. *Nano Energy* **104**, 107901 (2022).
26. Riccardi, M. & Martin, O. J. F. Electromagnetic Forces and Torques: From Dielectrophoresis to Optical Tweezers. *Chem. Rev.* (2023).
27. Huang, J. et al. Electrically programmable adhesive hydrogels for climbing robots. *Sci. Robot.* **6**, (2021).
28. Li, D. et al. Study on the Manipulation Strategy of Metallic Microstructures Based on Electrochemical-Assisted Method. *Micromachines (Basel)* **13**, 2151 (2022).
29. Kim, K. J. & Tadokoro, S. *Electroactive polymers for robotic applications* (Springer, London, 2007).
30. Shi, Y.-X. et al. Soft electrochemical actuators with a two-dimensional conductive metal-organic framework nanowire array. *J. Am. Chem. Soc.* **143**, 4017-4023 (2021).
31. Deng, Q. et al. Progress and prospective of electrochemical actuator materials. *Compos. Part A Appl. Sci. Manuf.* **165**, 107336 (2023).
32. Otero, T. F., Martinez, J. G., Fuchiwaki, M. & Valero, L. Structural electrochemistry from freestanding polypyrrole films: full hydrogen inhibition from aqueous solutions. *Adv. Funct. Mater.* **24**, 1265-1274 (2014).
33. Israelachvili, J. N. *Intermolecular and surface forces* (American Press, New York, 1992).
34. Sinniah, S. K., Steel, A. B., Miller, C. J. & Reutt-Robey, J. E. Solvent Exclusion and Chemical Contrast in Scanning Force Microscopy. *J. Am. Chem. Soc.* **118**, 8925-8931 (1996).
35. Noy, A., Vezenov, D. V. & Lieber, C. M. Chemical force microscopy. *Annu. rev. mater. sci.* **27**, 381-421 (1997).
36. Papastavrou, G. & Akari, S. Interaction forces between OH-groups in different solvents as observed by scanning force microscopy. *Colloids Surf. A Physicochem. Eng. Asp.* **164**, 175-181 (2000).
37. Raduge, C., Papastavrou, G., Kurth, D. G. & Motschmann, H. Controlling wettability by light: illuminating the molecular mechanism. *Eur. Phys. J. E* **10**, 103-114 (2003).
38. Kim, M. et al. Switchable Photonic Bio-Adhesive Materials. *Adv. Mater.* **33**, 2103674 (2021).
39. Serafin, J. M., Hsieh, S.-J., Monahan, J. & Gewirth, A. A. Potential dependent adhesion forces on bare and underpotential deposition modified electrode surfaces. *J. Phys. Chem. B* **102**, 10027-10033 (1998).
40. Campbell, S. D. & Hillier, A. C. Nanometer-scale probing of potential-dependent electrostatic forces, adhesion, and interfacial friction at the electrode/electrolyte interface. *Langmuir* **15**, 891-899 (1999).
41. Kuznetsov, V. & Papastavrou, G. Adhesion of Colloidal Particles on Modified Electrodes. *Langmuir* **28**, 16567-16579 (2012).

## 5. Electrochemical Grippers for Micro- and Nanorobotics: Manipulation by Tuning Surface Forces

42. Papastavrou, G. Combining electrochemistry and direct force measurements: from the control of surface properties towards applications. *Colloid Polym Sci.* **288**, 1201-1214 (2010).
43. Butt, H. J. Measuring electrostatic, van der Waals, and hydration forces in electrolyte solutions with an atomic force microscope. *Biophys. J.* **60**, 1438-1444 (1991).
44. Ducker, W. A., Senden, T. J. & Pashley, R. M. Direct measurement of colloidal forces using an atomic force microscope. *Nature* **353**, 239-241 (1991).
45. Kappl, M. & Butt, H. J. The colloidal probe technique and its application to adhesion force measurements. *Part. Part. Syst. Charact.* **19**, 129-143 (2002).
46. Yuan, C. C., Zhang, D. & Gan, Y. Invited Review Article: Tip modification methods for tip-enhanced Raman spectroscopy (TERS) and colloidal probe technique: A 10 year update (2006-2016) review. *Rev. Sci. Instrum.* **88**, 031101 (2017).
47. Karg, A. et al. A Versatile and Simple Approach to Electrochemical Colloidal Probes for Direct Force Measurements. *Langmuir* **37**, 13537-13547 (2021).
48. Mirkin, M. V. & Amemiya, S. *Nanoelectrochemistry* (CRC Press, Boca Raton, 2015).
49. Petrovic, S. Cyclic Voltammetry of Hexachloroiridate(IV): An Alternative to the Electrochemical Study of the Ferricyanide Ion. *Chem. Educ.* **5**, 231-235 (2000).
50. Ji, X., Banks, C. E., Crossley, A. & Compton, R. G. Oxygenated edge plane sites slow the electron transfer of the ferro-/ferricyanide redox couple at graphite electrodes. *ChemPhysChem* **7**, 1337-1344 (2006).
51. Butt, H.-J., Cappella, B. & Kappl, M. Force measurements with the atomic force microscope: Technique, interpretation and applications. *Surf. Sci. Rep.* **59**, 1-152 (2005).
52. Behrens, S. H. & Grier, D. G. The charge of glass and silica surfaces. *J. Chem. Phys.* **115**, 6716-6721 (2001).
53. Pericet-Camara, R., Papastavrou, G., Behrens, S. H. & Borkovec, M. Interaction between Charged Surfaces on the Poisson-Boltzmann Level: The Constant Regulation Approximation. *J. Phys. Chem. B* **108**, 19467-19475 (2004).
54. Rentsch, S., Pericet-Camara, R., Papastavrou, G. & Borkovec, M. Probing the validity of the Derjaguin approximation for heterogeneous colloidal particles. *Phys. Chem. Chem. Phys.* **8**, 2531-2538 (2006).
55. Trefalt, G., Palberg, T. & Borkovec, M. Forces between colloidal particles in aqueous solutions containing monovalent and multivalent ions. *Curr. Opin. Colloid Interface Sci.* **27**, 9-17 (2017).
56. Kaftan, O. et al. Probing multivalent host-guest interactions between modified polymer layers by direct force measurement. *J. Phys. Chem. B* **115**, 7726-7735 (2011).
57. Zyulkov, I. et al. Area-Selective ALD of Ru on Nanometer-Scale Cu Lines through Dimerization of Amino-Functionalized Alkoxy Silane Passivation Films. *ACS Appl. Mater. Interfaces* **12**, 4678-4688 (2020).
58. You, S. & Wan, M. P. Mathematical models for the van der Waals force and capillary force between a rough particle and surface. *Langmuir* **29**, 9104-9117 (2013).
59. Ramakrishna, S. N., Clasohm, L. Y., Rao, A. & Spencer, N. D. Controlling adhesion force by means of nanoscale surface roughness. *Langmuir* **27**, 9972-9978 (2011).

## 5. Electrochemical Grippers for Micro- and Nanorobotics: Manipulation by Tuning Surface Forces

60. Stevens, F., Lo, Y.-S., Harris, J. M. & Beebe, T. P. Computer modeling of atomic force microscopy force measurements: comparisons of Poisson, histogram, and continuum methods. *Langmuir* **15**, 207-213 (1999).
61. Hillier, A. C., Kim, S. & Bard, A. J. Measurement of double-layer forces at the electrode/electrolyte interface using the atomic force microscope: potential and anion dependent interactions. *J. Phys. Chem.* **100**, 18808-18817 (1996).
62. Serafin, J. M. & Gewirth, A. A. Measurement of adhesion force to determine surface composition in an electrochemical environment. *J. Phys. Chem. B* **101**, 10833-10838 (1997).
63. Rentsch, S., Siegenthaler, H. & Papastavrou, G. Diffuse Layer Properties of Thiol-Modified Gold Electrodes Probed by Direct Force Measurements. *Langmuir* **23**, 9083-9091 (2007).
64. Kuznetsov, V. & Papastavrou, G. Ion Adsorption on Modified Electrodes as Determined by Direct Force Measurements under Potentiostatic Control. *J. Phys. Chem. C* **118**, 2673-2685 (2014).
65. Borkowska, Z. & Hamelin, A. The influence of the crystallographic orientation on the double layer parameters of the Au/dimethylsulphoxide interface. *J. electroanal. Chem.* **241**, 373-377 (1988).
66. Trasatti, S. & Doubova, L. M. Crystal-face specificity of electrical double-layer parameters at metal/solution interfaces. *J. Chem. Soc. Faraday Trans.* **91**, 3311-3325 (1995).
67. Ahrens, P. et al. Influence of argon ion beam etching and thermal treatment on polycrystalline and single crystal gold electrodes Au (100) and Au (111). *J. Electroanal. Chem.* **832**, 233-240 (2019).
68. Liang, J. et al. Electrostatic footpads enable agile insect-scale soft robots with trajectory control. *Sci. Rob.* **6**, eabe7906 (2021).
69. Fischer, P. & Nelson, B. J. Tiny robots make big advances. *Sci. Rob.* (2021).
70. Bard, A. J. & Faulkner, L. R. *Fundamentals and applications* (Wiley New York, 2001).
71. Xu, K. & Su, R. Path planning of nanorobot: a review. *Microsyst. Technol.* **28**, 2393-2401 (2022).
72. Xu, K., Kalantari, A. & Qian, X. Efficient AFM-based nanoparticle manipulation via sequential parallel pushing. *IEEE Trans. Nanotechnol.* **11**, 666-675 (2011).
73. Requicha, A. A. G., Arbuckle, D. J., Mokaberi, B. & Yun, J. Algorithms and software for nanomanipulation with atomic force microscopes. *Int. J. Rob. Res.* **28**, 512-522 (2009).
74. Zhang, Z., Wang, X., Liu, J., Dai, C. & Sun, Y. Robotic Micromanipulation: Fundamentals and Applications. *Annu. Rev. Control Robot. Auton. Syst.* **2**, 181-203 (2019).
75. Zimmermann, S., Tiemerding, T. & Fatikow, S. Automated Robotic Manipulation of Individual Colloidal Particles Using Vision-Based Control. *IEEE ASME Trans. Mechatron.* **20**, 2031-2038 (2015).
76. Dey, U., Kumar, C. S. & Jacob, C. SEM image-guided manipulation with a feedback assistance system for automated nanohandling of a 4 DOF micromanipulator. *J. Micromech. Microeng.* **31**, 115006 (2021).
77. Sha, X., Sun, H., Zhao, Y., Li, W. & Li, W. J. A Review on Microscopic Visual Servoing for Micromanipulation Systems: Applications in Micromanufacturing, Biological Injection, and Nanosensor Assembly. *Micromachines* **10**, 843 (2019).
78. Zhou, L., Li, X., Zhu, B. & Su, B. An Overview of Antifouling Strategies for Electrochemical Analysis. *Electroanalysis* **34**, 966-975 (2022).

## 5. Electrochemical Grippers for Micro- and Nanorobotics: Manipulation by Tuning Surface Forces

---

79. Hanssen, B. L., Siraj, S. & Wong, D. K. Y. Recent strategies to minimise fouling in electrochemical detection systems. *Rev. Anal. Chem.* **35**, 1-28 (2016).
80. Lin, P. H. & Li, B. R. Antifouling strategies in advanced electrochemical sensors and biosensors. *Analyst* **145**, 1110-1120 (2020).
81. Fischer, L. M. et al. Gold cleaning methods for electrochemical detection applications. *Microelectron. Eng.* **86**, 1282-1285 (2009).
82. Fornof, A. R., Erdmann, M., David, R. & Gaub, H. E. Electric glue: electrically controlled polymer-surface adhesion. *Nano Lett.* **11**, 1993-1996 (2011).
83. Fritz, P. A. et al. Electrode Surface Potential-Driven Protein Adsorption and Desorption through Modulation of Electrostatic, van der Waals, and Hydration Interactions. *Langmuir* (2021).
84. Xu, J., Kwak, K. J., Lee, J. L. & Agarwal, G. Lifting and Sorting of Charged Au Nanoparticles by Electrostatic Forces in Atomic Force Microscopy. *Small* **6**, 2105-2108 (2010).
85. Cheng, H.-W. et al. Simple and Fast Method To Fabricate Single-Nanoparticle-Terminated Atomic Force Microscope Tips. *J. Phys. Chem. C* **117**, 13239-13246 (2013).
86. Helfricht, N. et al. Probing the adhesion properties of alginate hydrogels: a new approach towards the preparation of soft colloidal probes for direct force measurements. *Soft Matter* **13**, 578-589 (2017).
87. Hutter, J. L. & Bechhoefer, J. Calibration of atomic-force microscope tips. *Rev. Sci. Instrum.* **64**, 1868-1873 (1993).
88. Rabinovich, Y. I., Adler, J. J., Ata, A., Singh, R. K. & Moudgil, B. M. Adhesion between nanoscale rough surfaces: II. Measurement and comparison with theory. *J. Colloid. Interface Sci.* **232**, 17-24 (2000).

## 6. An integrated, exchangeable three- electrode electrochemical setup for AFM- based scanning electrochemical microscopy

*Andreas Karg*<sup>1,2</sup>, *Sebastian Gödrich*<sup>1</sup>, *Philipp Dennstedt*<sup>1,2</sup>, *Nicolas Helfricht*<sup>1</sup>,  
*Markus Retsch*<sup>2,3</sup>, *Georg Papastavrou*<sup>1,2,\*</sup>

<sup>1</sup>Physical Chemistry II, University of Bayreuth, 95447 Bayreuth, Germany;

<sup>2</sup>Bavarian Institute for Battery Technology, University of Bayreuth, 95448 Bayreuth

<sup>3</sup>Physical Chemistry I, University of Bayreuth, 95447 Bayreuth, Germany

Reprinted with permission from:

„An integrated, exchangeable three-electrode electrochemical setup for AFM-based scanning electrochemical microscopy“, [Andreas Karg](#), Sebastian Gödrich, Philipp Dennstedt, Nicolas Helfricht, Markus Retsch, Georg Papastavrou\*, *MDPI Sensors*, **2023**, 23 (11), 5228. DOI: 10.3390/s23115228

Under terms of the CC BY license

## 6. An integrated, exchangeable three-electrode electrochemical setup for AFM-based scanning electrochemical microscopy

**Abstract:** *Scanning electrochemical microscopy (SECM) is a versatile scanning probe technique that allows monitoring of a plethora of electrochemical reactions on a highly resolved local scale. SECM in combination with atomic force microscopy (AFM) is particularly well suited to acquire electrochemical data correlated to sample topography, elasticity, and adhesion, respectively. The resolution achievable in SECM depends critically on the properties of the probe acting as an electrochemical sensor, i.e., the working electrode, which is scanned over the sample. Hence, the development of SECM probes received much attention in recent years. However, for the operation and performance of SECM, the fluid cell and the three-electrode setup are also of paramount importance. These two aspects received much less attention so far. Here, we present a novel approach to the universal implementation of a three-electrode setup for SECM in practically any fluid cell. The integration of all three electrodes (working, counter, and reference) near the cantilever provides many advantages, such as the usage of conventional AFM fluid cells also for SECM or enables the measurement in liquid drops. Moreover, the other electrodes become easily exchangeable as they are combined with the cantilever substrate. Thereby, the handling is improved significantly. We demonstrated that high-resolution SECM, i.e., resolving features smaller than 250 nm in the electrochemical signal, could be achieved with the new setup and that the electrochemical performance was equivalent to the one obtained with macroscopic electrodes.*

### Introduction

Scanning electrochemical microscopy (SECM) is a well-established analytical technique that allows measuring electrochemical sample properties on the micro- and nanometer-scale<sup>1-6</sup>. SECM belongs to the so-called scanning probe techniques and the basic idea of SECM is to scan a small electrode over a sample and to detect in a locally resolved manner changes in current as a function of the lateral position on the sample and the distance to the sample, respectively. The technique has been presented first in 1989<sup>7</sup>. In the following decades, many different imaging modes have been developed<sup>1,3</sup>. However, independent from the imaging mode, some fundamental instrumental parameters determine the performance in SECM measurements. The parameters compromise the probe, the sample topography, the distance control between probe and sample, and the possibility to track and follow the surface

## 6. An integrated, exchangeable three-electrode electrochemical setup for AFM-based scanning electrochemical microscopy

---

topography of the sample<sup>3</sup>. Tracking surface topography and thus surface separation distance is essential as these have a strong influence on the electrochemical currents that are the primary measurement signal<sup>4</sup>.

Originally, SECM was based solely on micropipettes, which were scanned over the sample<sup>7-10</sup>. However, micropipette-based SECM was strongly limited in determining the surface topography in a non-destructive manner and with high lateral resolution<sup>11,12</sup>. In particular, it was and is difficult to control the force exerted on the sample during the imaging process, which is carried out mostly by shear-force detection<sup>9</sup>. The method of micropipette-based SECM is still under active development and some limitations have been overcome<sup>13,14</sup>. SECM probes from micropipettes provide also a number of advantages in terms of versatility of the probes and tuning them from specific applications, such as the detection of local ions. Hence, micropipettes in SECM have found applications in studying corrosion<sup>15</sup>, catalysis<sup>16</sup>, biological cells, or battery materials<sup>17-19</sup>. In particular, in the field of scanning ion conductance microscopy micropipette-based techniques are extensively used<sup>14</sup>.

The advent of AFM-based SECM allowed us to overcome many problems associated with micropipettes, resulting in a high lateral resolution as well as a non-destructive imaging. Moreover, the simultaneous acquisition of laterally resolved data on additional sample properties, such as adhesion or elastic response, is a further advantage of AFM-based SECM approaches. Unfortunately, AFM-SECM has long suffered from the difficult and tedious preparation of probes that combine a sharp AFM tip and an electrode on one cantilever<sup>20-26</sup>. Recently, batch preparation techniques for the fabrication of such SECM-cantilevers have been improved significantly and suitable cantilevers became available more widely<sup>12,25-27</sup>. In consequence, AFM-based SECM has been recently utilized increasingly in several fields such as battery<sup>17,18</sup> and corrosion research, catalysis<sup>28</sup>, and biology<sup>5</sup>.

Electrodes represent a crucial element not only in SECM but in all electrochemical experiments and electrode arrangements electrochemical cells are often of great importance<sup>29-31</sup>. In the case of SECM, not only the electrochemical sensitivity but also the spatial resolution in the electrochemical signal depends critically on the dimension and geometry of the working electrode, which is scanned as a probe over the sample surface. Therefore, it is not surprising, that the fundamental combined AFM-SECM sensors have recently received much attention<sup>32</sup>. The outline of the entire electrochemical cell is also of great importance for the performance of the instrumental

## 6. An integrated, exchangeable three-electrode electrochemical setup for AFM-based scanning electrochemical microscopy

setup<sup>29</sup>. The design of electrochemical cells for scanning probe microscopy has received only moderate interest in the past<sup>33,34</sup>. On the other hand, by now, electrochemical cells are commercially available from most AFM manufacturers. However, common to all standard designs for all AFM electrochemical cells is that they concentrate in their design on macroscopic working electrodes that are often used as samples. Hence, the position and the dimensions of the reference and counter electrode in the electrochemical cell are designed with respect to the second macroscopic working electrode.

However, the presence of macroscopic electrodes in the fluid cell are not necessary or even advantageous for all applications of SECM<sup>35</sup>. For various applications, the SECM-probe is the only or the primary working electrode, i.e., there is no need to keep a macroscopic sample of several mm<sup>2</sup>-area under potentiostatic control. In this case, the requirements with respect to the area of the counter electrode and the position of the reference electrode change substantially as the AFM-SECM probe corresponds to a nanoelectrode, which is incorporated into the AFM-cantilever. There are two general important rules in relation to electrochemical cells. First, the size of the counter electrode should be several times larger than the one of the working electrodes. Secondly, the reference electrode should be placed as close as possible to the working electrode, which is a requirement that leads to the use of devices like the Luggin-capillary<sup>29</sup>. Adapting these requirements to the nm-sized electrode on the AFM-cantilever leads to drastically new boundary conditions in designing the counter and reference electrodes, respectively, and their positions in the electrochemical cell. The counter electrode can be reduced significantly in size, and both the counter and the reference electrode can be placed on the glass packaging of the AFM-cantilever. This approach, which we refer to as SECM-Cantilevers/Echemcell, in which the cantilever and cell are now one unit, is based on pastes for screen-printed electrodes<sup>36</sup>. The latter became increasingly popular for analytical applications and provide reliable as well as inert electrode materials<sup>37-45</sup>. This new type of electrochemical cell for AFM-based SECM has been characterized for its electrochemical performance. We performed two types of experiments for this characterization. On one hand, cyclic voltammetric measurements with a well-defined redox couple allow us to verify not only the electrode on the SECM cantilever but also the function of the other electrodes by comparison of the cyclic voltammograms. By detecting the currents on the working electrode, e.g., the SECM-tip, as a function of the applied potential and comparing

## 6. An integrated, exchangeable three-electrode electrochemical setup for AFM-based scanning electrochemical microscopy

---

these currents to the ones reported previously for the same redox-couple in the liquid phase, the electrochemical properties of the electrode as well the other electrodes can be verified in an exemplary manner. On the other hand, SECM imaging with the newly developed cell and the comparison to the images as acquired with a standard cell provides additional verification for the suitability of the new cell in SECM-imaging applications.

### Materials and Methods

**Preparation of Integrated SECM-Cantilevers/Echemcell.** Commercial SECM-AFM cantilevers (Bruker, Santa Barbara, CA, USA) were painted by means of a Pt-paste (Platinum Polymer Paste, Sun Chemical Corp., Parsippany-Troy Hills, NJ, USA) and an Ag/AgCl-paste (60% Ag/40% AgCl in paintable format, Zimmer & Peacock, Royston, UK) through a homemade rubber-mask, resulting in an electrode geometry of approx. length 7 mm and approx. width 0.6 mm, respectively. Afterwards, the modified cantilever was dried for 30 min at 80 °C. The painted electrodes were electrically contacted using a PEI-insulated silver wire (0.125 mm in diameter, Advent Research Materials Ltd., Oxford, England) using conductive silver (Acheson 1415, Plano GmbH, Wetzlar, Germany) and UV-curing glue (NOA 63, Norland Products Inc., Jamesburg, NJ, USA). An additional insulating layer (Red insulating Varnish GC Waldom, GC Electronics, Rockford, IL, USA) was applied to the contacts. Scanning electron images were taken by means of a LEO1530 SEM (Carl Zeiss Microscopy GmbH, Oberkochen, Germany). Prior to the SEM measurements, the SECM cantilevers were sputtered with a layer of approx. 10 nm of carbon.

**Electrochemical Characterization.** Cyclic voltammetric measurements were performed by applying a potential via a CHI750i (CH Instruments, Inc., Austin, TX, USA). For long-term stability measurements, a circular Pt-macroelectrode (1 mm in diameter, Metrohm AG, Herisau, Switzerland) was used as a working electrode. A glass slide that has been cleaned in an ultrasonic bath in aqueous 2vol% Hellmanex solution (Hellmanex III, Hellma GmbH & Co. KG, Müllheim, Germany) was painted with Pt-paste and Ag/AgCl-paste in an analogous manner compared to the integrated SECM-cantilevers/Echemcell. These electrodes were applied as counter electrodes and reference electrodes, respectively. Cyclic voltammograms were recorded in an aqueous solution of 5 mM potassium ferrocyanide (99.95%, Sigma-Aldrich Inc., St.

## 6. An integrated, exchangeable three-electrode electrochemical setup for AFM-based scanning electrochemical microscopy

Louis, MO, USA), 5 mM potassium ferricyanide (99.98%, Sigma-Aldrich Inc, St. Louis, MO, USA) and 0.1 mM KNO<sub>3</sub> (99%, abcr GmbH, Karlsruhe, Germany) every 30 min for 3 h at a scan rate of 0.05 V/s. The experiments have been carried out under standard experimental conditions (room temperature and atmospheric pressure).

For the comparison of the electrochemical properties, also the integrated SECM-cantilever/Echemcell was characterized by cyclic voltammetry, where the electroactive cantilever tip was used as working electrode. In an electrochemical AFM cell, cyclic voltammetric measurements in an aqueous solution of 5 mM hexaammineruthenium(III) chloride (99%, abcr GmbH, Karlsruhe, Germany) and 0.1 mM KNO<sub>3</sub> (99%, abcr GmbH, Karlsruhe, Germany) were performed at a scan rate of 0.02 V/s with the painted electrodes connected as counter and reference electrodes to test the integrated SECM-cantilever/Echemcell. For comparison experiments, a chlorinated silver wire as a quasi reference electrode (0.125 mm in diameter, Advent Research Materials Ltd., Oxford, England) and a coiled Pt-wire (0.127 mm in diameter, Advent Research Materials Ltd., Oxford, England) were used as a counter electrode to compare it to a standard SECM setup. The wire electrodes and painted electrodes were referenced against a commercial saturated calomel electrode (RE-2B, Basi Inc., West Lafayette, IN, USA) using a high-resistance voltmeter (Keithley Instruments, Solon, OH, USA).

**Preparation of Gold Nano-Meshes.** Monolayers of spherical polystyrene beads ( $1.04 \pm 0.04 \mu\text{m}$  in diameter, Microparticles GmbH, Berlin, Germany) were produced as described by Retsch et al.<sup>46</sup>. Glass slides were cleaned for 15 min in an ultrasonic bath with a 2vol% aqueous of Hellmanex III (Hellma GmbH & co. KG, Müllheim, Germany), extensively rinsed with ultrapure water and dried under a nitrogen stream. The glass slides were functionalized by means of a liquid phase silanization for 1 h with an aqueous 1 vol% of a silane (N-trimethoxysilylpropyl-N,N,N-trimethylammonium chloride, 50% in methanol, abcr GmbH, Karlsruhe, Germany). Cationically functionalized glass slides were spin-cast with a 3 wt% polystyrene particle dispersion at a rotation speed of 4000 rpm. Freely floating monolayers were assembled at the air/water interface by slow immersion of the particle-coated glass substrate into a 0.1 mM SDS solution in MilliQ water. The aqueous phase was adjusted to pH 12 by adding a few drops of ammonia. The floating monolayer was transferred to a glass substrate and dried in air. Based on the approach of Stelling and coworkers, nanomeshes were produced from these monolayers<sup>47</sup>. The prepared monolayers

## 6. An integrated, exchangeable three-electrode electrochemical setup for AFM-based scanning electrochemical microscopy

were etched in a plasma reactor MiniFlecto (Plasma Technology GmbH, Herrenberg-Gültstein, Germany) with 75% argon and 25% oxygen at 80 W power at a pressure of 0.14 mbar. Etching was conducted for 20 min in order to obtain non-close packed monolayers with particles of 870 nm in diameter. A thin layer of chromium (thickness = 3 nm) as an adhesion promoter and a consecutive layer of gold (thickness = 50 nm) were deposited by thermal evaporation using a Balzers BA360 (Oerlikon Balzers Ltd., Balzers, Liechtenstein). The layer thickness was monitored via a SQM 160 microbalance (Sigma Instruments, INFICON Holding AG, Bad Ragaz, Switzerland). The remaining particles were removed using Scotch<sup>®</sup> tape (3M corp-. Saint Paul, MN; USA) leading to nanohole arrays in the gold film. These Au-nano-mesh substrates were cleaned for 10 min in an ultrasonic bath with a 2% aqueous Hellmanex III (Hellma GmbH & Co. KG, Müllheim, Germany) solution in ultrapure water. The surfactant was extensively rinsed off with ultrapure water and the substrates were placed in ethanol in an ultrasonic bath for 10 min and dried under a nitrogen stream.

**SECM Measurements.** Height and current images of the AFM-SECM measurements were acquired with a Dimension ICON (Bruker Corp., Billerica, MA, USA) equipped with a Nanoscope V controller (Bruker Corp., Billerica, MA, USA) in a partially closed electrochemistry fluid cell. This cell has been purposely designed on base of a commercially available electrochemical cell (Asylum Research Corp., Santa Barbara, CA, USA). The feed-throughs for the liquid exchange have been used for connection to the electrodes inside the cell. A homemade reference electrode from an Ag/AgCl-wire has been prepared by the following procedure. From PTFE-insulated Ag wires with a diameter of 0.125 mm (Advent Research Materials Ltd, Oxford, England) the insulation has been partially removed and the resulting free area has been electrochemically coated with a layer of AgCl using an automatic chlorination device (AC1-01, npi electronic GmbH, Tamm, Germany). As a counter electrode, a coiled Pt-wire (0.127 mm in diameter, Advent Research Materials Ltd, Oxford, England) with a total effective length of about 100 mm has been used.

When AFM-SECM measurements with integrated SECM-cantilevers/Echemcells were performed, a painted Ag/AgCl electrode acted as reference and a painted Pt-electrode acted as counter-electrode, respectively. The electrochemical-active SECM-cantilevers were used as primary working electrodes, while the gold-nanomesh substrates were used as secondary working electrodes, respectively. A constant potential of  $-0.5$  V was applied to the SECM-tip, while a potential of  $0.2$  V was applied

## 6. An integrated, exchangeable three-electrode electrochemical setup for AFM-based scanning electrochemical microscopy

to the gold-nanomesh for regeneration of the reduced species by means of a CHI750i potentiostat. The AFM-SECM measurements were performed in an aqueous solution of 5 mM hexaamminerruthenium(III) chloride with 0.1 M KNO<sub>3</sub> in PeakForce lift mode at a lift height of 40 nm. In order to eliminate line noise in the current signal, an active compensation device (HumBug noise eliminator, Quest Scientific Instruments Inc., North Vancouver, BC, Canada) was used. AFM height and current images were processed with NanoScope Analysis 1.80 (Bruker Bruker Corp., Billerica, MA, USA). The resulting current images were normalized to the current on the gold line-by-line, which was evaluated by means of a home-built procedure in IgorPro (Wavematrix, Inc., Lake Oswego, OR, USA).

### Results

**An Electrochemical Cell Integrated into the Glass Packaging of an AFM-SECM-Cantilever.** In AFM-SECM feedback mode, the SECM-cantilever is used for imaging as well as for characterizing the electrochemical properties of a sample surface <sup>7</sup>. Here, we present a newly developed electrochemical cell in direct integration with the SECM-cantilevers and their glass packaging. More specifically, we integrated the reference and the counter electrode directly on the cantilever glass packaging. Therefore, both were brought in the direct vicinity of the working electrode used for SECM imaging. More details will be given below. In order to test these integrated SECM-cantilevers/Echemcells, we compared them in their performance to 'classical' electrochemical cells. A 'classical' electrochemical cell is shown in a schematic representation in Figure 1a. Similar electrochemical cells for applications in AFM have been used in our groups for many years <sup>48–51</sup>. The design is based on the standard distribution of electrodes for electrochemical cells in AFM <sup>20,23</sup>. The large sample with dimensions of ca. 10 mm × 10 mm, which can act also as a working electrode, is located at the center of the cell. The corresponding counter electrode is placed in an approximately semi-circular configuration around the sample. We commonly utilize either Pt-wires, which we form in a spiral shape to increase the surface area, or Pt-nets as counter electrodes. The former has been utilized in the experiments presented here. As counter electrodes commonly either commercial solid-state reference electrodes (e.g., DriRef<sup>®</sup>) or silver wires that have been chlorinated, have been used in combined AFM/electrochemistry setups <sup>20,23,52</sup>.

## 6. An integrated, exchangeable three-electrode electrochemical setup for AFM-based scanning electrochemical microscopy

For this study, the SECM-cantilever, namely the electrode acting also as an AFM tip, acts as the primary working electrode. For some experiments, the large macroscopic electrode is used as 2nd working electrode. Electrochemical control of one or two working electrodes has been provided by means of a commercial bi-potentiostat. An image of the complete, unmodified SECM-cantilever, including the packaging made from glass, is shown in Figure 1a top right. This glass carrier is also used to immobilize the cantilever in the cantilever holder of the AFM head. In the electrochemical cell for the AFM (cf. Figure 1a), the counter electrode was a platinum wire, which has been coiled in order to increase the available surface area (cf. Figure 1a right bottom). A chlorinated silver wire (Ag/AgCl) serves as reference electrode <sup>12,48,49</sup>. For measurements at low ionic strength, the wire allows for a rather symmetric distance around the macroscopic working electrode located in the center of the fluid cell (cf. inset Figure 1a right bottom). The type of components shown in the images of Figure 1a represents the classical setup for AFM-based SECM and has been utilized in several studies from us <sup>12</sup> or other groups <sup>53,54</sup>.

Figure 1b shows the newly developed integrated SECM-cantilever/Echemcell, which places all three electrodes on the cantilever and its glass packaging, respectively. The schematic illustration (cf. Figure 1b left) shows the position of these electrodes. Under the condition that only the nm-sized electrode on the AFM-tip has to be electrochemically controlled, a more miniaturized setup becomes feasible, and the counter and reference electrode can be much smaller. Moreover, both electrodes can be placed much closer in the vicinity of the working electrode at the AFM-SECM tip. The inset on the right top of Figure 1b shows the same type of SECM-cantilevers as in Figure 1a (inset, top right) but this time includes the two additional electrodes, namely counter and reference electrode, that have been painted on the glass packaging. These on-substrate electrodes eliminate the need for additional electrodes in the measurement cell. Therefore, measurements in standard fluid cells (cf. Figure 1b right bottom) or even petri-dishes can be conducted. The detailed preparation and characterization of the integrated SECM-cantilevers/Echemcells will be given in the following.

## 6. An integrated, exchangeable three-electrode electrochemical setup for AFM-based scanning electrochemical microscopy

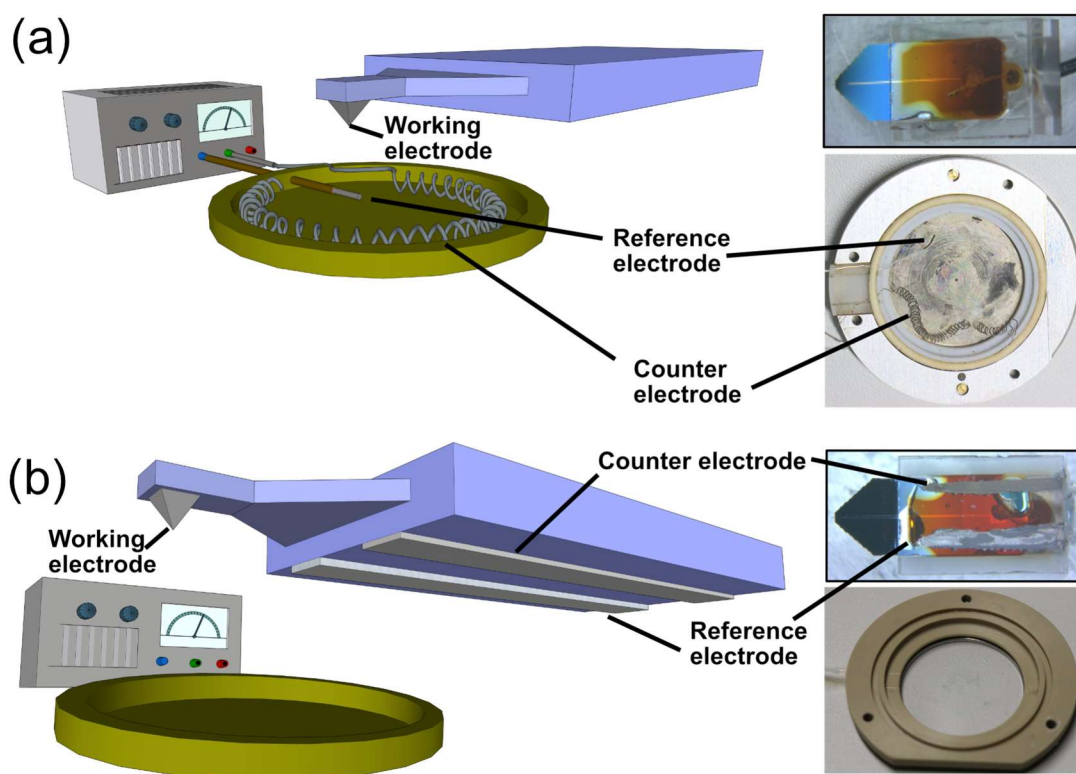


Figure 1. (a) Left: Schematic representation of the 'classical' setup for AFM-based SECM with macroscopic electrodes. A commercial AFM-SECM cantilever is connected to a potentiostat as one working electrode, while the sample is the second working electrode. The electrochemical cell is based on Ag/AgCl- and Pt-wires as quasi-reference and counter electrodes, respectively. Right: photographs show the commercial SECM-cantilever, as well as the electrochemical cell with reference and counter electrode. (b) Left: Schematic representation of the integrated SECM cantilever/Echemcell setup based on the commercial AFM-SECM cantilever and screen-printed electrodes on its glass packaging. Here, the working, reference and counter electrode are fully integrated into the SECM-cantilever chip (right, top). For a three-electrode experiment, no additional wiring in the fluid is required. Hence, a standard fluid cell is viable for measurements (right bottom).

### Preparation of AFM-SECM Cantilevers with Integrated Electrochemical Cell.

Figure 2 summarizes the preparation of a three-electrode electrochemical cell, which is integrated into commercial AFM-SECM cantilevers and their glass packaging. In Figure 2a, the general setup is shown in a schematic overview. The combined AFM-SECM cantilever has an isolated Pt-tip at its apex. This tip acts as a working electrode and is already present in the commercially available cantilever<sup>12</sup>. The two additional electrodes required for a complete electrochemical cell are situated on the glass packaging and must be added afterwards. Figure 2b illustrates the necessary preparation process for these electrodes on the glass substrate. Starting from the bare

## 6. An integrated, exchangeable three-electrode electrochemical setup for AFM-based scanning electrochemical microscopy

---

glass surface (cf. Figure 2b left top), a custom-made rubber mask is placed on the substrate. The mask from high-purity silicon rubber has openings with the outline of the two electrodes. In the following, the electrodes were painted on the substrate. The paints for the electrodes have been originally developed for screening printing processes but can also be deposited with a fine brush. For the counter electrode, we used a Pt-based paste and for the reference electrode an Ag/AgCl-based paste. Further details are given in the experimental section. The deposited pastes have been cured at high temperature (80 °C) followed by removal of the mask (cf. Figure 2b bottom). Finally, the two additional electrodes have been contacted by thin insulated wires. We used a procedure for the wire attachment and insulation that has been developed to produce electrochemical colloidal probes (cf. experimental section)<sup>51</sup>. Figure 2c shows the resulting integrated SECM-cantilever/Echemcell and its glass packaging. The low magnification overview image serves as orientation (Figure 2c central). Scanning electron microscopy images of the working electrode on the apex of the tip are shown in Figure 2c left top and center. Please notice that the integrated SECM-cantilever/Echemcell has been utilized for measurements and that the debris visible results from the transfer through the water/air interface and drying. Further SEM images show the microstructures of the dried Ag/AgCl paste (cf. Figure 2c, top right) and the Pt-paste (cf. Figure 2c, bottom right), which are used as a reference and counter electrode, respectively. For both, grains with defined borders are visible, while the grain size is significantly smaller for the Pt-paste. The configuration of the electrodes resembles slightly the one encountered for in situ electrochemical cells for transmission electron microscopy<sup>30,55,56</sup>.

## 6. An integrated, exchangeable three-electrode electrochemical setup for AFM-based scanning electrochemical microscopy

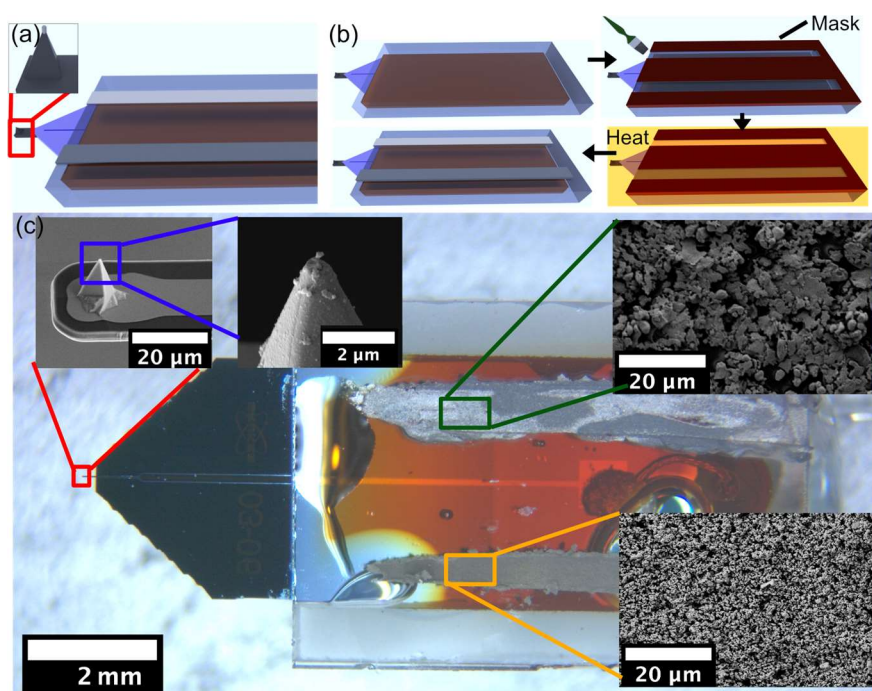


Figure 2. (a) Schematic representation of the integrated SECM-cantilever/Echemcell developed in this study. Inset: Ultramicroelectrode on the tip used for both imaging and electrochemical characterization. (b) Schematic representation of the preparation steps. (c) Optical microscopy image at low magnification of the integrated SECM-cantilever/Echemcell. The insets show scanning electron microscopy images of the combined AFM-SECM tip, as well as the microstructures of the dried Ag/AgCl-paste (dark green, top) and dried Pt-paste (orange, bottom).

**Characterization by Cyclic Voltammetry.** In order to evaluate the electrochemical performance of the integrated SECM-cantilever/Echemcell we did perform a number of cyclic voltammetry measurements. Cyclic voltammetry (CV) is a standard analytical technique that allows us to follow the oxidation and reduction of electroactive species at an electrode under potentiostatic control while applying a time-dependent triangular voltage signal and acquiring the resulting current. The CV technique is routinely used to characterize (ultra-)microelectrodes utilized for SECM probes<sup>23,54,57</sup> by conducting CV measurements with standard redox couples, such as hexacyanoferrate or ruthenium complexes, which have been extensively described in the literature<sup>29,57</sup>. In particular, CV is also useful to verify the function of nanoelectrodes, such as the electrodes on SECM cantilevers<sup>57,58</sup>. In consequence, CV allows also to verify the experimental setup, i.e., the entire electrochemical cell and not only the state of the nanoelectrode<sup>59</sup>. It should be pointed out that the following CV experiments are not intended to provide a statistical analysis, as the electrochemical process is already

## 6. An integrated, exchangeable three-electrode electrochemical setup for AFM-based scanning electrochemical microscopy

well-described<sup>57</sup>. This approach of performing measurements for a selected redox-couple is standard for the development of novel SECM probes<sup>57</sup>. By demonstrating that previously reported CVs can be reproduced the newly developed setup is benchmarked as any significant change in the electrochemical behaviour of the electrodes would lead in this respect to significant changes. In particular, this approach allows us to address also the stability of the electrode materials<sup>57</sup>.

In the first set of experiments, the electrochemical responses of the electrodes prepared by the here-presented pastes have been verified. The paste-based electrodes have been attributed the same roles as the integrated SECM-cantilever/Echemcell. The counter electrode has been prepared by the Pt-paste and the reference electrode by the Ag/AgCl-paste. The working electrode was a commercial circular Pt-macroelectrode with an electrode area of approximately 0.8 mm<sup>2</sup>. This Pt-macroelectrode was located in close vicinity to a glass substrate on which the Pt- and Ag/AgCl-paste were prepared in a completely analogous manner to the glass packaging of the SECM cantilevers. An image of the electrode setup is shown as an inset in Figure 3a (cf. for comparison to Figure 2 central). A cyclic voltammetric measurement with standard parameters (cf. Materials and methods) was repeated every thirty minutes for a total time interval of 3 h while keeping the electrode configuration constant during the whole time. The corresponding CVs in Figure 3a show the overall shape as expected for a macroelectrode with pronounced oxidation and reduction peaks. The position of the peaks and current densities are completely in line with the ones reported in literature for the used ferro/ferricyanide redox couple<sup>60,61</sup>. Moreover, Figure 3a demonstrates the long-term stability of the paste-based electrodes (cf. inset on the left side of the cyclic voltammogram). The absence of any further peaks in the cyclic voltammogram, indicating the absence of contaminations in the paste electrodes, should be noted as well.

Figure 3b shows a second set of CV experiments where the electrochemical performance of the electrodes of the integrated SECM-cantilever/Echemcell have been compared to the ones of a conventional setup using macroelectrodes. In this case, the working electrode was the SECM tip. Another CV with hexaammineruthenium(III) chloride has been performed. The different shape of the cyclovoltammogram in Figure 3b compared to Figure 3a has its origins in the very different dimensions of the working electrode. The sigmoidal shape is commonly observed for nanoelectrodes<sup>57,58</sup>. The CV in Figure 3b corresponds to the ones

## 6. An integrated, exchangeable three-electrode electrochemical setup for AFM-based scanning electrochemical microscopy

reported previously, which have been acquired with a similar type of SECM-cantilevers and the same redox couple <sup>12,54</sup>. Practically, no difference is observed between the two sets of experiments, one performed with standard setup (SECM-cantilever, macroscopic reference and working electrode in cell, cf. Figure 3b inset top, black curve) and the here-developed setup (integrated SECM-cantilever/Echemcell only, cf. Figure 3b inset bottom, red curve). We could not observe any offset in terms of the CV as acquired by the two electrochemical setups while the working electrode, i.e., the SECM-cantilever, remained constant. Moreover, no difference in peak height and shape in the two different CVs could be detected. From these results for an exemplary electrochemically active substance (i.e., hexaammineruthenium(III) chloride), we can conclude that the integrated SECM-cantilever/Echemcell provides a completely equivalent setup in terms of potentiostatic control to the one provided by macroscopic electrodes commonly found in fluid cells for electrochemistry by AFM.

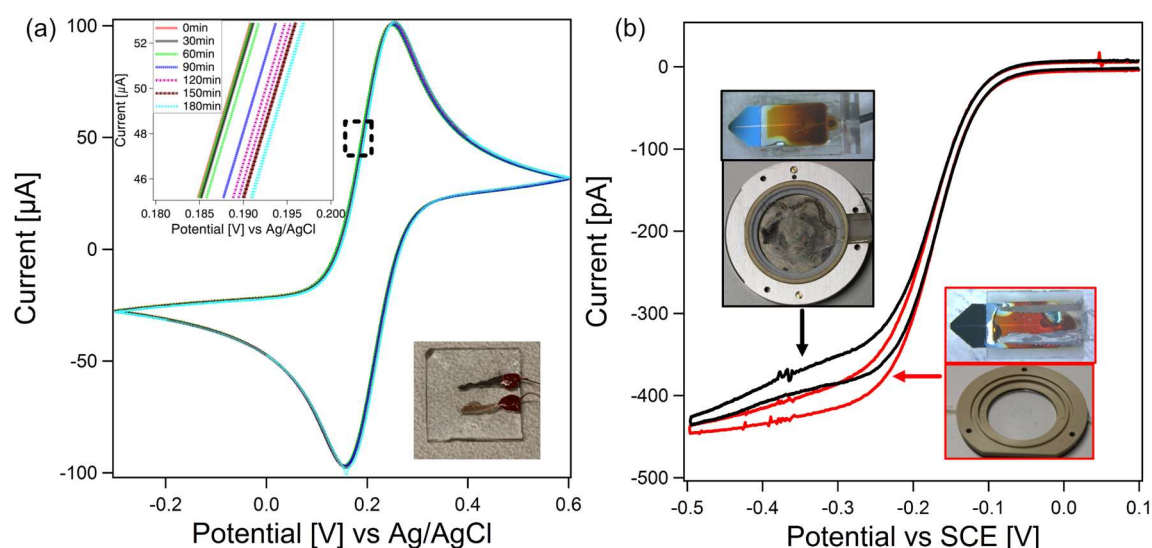


Figure 3. (a) Long-term stability experiment, using a commercial Pt-macroelectrode as working electrode and Ag/AgCl- and Pt-electrodes prepared analogously to the integrated SECM-cantilever/Echemcell. Cyclic voltammograms in ferricyanide (5 mM)/ferrocyanide (5 mM) were acquired every 30 min. On the macroscopic scale, no shift in the CVs could be detected. Inset: Zoom-in into long term CV, showing a difference of the CVs smaller than 6 mV over 3 h. No direct correlation between shift and time could be traced. (b) CVs of the AFM-SECM setup in hexaammineruthenium(III) chloride, a standard electrolyte used in AFM-SECM measurements <sup>12,54</sup>, using the cantilever tip as ultramicroelectrode. Black data: CVs as acquired by means of a 'classical' electrochemical fluid cell for AFM using Ag/AgCl- and Pt wires as reference and counter electrodes. Red data: CVs acquired solely by integrated SECM-cantilever/Echemcell.

## 6. An integrated, exchangeable three-electrode electrochemical setup for AFM-based scanning electrochemical microscopy

**SECM-Measurements with the Integrated Electrochemical Cell.** The most important corroboration for the integrated SECM-cantilever/Echemcell is its performance for imaging in SECM-AFM applications. As a test substrate for SECM imaging, we did choose so-called gold nano-mesh electrodes. These electrodes have been used already in the past as model systems to determine the resolution achievable by the SECM-cantilevers<sup>12,27</sup>. The nano-meshes were prepared by means of colloidal lithography<sup>46,47</sup>. Figure 4a summarizes in a schematic manner the preparation of such nano-meshes. Briefly, a densely packed layer of colloidal polystyrene particles is transferred to a functionalized glass substrate. The particles are etched by exposure to oxygen plasma and a thin layer of gold is evaporated onto the substrate. After the mechanical removal of the polystyrene particles, a nano-mesh of gold with defined hole sizes on an insulator surface is the result. The detailed procedure utilized here has been described elsewhere more in detail<sup>47</sup>. These nano-meshes are excellent test samples for SECM due to their defined structure with conducting gold and insulating holes wielding a glass surface<sup>12</sup>. Here, we did prepare Au nano-meshes with a whole diameter of 870 nm and a center of hole to center of hole separation of 1040 nm.

During SECM measurements, various feedback modes are possible<sup>58</sup>. Here, the two working electrodes, i.e., the Au-nano-mesh and the SECM tip, are independently controlled by a bi-potentiostat. The SECM measurements were performed in a 5 mM solution of hexaammineruthenium(III) chloride in dual-pass mode. In the first pass, the surface topography has been obtained by PeakForceTapping in liquid. For the second scan, a constant lift-height of 40 nm has been maintained and the current of the SECM-signal in function of the lateral position has been acquired. For the measurements with the standard electrochemical cell, a negative potential of  $\varphi_{Tip} = -0.50$  V vs. SCE was applied to the SECM-tip, while maintaining a constant potential at the gold-nano-mesh electrode with  $\varphi_{Mesh} = 0.20$  V vs. SCE. Consequently, the ruthenium is reduced at the SECM tip and re-oxidized at the nano-mesh electrode.

Figure 4b illustrates the difference in the resulting currents detected when the tip is situated over the nano-mesh electrode or the insulator surface. The reduction of oxidized species occurs at the electrochemical active SECM tip when the negative potential  $\varphi_{Tip}$  is applied. The current will depend on the concentration of  $Ru^{3+}$ -ions. If this reduction takes place over the Au-electrode of the nano-mesh the local concentration will be higher than in the bulk due to the additional regenerated former

## 6. An integrated, exchangeable three-electrode electrochemical setup for AFM-based scanning electrochemical microscopy

$\text{Ru}^{2+}$ -ions. The oxidation and regeneration of  $\text{Ru}^{2+}$ - to  $\text{Ru}^{3+}$ -ions take place at the Au-part of the nano-mesh when the potential  $\varphi_{mesh}$  is applied. However, in the insulator parts of the nano-mesh, no regeneration takes place and the  $\text{Ru}^{3+}$ -ion-concentration is reduced. These two processes are also often referred to as positive and negative feedback, respectively, in SECM <sup>58,62</sup>. It should be noted that both processes are amplified in effect with reduced distance to the solid/liquid interface (cf. lower graph of Figure 4b). For negative feedback, the diffusion of  $\text{Ru}^{3+}$ -ions is reduced compared to the bulk. For positive feedback, the regenerated concentration is highest near the electrode at  $\varphi_{mesh}$ . Figure 4c summarizes the expected currents for the experiments. For the Au-part of the nano-mesh, a positive feedback signal and thus a high current is expected as schematically illustrated. By contrast, in the holes of the mesh with the glass surface, negative feedback takes place, and a reduced current should be detected.

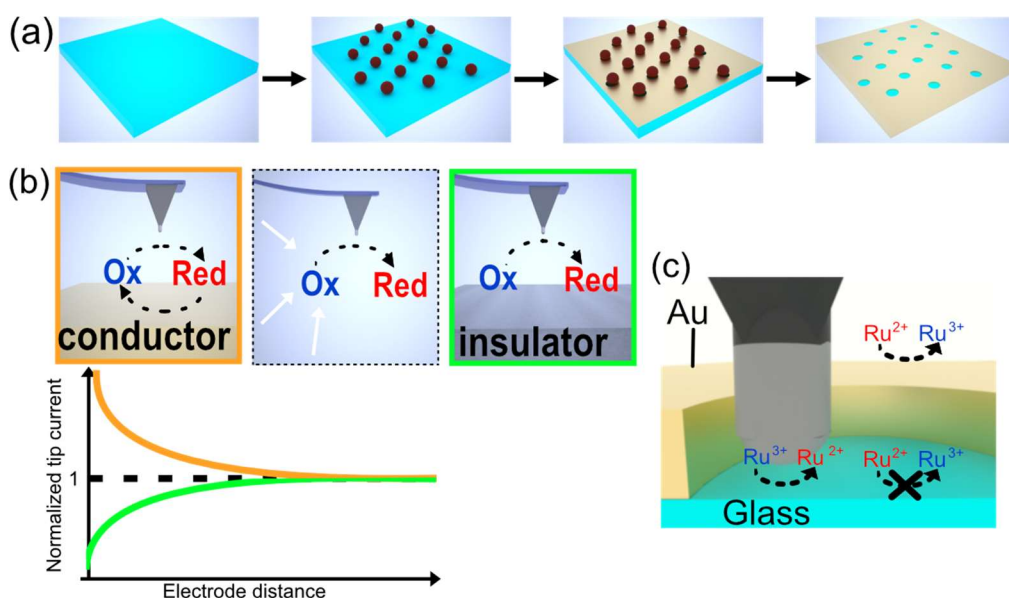


Figure 4. (a) Schematic production of gold nano-meshes used as a test sample for AFM-SECM measurements. (b) Working principle of SECM feedback mode under bi-potentiostatic control. Dashed lines indicate electron transfer reactions on the electrode, while white arrows indicate diffusion of redox species. The schematic graph of the corresponding normalized tip current for positive (orange) and negative (green) feedback demonstrates the dependency on tip-sample distance. The dashed line marks the diffusion-limited bulk current in the bulk. (c) Schematic representation of SECM feedback and electron transfer reaction on nano-mesh electrodes for the SECM experiments conducted.

Figures 5a,b show the results of AFM-SECM measurements conducted in PeakForceTapping mode: one time in a conventional electrochemical cell with

## 6. An integrated, exchangeable three-electrode electrochemical setup for AFM-based scanning electrochemical microscopy

---

macroscopic reference and counter electrodes (cf. Figure 5a) and one time with only the integrated SECM-cantilever/Echemcell (cf. Figure 5b), respectively. In both cases, the gold nano-mesh acted as a second working electrode, leading to a regeneration of oxidized species near its surface. The height images (top graphs) show in both cases the typical features of the nano-mesh electrode. The total height was 50 nm for the Au-layer and a diameter of 870 nm for the holes in the mesh. The slight difference in the resolution between the two topographic images is attributed to the wear of the tip as Figure 5b has been acquired directly before Figure 5a by means of the same SECM cantilever.

The current images (cf. bottom of Figure 5a and 5b, respectively) show nearly exactly the same characteristics in terms of current and lateral resolution. As expected from Figure 4c, the current is reduced in the areas of holes. For both images, the detected current has been line fitted to compensate for drift effects. Instrumental drift does lead in particular to uncertainty in terms of the separation between probe and sample. The latter has a large effect on the detected currents<sup>4</sup>. PeakForce Tapping mode leads to a significant reduction of this effect<sup>12,63</sup>. Moreover, the dimension of the SECM probe is of critical importance for achievable resolution<sup>4</sup>. Taking into account the tip-wear during the previous imaging, no difference between the two images can be detected, illustrating the comparable performance of a classical electrochemical cell and the integrated SECM-cantilever/Echemcell. From the current image, a lateral resolution better than 250 nm can be clearly derived. This value is in line with the one reported previously for the same type of SECM cantilevers<sup>12</sup>.

## 6. An integrated, exchangeable three-electrode electrochemical setup for AFM-based scanning electrochemical microscopy

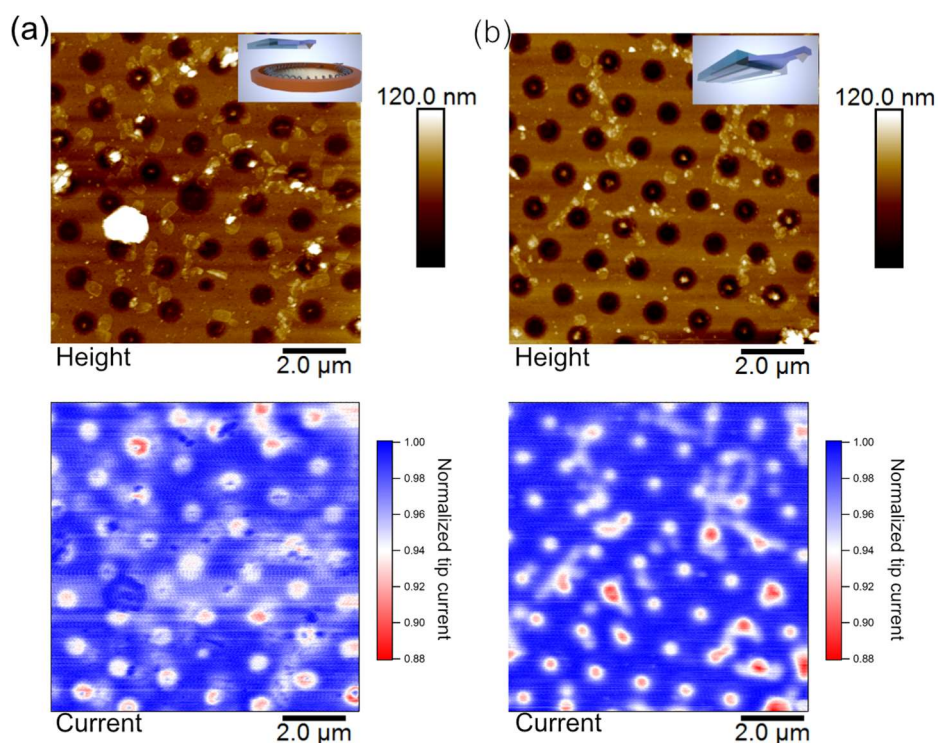


Figure 5. (a) AFM-SECM images of simultaneously acquired topography and tip current at an electrode distance of 40 nm using the ‘standard’ AFM-SECM setup with macroscopic electrodes. (b) AFM-SECM images acquired with the integrated SECM-cantilever/Echemcell. The current signal for SECM-current images was normalized line by line to current on gold for better visibility.

### Discussion

The advent of batch fabrication and commercially available cantilevers with reproducible characteristics for SECM<sup>12,20,32</sup> has led to an increased interest in applying AFM-based SECM in various fields, such as battery research<sup>17–19</sup>, corrosion<sup>15</sup>, catalysis<sup>16</sup> or biology<sup>5</sup>. While the batch processing as well as the reproducible production of SECM tips were in the focus for technical developments in AFM-based SECM in recent years, we believe that it is now time to focus on the electrochemical cell. The design idea of the here-presented integrated SECM-cantilever/Echemcell is similar to recently developed electrochemical cells for in situ and in operando transmission electron microscopy (TEM)<sup>30,55,56,64,65</sup>. Another field where miniaturization of the electrochemical cell has taken place is the technique of scanning electrochemical cell microscopy. However, for this technique, the configuration of the electrodes is not comparable to the here presented setup. The integration of the complete electrochemical cell onto the exchangeable parts, namely the cantilever

## 6. An integrated, exchangeable three-electrode electrochemical setup for AFM-based scanning electrochemical microscopy

---

(working electrode) and its glass packaging (counter and reference electrode), will provide several advantages. First, the reference electrode is placed near the working electrode(s). For the extremely small SECM tips the ohmic drop is not highly relevant<sup>58</sup>. However, if the sample working electrode has only an active area of a few mm<sup>2</sup>, then the integrated SECM-cantilever/Echemcell might still be used as a counter electrode, which would be placed at the shortest possible distance for the second working electrode, thereby reducing ohmic drop effects. Second, the reference electrode would be placed very near to both working electrodes and be practically equidistant from both. Third, one of the biggest advantages is the resulting miniaturization of the electrochemical cell by the integrated SECM-cantilever/Echemcell. Thus, measurements in drop cells or small volume cells as favored in some biological applications (e.g., protein adsorption) become possible. A further advantage would be that the SECM working electrode can be tested with very moderate experimental effort by just immersing it in a vessel containing a solution with a suitable redox-couple and performing cyclic voltammetry. Moreover, the integrated SECM-cantilever/Echemcell would prevent the 'running dry' of reference electrodes, which is a common source of errors in fluid cells with macroscopic electrodes due to the resulting overpotentials that destroy often the SECM-cantilever. However, the resulting miniaturization of the whole liquid cell might lead to an overall reduction of thermal drifts, which represents a major limitation for the performance of SECM<sup>4</sup>.

The implementation of the SECM-cantilever/Echemcell is based on pastes that have been developed for the screen printing of electrodes on glass substrates. Screen-printed electrodes have by now a long history in electrochemistry and their preparation has been optimized in recent years<sup>66,67</sup>. Hence, the here-used preparation process by painting the electrodes with a brush on the glass packaging can be certainly optimized. It will lead to more homogenous and thinner electrodes that can be cured in a more reliable manner. Generally, the preparation of the two additional electrodes by sieve printing could be easily integrated into the workflows of preparing SECM-cantilevers. As a result, the homogeneity, form, and area of the reference and working electrode would be better defined. If the transfer of the pastes to the glass packaging is performed before the assembly of packaging and cantilever, higher curing temperatures are achievable, thus allowing for increased chemical resistance and a wider choice of pastes for the electrodes. Nevertheless, using the here-presented preparation, resistance to chemicals should be already good enough even for solution

## 6. An integrated, exchangeable three-electrode electrochemical setup for AFM-based scanning electrochemical microscopy

---

environments common for SECM studies in battery materials<sup>68–70</sup>. Here, curing took place at temperatures below 100 °C. Screen printed Ag/AgCl electrodes are also used for various analytical and monitoring applications<sup>71,72</sup>. Hence, a high degree of reproducibility is ensured, and a wealth of experience in terms of the stability of such electrodes under different conditions exist. In particular, the quality of the reference electrodes is most likely sufficient for applications in AFM-based SECM. Future improvements of the design could be further miniaturization by preparing the electrodes directly on the cantilever chip instead of the glass carrier.

### **Acknowledgments**

The authors thank C. Clute for some initial experiments leading to this research, P. Markus for his help with the loaders for the data analysis, and C. Stelling for the production of the nano-mesh substrates.

## References

1. Bard, A. J. & Mirkin, M. V. *Scanning electrochemical microscopy* (CRC Press, Boca Raton, FL, 2012).
2. Wittstock, G., Burchardt, M., Pust, S. E., Shen, Y. & Zhao, C. Scanning electrochemical microscopy for direct imaging of reaction rates. *Angew. Chem. Int. Ed.* **46**, 1584-1617 (2007).
3. Polcari, D., Dauphin-Ducharme, P. & Mauzeroll, J. Scanning electrochemical microscopy: a comprehensive review of experimental parameters from 1989 to 2015. *Chemical reviews* **116**, 13234-13278 (2016).
4. Kai, T., Zoski, C. G. & Bard, A. J. Scanning electrochemical microscopy at the nanometer level. *Chem. Com.* **54**, 1934-1947 (2018).
5. Bentley, C. L. et al. Nanoscale Electrochemical Mapping. *Anal. Chem.* **91**, 84-108 (2018).
6. Lai, Z. et al. Small-Area Techniques for Micro-and Nanoelectrochemical Characterization: A Review. *Analytical Chemistry* **95**, 357-373 (2023).
7. Bard, A. J., Fan, F. R. F., Kwak, J. & Lev, O. Scanning electrochemical microscopy. *Anal. Chem.* **61**, 132-138 (1989).
8. Kwak, J. & Bard, A. J. Scanning electrochemical microscopy. Theory of the feedback mode. *Anal. Chem.* **61**, 1221-1227 (1989).
9. Ludwig, M., Kranz, C., Schuhmann, W. & Gaub, H. E. Topography feedback mechanism for the scanning electrochemical microscope based on hydrodynamic forces between tip and sample. *Rev. Sci. Instrum.* **66**, 2857-2860 (1995).
10. Holder, M. N., Gardner, C. E., Macpherson, J. V. & Unwin, P. R. Combined scanning electrochemical-atomic force microscopy (SECM-AFM): Simulation and experiment for flux-generation at un-insulated metal-coated probes. *J. Electroanal. Chem.* **585**, 8-18 (2005).
11. Salomo, M., Pust, S. E., Wittstock, G. & Oesterschulze, E. Integrated cantilever probes for SECM/AFM characterization of surfaces. *Microelectron. Eng.* **87**, 1537-1539 (2010).
12. Nellist, M. R. et al. Atomic force microscopy with nanoelectrode tips for high resolution electrochemical, nanoadhesion and nanoelectrical imaging. *Nanotechnology* **28**, 095711 (2017).
13. Bretag, A. H. The glass micropipette electrode: A history of its inventors and users to 1950. *Journal of General Physiology* **149**, 417-430 (2017).
14. Zhu, C., Huang, K., Siepser, N. P. & Baker, L. A. Scanning ion conductance microscopy. *Chem. Rev.* **121**, 11726-11768 (2020).
15. Traxler, I., Singewald, T. D., Schimo-Aichhorn, G., Hild, S. & Valtiner, M. Scanning electrochemical microscopy methods (SECM) and ion-selective microelectrodes for corrosion studies. *Corros. Rev.* **40**, 515-542 (2022).
16. Santana Santos, C., Jaato, B. N., Sanjuán, I., Schuhmann, W. & Andronescu, C. Operando Scanning Electrochemical Probe Microscopy during Electrocatalysis. *Chem. Rev.* **123**, 4972-5019 (2023).
17. Santos, C. S., Botz, A., Bandarenka, A. S., Ventosa, E. & Schuhmann, W. Correlative Electrochemical Microscopy for the Elucidation of the Local Ionic and Electronic Properties of the Solid Electrolyte Interphase in Li-Ion Batteries. *Angew. Chem. Int. Ed.* **61**, e202202744 (2022).

## 6. An integrated, exchangeable three-electrode electrochemical setup for AFM-based scanning electrochemical microscopy

18. Daboss, S., Rahmanian, F., Stein, H. S. & Kranz, C. The potential of scanning electrochemical probe microscopy and scanning droplet cells in battery research. *Electrochem. Sci. Adv.* **2**, e2100122 (2022).
19. He, R., Zhou, L., Tenent, R. & Zhou, M. Basics of Scanning Electrochemical Microscope and its Application in Characterizations of Lithium-Ion Batteries: A Brief Review. *Mater. Chem. Front.* **7**, 662-678 (2023).
20. Macpherson, J. V. & Unwin, P. R. Combined Scanning Electrochemical-Atomic Force Microscopy. *Anal. Chem.* **72**, 276-285 (2000).
21. Abbou, J., Demaille, C., Druet, M. & Moiroux, J. Fabrication of Submicrometer-Sized Gold Electrodes of Controlled Geometry for Scanning Electrochemical-Atomic Force Microscopy. *Anal. Chem.* **74**, 6355-6363 (2002).
22. Dobson, P. S., Weaver, J. M. R., Holder, M. N., Unwin, P. R. & Macpherson, J. V. Characterization of Batch-Microfabricated Scanning Electrochemical-Atomic Force Microscopy Probes. *Anal. Chem.* **77**, 424-434 (2005).
23. Pobelov, I. V. et al. Electrochemical current-sensing atomic force microscopy in conductive solutions. *Nanotechnology* **24**, 115501-115511 (2013).
24. Kranz, C. Recent advancements in nanoelectrodes and nanopipettes used in combined scanning electrochemical microscopy techniques. *The Analyst* **139**, 336-352 (2014).
25. Wain, A. J., Pollard, A. J. & Richter, C. High-Resolution Electrochemical and Topographical Imaging Using Batch-Fabricated Cantilever Probes. *Anal. Chem.* **86**, 5143-5149 (2014).
26. Eifert, A., Mizaikoff, B. & Kranz, C. Advanced fabrication process for combined atomic force-scanning electrochemical microscopy (AFM-SECM) probes. *Micron* **68**, 27-35 (2015).
27. Huang, Z. et al. PeakForce Scanning Electrochemical Microscopy with Nanoelectrode Probes. *Microscopy Today* **24**, 18-25 (2016).
28. Nellist, M. R. et al. Potential-sensing electrochemical atomic force microscopy for in operando analysis of water-splitting catalysts and interfaces. *Nature Energy* **3**, 46-52 (2018).
29. Bard, A. J., Faulkner, L. R. & White, H. S. *Electrochemical methods: fundamentals and applications* (Wiley, Hoboken, NJ, 2022).
30. Fahrenkrug, E., Alsem, D. H., Salmon, N. & Maldonado, S. Electrochemical measurements in in situ TEM experiments. *J. Electrochem. Soc.* **164**, H358 (2017).
31. Stricker, E. A., Ke, X., Wainright, J. S., Unocic, R. R. & Savinell, R. F. Current density distribution in electrochemical cells with small cell heights and coplanar thin electrodes as used in ec-S/TEM cell geometries. *J. Electrochem. Soc.* **166**, H126 (2019).
32. Kranz, C. et al. Integrating an ultramicroelectrode in an AFM cantilever: combined technology for enhanced information. *Anal. Chem.* **73**, 2491-2500 (2001).
33. Spaine, T. W. & Baur, J. E. A positionable microcell for electrochemistry and scanning electrochemical microscopy in subnanoliter volumes. *Anal. Chem.* **73**, 930-938 (2001).
34. Turcu, F., Schulte, A. & Schuhmann, W. Scanning electrochemical microscopy (SECM) of nanolitre droplets using an integrated working/reference electrode assembly. *Anal. Bioanal. Chem.* **380**, 736-741 (2004).

## 6. An integrated, exchangeable three-electrode electrochemical setup for AFM-based scanning electrochemical microscopy

35. Knittel, P., Bibikova, O. & Kranz, C. Challenges in nanoelectrochemical and nanomechanical studies of individual anisotropic gold nanoparticles. *Faraday Discussions* **193**, 353-369 (2016).
36. Foster, C. W., Kadara, R. O. & Banks, C. E. in *Screen-printing electrochemical architectures* 13-23 (Springer, Heidelberg, Germany, 2016).
37. Renedo, O. D., Alonso-Lomillo, M. A. & Martinez, M. J. A. Recent developments in the field of screen-printed electrodes and their related applications. *Talanta* **73**, 202-219 (2007).
38. Shen, X., Ju, F., Li, G. & Ma, L. Smartphone-Based Electrochemical Potentiostat Detection System Using PEDOT: PSS/Chitosan/Graphene Modified Screen-Printed Electrodes for Dopamine Detection. *Sensors* **20**, (2020).
39. Muschiatti, A., Serrano, N., Ariño, C., Díaz-Cruz, M. S. & Díaz-Cruz, J. M. Screen-Printed Electrodes for the Voltammetric Sensing of Benzotriazoles in Water. *Sensors* **20**, (2020).
40. Martínez-Periñán, E., Gutiérrez-Sánchez, C., García-Mendiola, T. & Lorenzo, E. Electrochemiluminescence Biosensors Using Screen-Printed Electrodes. *Biosensors* **10**, (2020).
41. Torres-Rivero, K. et al. Direct As(V) Determination Using Screen-Printed Electrodes Modified with Silver Nanoparticles. *Nanomaterials* **10**, (2020).
42. Antuña-Jiménez, D., González-García, M. B., Hernández-Santos, D. & Fanjul-Bolado, P. Screen-Printed Electrodes Modified with Metal Nanoparticles for Small Molecule Sensing. *Biosensors* **10**, 9 (2020).
43. Mincu, N.-B. et al. Screen-Printed Electrodes (SPE) for In Vitro Diagnostic Purpose. *Diagnostics* **10**, 517 (2020).
44. Costa-Rama, E. & Fernández-Abedul, M. T. Paper-Based Screen-Printed Electrodes: A New Generation of Low-Cost Electroanalytical Platforms. *Biosensors* **11**, (2021).
45. Gomes, R. S. et al. Plastic Antibody of Polypyrrole/Multiwall Carbon Nanotubes on Screen-Printed Electrodes for Cystatin C Detection. *Biosensors* **11**, (2021).
46. Retsch, M. et al. Fabrication of Large-Area, Transferable Colloidal Monolayers Utilizing Self-Assembly at the Air/Water Interface. *Macromol. Chem. Phys.* **210**, 230-241 (2009).
47. Stelling, C., Mark, A., Papastavrou, G. & Retsch, M. Showing particles their place: deterministic colloid immobilization by gold nanomeshes. *Nanoscale* **8**, 14556-14564 (2016).
48. Rentsch, S., Siegenthaler, H. & Papastavrou, G. Diffuse Layer Properties of Thiol-Modified Gold Electrodes Probed by Direct Force Measurements. *Langmuir* **23**, 9083-9091 (2007).
49. Kuznetsov, V. & Papastavrou, G. Adhesion of Colloidal Particles on Modified Electrodes. *Langmuir* **28**, 16567-16579 (2012).
50. Kuznetsov, V. & Papastavrou, G. Ion Adsorption on Modified Electrodes as Determined by Direct Force Measurements under Potentiostatic Control. *J. Phys. Chem. C* **118**, 2673-2685 (2014).
51. Karg, A. et al. A Versatile and Simple Approach to Electrochemical Colloidal Probes for Direct Force Measurements. *Langmuir* **37**, 13537-13547 (2021).
52. Gullo, M. R. et al. Characterization of microfabricated probes for combined atomic force and high-resolution scanning electrochemical microscopy. *Analytical chemistry* **78**, 5436-5442 (2006).

## 6. An integrated, exchangeable three-electrode electrochemical setup for AFM-based scanning electrochemical microscopy

53. Walker, S. M., Marcano, M. C., Bender, W. M. & Becker, U. Imaging the reduction of chromium (VI) on magnetite surfaces using in situ electrochemical AFM. *Chemical Geology* **429**, 60-74 (2016).
54. Knittel, P., Zhang, H., Kranz, C., Wallace, G. G. & Higgins, M. J. Probing the PEDOT:PSS/cell interface with conductive colloidal probe AFM-SECM. *Nanoscale* **8**, 4475-4481 (2016).
55. Leenheer, A. J., Sullivan, J. P., Shaw, M. J. & Harris, C. T. A sealed liquid cell for in situ transmission electron microscopy of controlled electrochemical processes. *J. Microelectromech. Syst.* **24**, 1061-1068 (2015).
56. Taheri, M. L. et al. Current status and future directions for in situ transmission electron microscopy. *Ultramicroscopy* **170**, 86-95 (2016).
57. Compton, R. G. & Banks, C. E. *Understanding voltammetry* (Imperial College Press, London, 2010).
58. Mirkin, M. V. & Amemiya, S. *Nanoelectrochemistry* (CRC Press, Boca Raton, 2015).
59. Criscuolo, F., Galfione, M., Carrara, S. & De Micheli, G. All-solid-state Reference Electrodes for analytical applications. *2019 IEEE 8th International Workshop on Advances in Sensors and Interfaces (IWASI) 2019 IEEE 8th International Workshop on Advances in Sensors and Interfaces*, 66-69 (2019).
60. Petrovic, S. Cyclic Voltammetry of Hexachloroiridate(IV): An Alternative to the Electrochemical Study of the Ferricyanide Ion. *Chem. Educ.* **5**, 231-235 (2000).
61. Ji, X., Banks, C. E., Crossley, A. & Compton, R. G. Oxygenated edge plane sites slow the electron transfer of the ferro-/ferricyanide redox couple at graphite electrodes. *ChemPhysChem* **7**, 1337-1344 (2006).
62. Sun, P., Laforge, F. O. & Mirkin, M. V. Scanning electrochemical microscopy in the 21st century. *Phys. Chem. Chem. Phys.* **9**, 802-823 (2007).
63. Knittel, P., Mizaikoff, B. & Kranz, C. Simultaneous Nanomechanical and Electrochemical Mapping: Combining Peak Force Tapping Atomic Force Microscopy with Scanning Electrochemical Microscopy. *Analytical Chemistry* **88**, 6174-6178 (2016).
64. Zeng, Z. et al. Visualization of electrode–electrolyte interfaces in LiPF<sub>6</sub>/EC/DEC electrolyte for lithium ion batteries via in situ TEM. *Nano Letters* **14**, 1745-1750 (2014).
65. Girod, R., Nianias, N. & Tileli, V. Electrochemical behavior of carbon electrodes for in situ redox studies in a transmission electron microscope. *Microsc. Microanal.* **25**, 1304-1310 (2019).
66. Ferrari, A. G.-M., Rowley-Neale, S. J. & Banks, C. E. Screen-printed electrodes: Transitioning the laboratory in-to-the field. *Talanta Open* **3**, 100032 (2021).
67. Singh, S., Wang, J. & Cinti, S. An overview on recent progress in screen-printed electroanalytical (bio) sensors. *ECS Sensors Plus* (2022).
68. Ventosa, E. & Schuhmann, W. Scanning electrochemical microscopy of Li-ion batteries. *Phys. Chem. Chem. Phys.* **17**, 28441-28450 (2015).
69. Mahankali, K., Thangavel, N. K. & Reddy Arava, L. M. In Situ Electrochemical Mapping of Lithium–Sulfur Battery Interfaces Using AFM–SECM. *Nano Letters* **19**, 5229-5236 (2019).
70. Zhang, Z. et al. Operando Electrochemical Atomic Force Microscopy of Solid-Electrolyte Interphase Formation on Graphite Anodes: The Evolution of SEI Morphology and Mechanical Properties. *ACS Appl. Mater. Interfaces* **12**, 35132-35141 (2020).

## 6. An integrated, exchangeable three-electrode electrochemical setup for AFM-based scanning electrochemical microscopy

---

71. Liao, W. Y. & Chou, T. C. Fabrication of a planar-form screen-printed solid electrolyte modified Ag/AgCl reference electrode for application in a potentiometric biosensor. *Anal. Chem.* **78**, 4219-4223 (2006).
72. Guth, U., Gerlach, F., Decker, M., Oelßner, W. & Vonau, W. Solid-state reference electrodes for potentiometric sensors. *J. Solid State Chem.* **13**, 27-39 (2009).

## List of Publications

- 1. A Versatile and Simple Approach to Electrochemical Colloidal Probes for Direct Force Measurements**  
Andreas Karg, Tamino Rößler, Andreas Mark, Paul Markus, Tobias Lauster, Nicolas Helfricht, Georg Papastavrou\*  
*Langmuir*, **2021**, 37 (46), 13537. DOI: 10.1021/acs.langmuir.1c01557
- 2. Electrochemical Grippers for Micro- and Nanorobotics: Manipulation by Tuning Surface Forces**  
Andreas Karg, Volodymyr Kuznetsov, Nicolas Helfricht, Markus Lippitz, Georg Papastavrou\*  
*Scientific Reports*, **2023**, 13 (1), 7885. DOI: 10.1038/s41598-023-33654-6
- 3. An integrated, exchangeable three-electrode electrochemical setup for AFM-based scanning electrochemical microscopy**  
Andreas Karg, Sebastian Gödrich, Philipp Dennstedt, Nicolas Helfricht, Markus Retsch, Georg Papastavrou\*  
*MDPI Sensors*, **2023**, 23 (11), 5228. DOI: 10.3390/s23115228

# Danksagung

Zu guter Letzt ist es an der Zeit, all denjenigen zu danken, ohne die diese Arbeit nicht möglich gewesen wäre!

Als erstes gilt mein aufrichtiger Dank meinem Betreuer Prof. Dr. Papastavrou. Vielen Dank für das entgegengebrachte Vertrauen, die lehrreiche Betreuung, wissenschaftliche Diskussionen und stete Motivation. Herzlichen Dank.

Des Weiteren danke ich meinen Kooperationspartnern für die sehr erfolgreiche Zusammenarbeit. Ich bedanke mich bei Prof. Dr. Markus Lippitz für die tollen Projekte und wissenschaftlichen Diskussionen. Prof. Dr. Markus Retsch danke ich für die spannenden Substrate für SECM Experimente und die wissenschaftlichen Diskussionen. Außerdem danke ich dem „Operator“ Patrick Knödler, für seine Hilfe und Arbeit an der FIB. Danke für die spaßige und lehrreiche Zusammenarbeit.

Danke an Nicolas Helfricht für die vielfältigen wissenschaftlichen und menschlichen Ratschläge, seinen unermüdlichen Einsatz bei den Papern und dafür, dass du versucht hast, mir mit Nachrichten abends und am Wochenende die Arbeit an den Papern neben dem Berufsleben zu erleichtern!

Meinen altvorderen Nicolas Helfricht, Sebastian Gödrich und Andreas Mark gilt besonderer Dank für den herzlichen Empfang in der Gruppe, stets angenehme und freundschaftliche Zusammenarbeit, spannende wissenschaftliche Diskussionen und das Einweihen in die Geheimnisse der Kraftmikroskopie. Bei Andreas bedanke ich mich zusätzlich für die Hilfestellungen bei allen elektrochemischen Problemen, und den sportlichen Ehrgeiz, den wir zusammen erweckt haben.

Außerdem gilt mein Dank „Lehrstuhlmama“ Sybille Zimmermann, die stets gut gelaunt bei allen organisatorischen Problemen half, und mich zusätzlich mit Ihrem Vorrat vor Unterzuckerung bewahrte.

Danke auch an meine wechselnden Bürokolleg\*Innen Agnes, Tamino, Katharina, Max, Lukas, Steffen und nochmal Andreas für eine spaßige, entspannte und dennoch produktive Arbeitsatmosphäre. Danke auch an Paul Markus (den Iconflüsterer und

## Danksagung

---

zweiten großartigen Zuckerspender), Nadine Raßman und Sebastian Sittl (der auch den sportlichen Ehrgeiz teilt) für spannende Kaffeepausen und Feierabendbiere, bei denen auch, aber nicht nur spannende wissenschaftliche Ideen diskutiert wurden.

Danke an Wolfgang Häfner, Markus Hund, Carmen Kunert und Petra Zippelius für die Hilfe bei technischen Problemen, Messungen und diverse Umzugsarbeiten.

Weiterhin gebührt Dank dem „Hiwi“-Clan Tamino, Matthias und Philipp für die Unterstützung bei diversen Projekten und Bastelarbeiten.

Bei Tamino, den ich vom ersten Praktikum bis zum Fast-Beginn der Promotion begleiten konnte, bedanke ich mich zusätzlich für die Hilfe mit den Probes, und die angenehme Zusammenarbeit während deiner Bachelorarbeit und weit darüber hinaus.

Dank gilt auch meinen Praktikanten Andos, Tamino, Marius und Sebastian für eure Unterstützung.

Dem Freundefreitag und gilt Dank für wissenschaftliche Diskussionen, Uni-Tratsch, moralischer Unterstützung, das Genießen der Hochs und das Ausgleichen der Tiefs der Promotion.

Ich danke dem Bayerischen Batteriezentrum für die Finanzierung, und dem e-fellows-Netzwerk für die Förderung.

Danke meiner Frau Julia, du warst immer für mich da, hast mich dauernd unterstützt und mir den Rücken freigehalten.

Zu guter Letzt Danke ich meiner Familie. Danke an meine Eltern Alfred und Viktoria, und meine Brüder Simon und Johannes für eure dauerhafte und fortwährende Unterstützung.

## Herzliches Dankeschön!

# **(Eidesstattliche) Versicherungen und Erklärungen**

(§ 8 Satz 2 Nr. 3 PromO Fakultät)

Hiermit versichere ich eidesstattlich, dass ich die Arbeit selbstständig verfasst und keine anderen als die von mir angegebenen Quellen und Hilfsmittel benutzt habe (vgl. Art. 64 Abs. 1 Satz 6 BayHSchG).

(§ 8 Satz 2 Nr. 3 PromO Fakultät)

Hiermit erkläre ich, dass ich die Dissertation nicht bereits zur Erlangung eines akademischen Grades eingereicht habe und dass ich nicht bereits diese oder eine gleichartige Doktorprüfung endgültig nicht bestanden habe.

(§ 8 Satz 2 Nr. 4 PromO Fakultät)

Hiermit erkläre ich, dass ich Hilfe von gewerblichen Promotionsberatern bzw. -vermittlern oder ähnlichen Dienstleistern weder bisher in Anspruch genommen habe noch künftig in Anspruch nehmen werde.

(§ 8 Satz 2 Nr. 7 PromO Fakultät)

Hiermit erkläre ich mein Einverständnis, dass die elektronische Fassung meiner Dissertation unter Wahrung meiner Urheberrechte und des Datenschutzes einer gesonderten Überprüfung unterzogen werden kann.

(§ 8 Satz 2 Nr. 8 PromO Fakultät)

Hiermit erkläre ich mein Einverständnis, dass bei Verdacht wissenschaftlichen Fehlverhaltens Ermittlungen durch universitätsinterne Organe der wissenschaftlichen Selbstkontrolle stattfinden können.

---

Ort, Datum, Unterschrift